

**POTENTIAL OF OPTICAL ANALYSIS METHODS  
FOR INVESTIGATIONS OF PESTICIDES ON  
BIOLOGICAL RELEVANT SURFACES AND IN  
THE ENVIRONMENT**

Von der Naturwissenschaftlichen Fakultät der  
Gottfried Wilhelm Leibniz Universität Hannover  
zur Erlangung des Grades

Doktor der Naturwissenschaften

Dr. rer. nat.

genehmigte Dissertation

von

Dipl.-Phys. Harald Hake

geboren am 07. November 1974 in Langenhagen

2007

Referentin	Prof. Dr. Angelika Anders–von Alften Institut für Biophysik, Gottfried Wilhelm Leibniz Universität Hannover, Hannover, Germany
Korreferent	Prof. Dr. Israel Schechter Technion – Israel Institute of Technology, Haifa, Israel
Tag der Promotion	05. September 2007

## Abstract

In this work optical methods are evaluated in regard to analysis of pesticides in environmental compartments and on biological surfaces such as leaves. Laser induced fluorescence (LIF) spectroscopy is suitable for fast *in situ* measurements and can be used for non-invasive and online screening of pesticide distributions. For investigations of pesticide colloidal suspensions in water, laser induced plasma breakdown detection (LIBD) is utilized. LIBD has the potential to detect nano-sized particulates at low concentrations.

Pesticides are an integral part of modern agriculture and are used to increase production and improve products. Today, there is a huge variety of different pesticides used as herbicides, fungicides, insecticides, growth regulators, etc. Usually, pesticides are solved in water and then sprayed onto a field where an over-coverage is common to ensure the full effect of pesticide application. Under-coverage means ineffective action, which is of considerable economical concern. Over-coverage, however, leads to pesticides in the soil and from there these substances are flushed out as run-off into rivers as well as into the ground water. Therefore, many countries have regulations which restrict the presence of such substances in water, especially in drinking water. When such limits are exceeded, considerable effort is required for remediation.

In view of all these factors, it is desirable to limit agricultural usage of pesticides to an optimal dosage. Therefore, a convenient, fast and non-invasive method is required to estimate the actual coverage of plants. In this thesis, optical methods are investigated in regard to their potential for a fast assessment of pesticide coverage in view of a field application. Optical methods are fast, non-invasive and can be automated for on-line analysis. One major problem of applying such methods for detection of compounds on biological material is the optical activity of this underlying material itself. Plants contain chromophores which could cause light emission (e.g. fluorescence of chlorophyll) or interfere with spectroscopic detection due to physiological effects. To overcome such matrix effects, investigations of spectral influences of an added labeling compound interacting with the pesticides are suggested. For the detection laser induced fluorescence (LIF) spectroscopy is used and spectral influences such as shifts in fluorescence emission or quenching effects will be addressed, as well as changes in fluorescence lifetime.

In this thesis the potential of laser induced breakdown detection (LIBD) is evaluated for small particulates at low concentrations. Colloid analysis is typically not included in water chemical standard analysis which is normally limited to particle diameters above 450 nm due to filtering. A pulsed laser beam is focused into a sample. The necessary laser pulse energy for generating a plasma is lower for solid matter than for liquids and much lower than for gases. The pulse energy is adjusted, so that there are no plasma events in water but a breakdown event is triggered when a solid particle moves into the focus of the laser beam. These events are counted in relation to the number of laser pulses which leads to a breakdown probability depending mainly on particle size and concentration. In this thesis, concentration measurements are carried out with model substances (e.g. silica dioxide) in view of an application for the detection of pesticide active components which show poor solubility and, thus, are likely to form colloids.

**Keywords:** Pesticide Detection, Fluorescence Spectroscopy, Laser Induced Plasma Detection



# Kurzzusammenfassung

Zielsetzung dieses Dissertationsprojektes war die Untersuchung optischer Methoden im Hinblick auf eine Analyse von Pestiziden in Umweltkompartimenten, sowie auf biologisch relevanten Oberflächen. Die Laser induzierte Fluoreszenzspektroskopie (LIF) ist in diesem Zusammenhang geeignet, um schnelle *in situ* Messungen und ein nicht invasives online Screening von Pestizidverteilungen durchzuführen. Für Untersuchungen von Pestizid-Colloidsuspensionen im Wasser, wurde die Laser induzierte Breakdown Detektion (LIBD) genutzt. LIBD hat das Potential, Nanopartikel in niedrigen Konzentrationen detektieren zu können.

Pestizide sind integraler Bestandteil moderner Landwirtschaft im Hinblick auf gesteigerte Produktion und verbesserte Produkte. Heute gibt es eine Vielzahl verschiedener Pestizide, welche als Herbizide, Fungizide, Insektizide, Wachstumsregulatoren, usw. genutzt werden. Üblicherweise werden die Pestizide in Wasser gelöst und dann auf ein Feld gesprüht, wobei eine Überdosierung zur Entfaltung des vollen Effekts der Pestizidanwendung üblich ist. Eine unvollständige Bedeckung bedeutet dabei ineffektive Wirkung, was ökonomische Folgen nach sich zieht. Durch die Überdosierung gelangen Pestizide in den Boden und in Gewässer sowie in das Grundwasser. Daher werden in vielen Staaten Grenzwerte für Gewässer und speziell für Trinkwasser vorgeschrieben. Werden die Grenzwerte überschritten, sind große Anstrengungen für eine Sanierung notwendig.

In dieser Arbeit werden optische Methoden mit dem Potenzial zur schnellen Beurteilung von Pestizidbedeckungen in Hinblick auf eine Feldanwendung vorgestellt. Optische Methoden zählen zu den schnellen und nicht invasiven Verfahren und können für eine online Analyse automatisiert werden. Ein Problem bei der Detektion von Substanzen ist das pflanzliche Material selbst. Pflanzen enthalten Chromophore, wie etwa Chlorophyll in den Blättern, welche fluoreszieren und können zusätzlich durch physiologische Effekte spektroskopische Messungen stören. Um diese Matrixeffekte zu Umgehen, wurden die Wechselwirkungen eines zugefügten Markers mit den Pestiziden analysiert. Laser induzierte Fluoreszenzspektroskopie wurde zur Detektion eingesetzt und spektrale Verschiebungen oder veränderte Halbwertszeiten der Fluoreszenzlebensdauern beim Zusammenwirken mit dem Marker untersucht.

In der chemischen Wasserstandartanalyse werden typischerweise Filter mit einer Porengröße von 450 nm eingesetzt, was zu einer Unterschätzung von Colloiden führt. In dieser Arbeit wird das Potential der Laser induzierten Breakdown Detektion (LIBD) im Hinblick auf eine Bestimmung von kleinen Partikeln in niedrigen Konzentrationen untersucht. Hierbei wird ein gepulster Laserstrahl in eine Probe fokussiert. Die nötige Pulsenergie für eine Plasmagenertation ist bei Festkörpern niedriger als für Flüssigkeiten und viel niedriger als für Gase. Bewegt sich ein Festkörperpartikel in die Fokusregion, kommt es zum Plasmabreakdown. Die Anzahl der Plasmaereignisse relativ zur Anzahl der Pulse ergibt eine Breakdown-Wahrscheinlichkeit, welche hauptsächlich von der Größe und Konzentration der Partikel abhängt. Im Rahmen dieser Arbeit wurden Messungen mit Modellsubstanzen (z.B. Silikondioxid) durchgeführt. Dies geschah im Hinblick auf Untersuchungen von Wirkstoffen der Pestizide, welche Aufgrund ihrer schlechten Wasserlöslichkeit mit großer Wahrscheinlichkeit Colloide bilden.

**Schlagerworte:** Pestizid Detektion, Fluoreszenzspektroskopie, Laserinduzierte Plasma Detektion



# Contents

Abstract . . . . .	iii
Kurzzusammenfassung . . . . .	v
List of Abbreviations . . . . .	xi
<b>1 Introduction</b>	<b>1</b>
<b>2 Theoretical Considerations</b>	<b>5</b>
2.1 Fluorescence Spectroscopy . . . . .	6
2.1.1 Fluorescence . . . . .	6
2.1.2 Fluorescence Detection and Imaging . . . . .	8
2.1.3 Time Resolved Fluorescence Spectroscopy . . . . .	9
2.2 Plasma Breakdown Detection . . . . .	9
2.2.1 Laser Induced Plasma . . . . .	10
2.2.2 Determination of Breakdown Probability and Particle Concentration	12
2.3 Biological and Chemical Foundations . . . . .	15
2.3.1 Colloids in an Aqueous Environment . . . . .	15
2.3.2 Pesticides . . . . .	16
<b>3 Material and Methods</b>	<b>21</b>
3.1 Laser Induced Fluorescence . . . . .	21
3.1.1 Nitrogen Laser System for Fast Optical Assessment . . . . .	21
3.1.2 Nd:YAG Laser System for Time Resolved Measurements . . . . .	24
3.2 Laser Induced Breakdown Detection . . . . .	28
3.2.1 Nd:YAG-Laser System for Plasma Breakdown Induction . . . . .	28

3.3	Fluorescence Measurements . . . . .	30
3.3.1	Direct CCD Imaging under UV Irradiation . . . . .	30
3.3.2	Fluorescence Microscope . . . . .	30
3.4	Material and Chemicals . . . . .	31
3.4.1	Solvents . . . . .	31
3.4.2	Fluorescing Particulates . . . . .	32
3.4.3	Pesticides and their Matrix . . . . .	34
<b>4</b>	<b>Results and Discussion</b>	<b>37</b>
4.1	Optical Assessment of Pesticide Coverage . . . . .	38
4.1.1	Auto-Fluorescence Spectra of Particulate Dyes on Surfaces . . . . .	39
4.1.1.1	Fluorescence of Particulate Dyes on a Glass Surface . . . . .	39
4.1.1.2	Fluorescence of Particulate Dyes on a Leaf Surface . . . . .	46
4.1.2	Auto-Fluorescence Spectra of Pesticide Droplets on Surfaces . . . . .	48
4.1.2.1	Fluorescence of Pesticide Droplet on a Glass Surface . . . . .	48
4.1.2.2	Fluorescence of Pesticide Droplet on a Leaf Surface . . . . .	52
4.1.3	Dissolution of Dye Micro-Crystals in Droplets . . . . .	54
4.1.4	Effects of Pesticides on <i>Rhodamine 6G</i> Fluorescence . . . . .	57
4.1.4.1	Effects of Pesticides on Fluorescence Intensities . . . . .	57
4.1.4.2	Analysis of Spectral Shifts . . . . .	59
4.1.4.3	Investigation of Fluorescence Decay Times . . . . .	62
4.1.5	Obtaining Imaging Data of Pesticide Coverage on Leaves . . . . .	68
4.1.5.1	Scanning Data . . . . .	68
4.1.5.2	Imaging Data . . . . .	70
4.2	Quantification of Pesticide Colloidal Suspension . . . . .	73
4.2.1	Breakdown Probability Detection . . . . .	73
4.2.1.1	Breakdown Probability at Varying Colloid Concentrations . . . . .	79
4.2.1.2	Breakdown Probability at Varying Laser Power . . . . .	80



---

4.2.2	Automated Data Evaluation . . . . .	82
4.2.2.1	Counting Breakdown Events in Colloidal Suspension .	83
4.2.2.2	Estimating Breakdown Area in Colloidal Suspension .	91
4.2.3	Correlating the Breakdown Probability and its Estimated Area . .	92
4.2.3.1	Analysis of Multiple Events Based on Area Estimation	95
<b>5</b>	<b>Summary and Conclusion</b>	<b>97</b>
<b>A</b>	<b>Pesticide Properties and Data Sheets</b>	<b>101</b>
	<b>List of Figures</b>	<b>111</b>
	<b>List of Tables</b>	<b>115</b>
	<b>Bibliography</b>	<b>117</b>



# List of Abbreviations

<b>AFM</b>	atomic force microscopy
<b>BBO</b>	$\beta$ -barium borate ( $\beta$ -BaB <sub>2</sub> O <sub>4</sub> )
<b>CCD</b>	charged coupled device
<b>DDT</b>	dichloro-diphenyl-trichloroethane (insecticide)
<b>EEM</b>	excitation-emission matrix
<b>EPA</b>	United States Environmental Protection Agency
<b>FIFRA</b>	Federal Insecticide, Fungicide, and Rodenticide Act
<b>HR</b>	highly reflective
<b>HRAC</b>	Herbicide Resistance Action Committee
<b>ICCD</b>	intensified CCD
<b>IR</b>	infrared
<b>KDP</b>	potassium dihydrogen phosphate (KH <sub>2</sub> PO <sub>4</sub> )
<b>LIBD</b>	laser induced breakdown detection
<b>LIBS</b>	laser induced (plasma) breakdown spectroscopy (also LIPS sometimes)
<b>LIF</b>	laser induced fluorescence
<b>MCP</b>	micro-channel plate
<b>Nd:YAG</b>	neodymium-doped yttrium aluminium garnet (Nd:Y <sub>3</sub> Al <sub>5</sub> O <sub>12</sub> )
<b>NIR</b>	near infrared
<b>OPO</b>	optical parametric oscillator
<b>PC</b>	personal computer
<b>PCS</b>	photon correlation spectroscopy
<b>PMT</b>	photomultiplier tube
<b>POP</b>	persistent organic pollutants
<b>PSI</b>	photosystem I
<b>PSII</b>	photosystem II
<b>Q-switch</b>	quality-switch

<b>REM</b>	reflection electron microscopy
<b>SEM</b>	scanning electron microscopy
<b>SHG</b>	second harmonic generation (frequency doubling)
<b>THG</b>	third harmonic generation (frequency tripling)
<b>TR-LIF</b>	time resolved LIF
<b>UNEP</b>	United Nations Environmental Programme
<b>UV</b>	ultraviolet
<b>VIS</b>	visible (spectral region)
<b>WHO</b>	World Health Organisation
<b>WTM</b>	wave-time matrix

# Chapter 1

## Introduction

In 2001 the Stockholm Convention on persistent organic pollutants (POPs) was signed by many countries under the United Nations Environmental Programme (UNEP). The goal of this treaty is the reduction and ultimately the complete elimination of persistent pollutants which have an impact on the environment. These pollutants include organochlorine pesticides, a widely known compound being the insecticide DDT (dichloro-diphenyl-trichloroethane). In the mid-1960s the concern for environmental issues by a few individuals turned into an environmental movement. *Rachel Carson* published her best selling book "*Silent Spring*" in 1962, where the impact of pesticides getting into the food chain, on the environment and human health is detailed. Carson especially focused on DDT and follow up research led to its ban. Public awareness of environmental problems was greatly enhanced by the best-seller, so it could be nominated for starting the environmental movement and awakening the interest on such problems by scientific, social, and political groups. In the following years, new interest groups were founded, notably Greenpeace, and concern about environmental problems such as air or water pollution or oil spills became of general interest.

Nevertheless, the production and use of pesticides has also increased worldwide. Pesticides are an integral part of modern agriculture and are used to increase production and improve products. Today, there is a wide variety of different pesticides used as herbicides, fungicides, insecticides, growth regulators, etc. Despite the regulations by governmental agencies for production of these compounds and to bring them on the market, the volume of pesticide usage has increased. Worldwide sales of pesticides were \$ 30 billion in 1996. In 1995 in the United States two crops (cotton and corn) used around 90 % of the insecticides and 80 % of the herbicides applied to crops [1]. For the U.S., annual used expenditures on pesticides have increased from \$ 6.3 billion (\$ 3.8 billion for herbicides and plant growth regulators (PRG)) in 1982 to \$ 11 billion (\$ 6.6 billion for herbicides and PGR) in 1996 [2]. The EPA report [2] also states that (for the U.S.) the most com-

monly used conventional\* pesticide active ingredient in the agricultural marked sector in 2001 was *Glyphosate* with 85 – 90 million pounds (in 1987 place seven with 6 – 8 million pounds) followed by *Atrazine* with 74 – 80 million pounds (in 1987 first place with 71 – 76 million pounds). Fifth place was taken by *2,4-D* with 28 – 33 million pounds (in 1987 also fifth place with 29 – 33 million pounds). Atrazine is still one of the most widely used herbicides, but in Germany it is banned from use since 1991 and in Austria since 1995 because it can get into the ground and drinking water where it can still be detected. Although the research on these products continues and pesticides became less hazardous regarding environmental issues (e.g. they are becoming less persistent), pesticide entry into the environment is a major risk factor and may have hazardous effects upon humans and animals [3, 4]. Development of new products is very cost intensive, so research is usually restricted to pesticides for crops with a huge market, e.g. wheat, corn, or soy beans.

Common practice for pesticide application is solving the trading unit in water and then spraying it on the plants in a field. In order to achieve the desired effect and to use a given pesticide to its full extent, a complete coverage must be achieved. Too low coverage means ineffective action, which is of considerable economical concern. Therefore, the usual case is an over-coverage to ensure the full effect of pesticide application. This overdosing has great economical and environmental impact. The expenses for pesticides are not negligible and reducing waste becomes more and more important. Also, the environmental impact is not to be underestimated. Over-coverage leads to pesticides in the soil and from there these substances are flushed out as run-off into rivers as well as into the ground water [5, 6]. Therefore, many countries have regulations which restrict the presence of such substances in water, especially in drinking water. When such limits are exceeded, considerable effort is required for remediation. Moreover, some of the used compounds have a long biological lifetime and, therefore, can be detected after years of application (especially the organochlorine pesticides are very persistent).

With the increased use of pesticides, an evaluation of risks to humans and to the environment became more and more important. New methods in environmental analysis became available, especially optical methods had an increased application since the development of the laser in about 1960. In environmental analysis a broad spectrum of problems has to be addressed which results in manifold requirements of a suitable method, depending on the challenge. Optical methods have the advantage of being non-invasive, contact-free and can be used with no preparation of the sample. The relatively simple setup, consisting of an irradiation source, the sample and a detector (refer to *Figure 2.1*) makes these methods good tools of in-situ analysis and they can also be used in vivo, which is essential for

---

\**Conventional Pesticides (EPA definition [2]):* Pesticides that are chemicals or other substances developed and produced primarily or only for use as pesticides. An example is DDT, which was developed and used almost exclusively as a pesticide. Also includes biological and biochemical pesticides, e.g. *Bacillus thuringiensis*.

many biological samples. Due to short interaction times of a sample with electromagnetic radiation, optical methods can be used for monitoring samples in real time. To obtain results immediately is another principal argument for optical methods, which allows on-line monitoring of samples. This is an important factor in process control as well as in environmental analysis.

In this thesis two optical methods for environmental analysis were employed. Laser induced fluorescence (LIF) was used for an optical assessment of pesticide coverage on leaves. A mapping of coverage will help to reduce pesticide use and thus lower the entry into the environment. Pesticides are usually composed of an active compound in an emulsion. If the active compound, which normally has poor solubility, gets into the soil or ground water due to over-coverage by the spraying application they are likely to form colloids. These nanosized particulates are not detected by conventional water analysis due to their small size, so the second method is directed at the detection of these particulates. Laser induced breakdown detection (LIBD) has the ability to detect nanosized particles by monitoring plasma emissions. The method is applied in aerosol detection [7, 8], investigations of drinking water [9, 10, 11] and natural waters [12, 13, 14], and groundwater colloid characterization [15, 16, 17]. The setup is similar to laser induced breakdown spectroscopy (LIBS) but no spectral information is needed, therefore, experimental complexity is reduced. As second part of this thesis, the application of LIBD for a detection of aqueous colloids is investigated in view of an application for analysis of pesticide colloidal suspensions. The experiments in this part were done at the Technion (Technion - Israel Institute of Technology, Haifa, Israel) and supported by the Max Planck Gesellschaft with a Minerva Research Grant.

Feasibility of employing LIBD for probing particle size distributions [18] in natural surface waters has been investigated [19]. Solid particles are present in natural waters with size distributions ranging from a few nanometer to suspended particles of some micrometer [20, 21]. Due to their small size, colloids have the potential to transport contaminants over long distances [22] which is of particular interest in context of radionuclide migration [23, 24].

For the use of LIF, fluorescence markers were used (primary fluorescing dyes) and applied to the surface of a leaf. When water is sprayed on the leaf the fluorescing particulates solve in the droplet and a signal could be detected when excited with a suitable wavelength. The approach in this thesis is to monitor changes in this fluorescence signature in the presence of pesticides. Spectral shifts could be observed and depending on the concentration even quantitative statements could be made. Shifts in fluorescence decay times were also investigated as well as increase or decline of signal intensity.

For the LIBD measurements, breakdown probability was investigated in dependence of concentration and power density. Here, the optical measurement of events was used. Additionally, the area of the events was monitored. Event area could be used as well as the

breakdown probability, but the estimation of the area has the advantage of taking multiple events into account, due to their larger total area. This results in a better differentiation of concentrations at high breakdown probability even if the probability has reached one hundred percent.



## Chapter 2

# Theoretical Considerations

Spectroscopy is the investigation of material by analyzing the emission, absorption or scattering of radiation, sound or particles. Historically, it is the study of interactions of visible light and matter, however, today this field of science is broadened by not only using visible light but a wide variety of radiation.

Spectroscopy is often used for compound detection and identification and can be classified by the physical quantity under investigation. Examples include *Absorption Spectroscopy*, *Fluorescence Spectroscopy*, *Infrared Spectroscopy*, or *Raman Spectroscopy*.

A general experimental setup for spectroscopy measurements is illustrated in *Figure 2.1*. Usually, the sample material is irradiated followed by some kind of interaction. This results in an emission, typically of radiation or sound waves, which is recorded by the detector. A spectrum is recorded and this can be used to analyze the material under investigation.

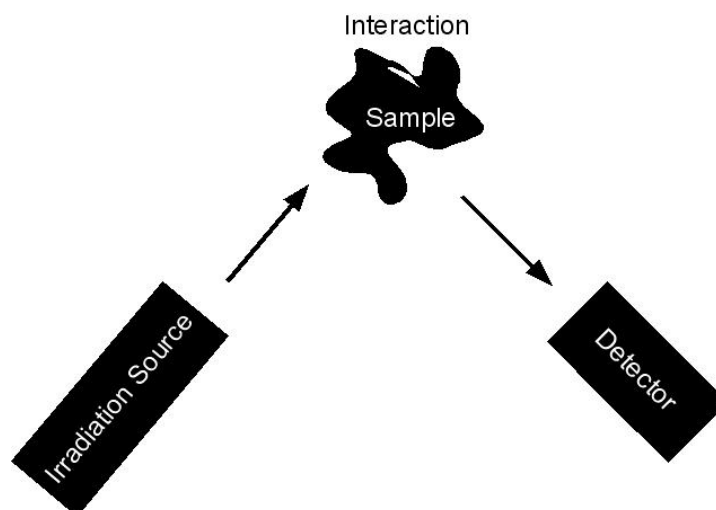


**Figure 2.1:** General experimental setup for measurements using spectroscopy. As can be seen in this simplified illustration, there is usually some kind of incident radiation leading to an interaction with the sample (e.g. absorption, scattering, fluorescence). Generally, this results in an emission which is monitored by a detector.

In this thesis two spectroscopic methods were employed, namely, *Laser induced Fluorescence (LIF) Spectroscopy* and *Laser induced Plasma Breakdown Detection (LIBD)*. The following sections will give a short overview over the theoretical background of these methods and will also give some historical information.

## 2.1 Fluorescence Spectroscopy

Fluorescence spectroscopy measures fluorescence emission for compound identification or compound detection. Referring to *Figure 2.1*, the interaction with the sample is absorption which leads to an emission of fluorescence radiation. Often, laser are used as excitation source. Then the method is referred to as laser induced fluorescence (LIF) spectroscopy.

Laser induced fluorescence (LIF) spectroscopy allows a selective irradiation of absorption bands. Due to the discrete nature of energy levels, excitation by lasers is used which results in a better compound detection or identification.

A typical system for laser induced fluorescence spectroscopy consists of a laser as excitation source. Here, neodymium-doped yttrium aluminum garnet (Nd:YAG) laser are common, due to their high power output and due to frequency multiplication wavelength in the green and ultraviolet (UV) spectral region can be used. For an easier handling, nitrogen laser are also used. These laser systems are running in a pulsed mode, which allows an identification of fluorescence life time.

The radiation of the excitation source undergoes an interaction with the sample. The absorption of the radiation is of importance for fluorescence spectroscopy, but other effects may also occur (e.g. scattering). The sample can then emit energy in form of fluorescence.

Fluorescence emission is typically conducted via optical fibers to the detection system. Here, a spectrometer is commonly used for spectral dispersion of the radiation. Detection is carried out by a charged coupled device (CCD) camera. The recorded spectra are then processed by a personal computer (PC).

Nowadays, CCD cameras are common as detector but photo multiplier tubes (PMT) are used at very weak signal intensity or if spectral information is not needed.

### 2.1.1 Fluorescence

In general, fluorescence is the dissipation of energy by an emission of radiation. For laser induced fluorescence spectroscopy, radiation from a laser beam has to be absorbed leading to electronically excited state in the molecule (or atom). The excitation energy  $E = h\nu$

( $h\nu$  is the photon energy of radiation, where  $h = 6.6 \cdot 10^{-34}$  Js (Planck's constant) and  $\nu$ : frequency) has to be high enough to reach the first electronically excited state ( $S_1$ ) from the ground state ( $S_0$ ), using laser excitation in the UV it is usually sufficient to excite the sample in higher energy levels. Due to non-radiative relaxation via internal conversion (IC) the excited electron passes over to the  $S_1$  energy level. From here, there are several competing pathways for relaxation. The energy can be dissipated as non radiative relaxation (e.g. as heat) or the excited molecule can relax by conversion (intersystem crossing (ISC)) to a triplet state ( $T_1$ ). This may result in a subsequent nonradiative relaxation or in the dissipation of energy by phosphorescence ( $T_1 \rightarrow S_0$ ). A radiationless energy transfer from the excited molecule to a second molecule, may also lead to a decrease in fluorescence intensity.

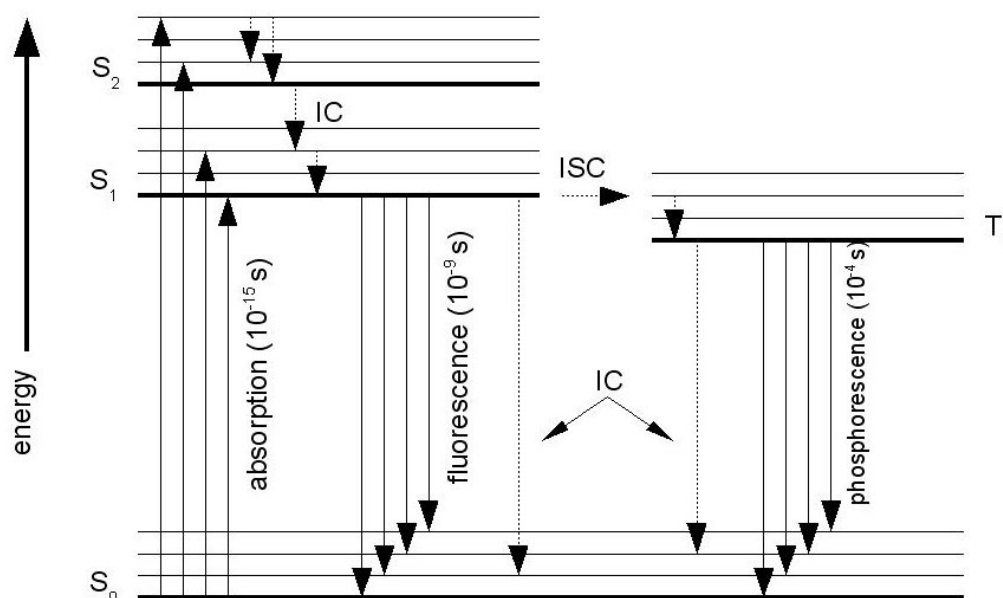


**Figure 2.2:** Jablonski diagram illustrating the various processes of energy transfer. Phosphorescence is taken into account but only for completeness of the competing processes.  $S_0, S_1$  and  $S_2$  are singlet states,  $T_1$  is a triplet state, ISC: intersystem crossing, IC: internal conversion, dotted arrows stand for non-radiative relaxation, and solid arrows for emission of radiation (and for absorption).

Relaxation of a molecule in the first electronically excited state,  $S_1$ , to the ground state,  $S_0$ , can also occur by emission of a photon. This process,  $S_1 \rightarrow S_0$ , by emission of radiation is called fluorescence. In *Figure 2.2* these processes are illustrated by a Jablonski diagram.

Absorption and internal conversion processes are in a time scale of  $10^{-12}$  s to  $10^{-15}$  s, whereas fluorescence emission is typically at  $10^{-9}$  s but can be as long as some microseconds. In comparison, phosphorescence is in the order of  $10^{-4}$  s to 10 s or even longer. The time (half life) a molecule remains in an excited state is referred to as fluorescence life time or fluorescence decay time. As can be derived from the time constants mentioned

above, for measuring this parameter, fast equipment (in the time scale of the parameter in question) is needed.

**Fluorescence Intensity and Quantum Yield** Quantum yield is an important characteristic of a fluorophore. It is derived from the number of emitted (fluorescence) photons relative to the number of absorbed photons. Fluorophores with a very high quantum yield, such as rhodamines, show the highest fluorescence intensity. Typically, radiative decay by emitting fluorescence competes with non-radiative decay mechanisms. For substances, where the non-radiative decay rate is much smaller than the rate of radiative decay, the quantum yield can be close to unity.

A wide variety of processes can decrease the intensity of fluorescence. Such a decrease in intensity is called *quenching*. As described above, quenching can occur when the excited substance collides with another molecule (the *quencher*) in a solution. In the process of collisional quenching the molecules are not chemically altered, but the fluorophore is deactivated. Carotenoids or oxygen are examples of good quenchers. Aside from collisional quenching, fluorescence intensity decrease can occur by other processes, such as the formation of nonfluorescing complexes with the quencher molecules [25].

**Fluorescence Lifetime** Fluorescence lifetime is another important parameter of a fluorophore. It determines the time available to interact with its environment. Fluorescence lifetime,  $\tau$ , is defined as the time a molecule stays in the excited state before deactivation into the ground state. This process typically follows an exponential decay, so few molecules would emit their photons at exactly  $t = \tau$ . For a single exponential decay,

$$I(t) = I_0 \exp\left(-\frac{t}{\tau}\right),$$

63 % of the molecules have been deactivated before  $t = \tau$  and 37 % afterwards.

Generally, fluorescence lifetimes are about 10 ns but can vary from  $10^{-9}$  s to  $10^{-7}$  s and are influenced by the presence of heavy atoms, which typically result in shorter lifetimes and lower fluorescence quantum yields.

### 2.1.2 Fluorescence Detection and Imaging

Fluorescence measurements can be grouped in two types of experiments. One being the measurement of steady-state fluorescence emission the other being time resolved fluorescence emission measurements.

Steady-state fluorescence is an integral measurement since fluorescence decay is in the nanosecond time-scale. For this kind of measurements a continuous excitation is needed and the detection of emission can be carried out. For time resolved measurements instrumentation is required which can produce a excitation pulse of nanosecond or sub-nanosecond duration. Additionally, the detector must have a response in the nanosecond timescale.

Typically, a CCD camera is used for the detection of fluorescence radiation. The emitted radiation is coupled into a spectrometer where the incident radiation is dispersed by a grating. A part of the spectrum is imaged onto the CCD camera and recorded. In a typical CCD camera, a hardware binning is activated accumulating all charges in one column. When spectral information is important it does not matter where in a column a charge is produced, but this mode of operation is much faster than reading out all pixel.

### 2.1.3 Time Resolved Fluorescence Spectroscopy

The decay times of a given sample can be used as an additional parameter for compound identification. For time resolved measurements additional experimental effort has to be met. The CCD camera has to be gateable and this shutter must be very fast (in the order of the timescale in question). Also a delay generator is needed to produce exactly timed signals.

Why using time resolved measurements, when the instrumental expense is much higher than for steady-state fluorescence measurements? Time resolved measurements have the potential to reveal whether quenching is due to diffusion or to complex formation with ground-state fluorophores [25]. Also, macromolecules often exist in more than a single conformation and the decay time of fluorescence may depend on the conformational state. Therefore, time resolved measurements may detect two decay times and thus the presence of more than one conformation. Steady-state fluorescence would, in this example, only reveal an averaged intensity, dependent on the two decay times.

## 2.2 Plasma Breakdown Detection

In this section, laser induced plasma breakdown detection is described. Referring to *Figure 2.1*, irradiation is done by a laser beam which is focused into the sample. In this case the interaction is the generation of a plasma in the focal region and here, acoustic waves as well as radiation can be detected.

In various scientific fields laser induced breakdown of matter has been investigated. Laser induced plasma breakdown detection (LIBD) has the ability to detect fine particulate matter in liquids as shown by Kitamori et al. [26, 27] at about 1990. The method was employed for monitoring particulate impurities in purified liquids, such as ultra pure water used in the manufacturing of semiconductors. The results suggest the ability to discriminate the size of particulate matter and in following works it is shown that particle size dependence on the method could be measured [28].

LIBD has shown the potential for a direct detection of nanosized particulates (colloids) in a liquid environment. A focused laser beam generates a plasma on single particulates and the resulting emission can be detected. This emission is in form of a sound wave or radiation, so either an acoustic or an optical signal can be used for monitoring plasma events. The method is based on the different breakdown threshold values and these are lowest for solid material. Liquids have a higher threshold and gases the highest, so plasma breakdown threshold values are in the order: solid material < liquids  $\ll$  gases.

Exploiting this fact, the laser pulse energy is adjusted such that in the pure liquid no plasma breakdown events occur. In the presence of colloids in the focal volume, however, the breakdown threshold value at the particle is exceeded [29, 30]. By monitoring many laser pulses and evaluating the distribution of plasma events (requires optical detection), the mean particle diameter can be estimated. The particle size together with the breakdown probability (BD), resulting from the number of events per number of laser pulses, allows the computation of the particle concentration.

The method is very sensitive to particles smaller than ca. 50 nm and at low concentrations. Additionally, due to the much higher threshold value for gaseous material, the method is insusceptible to gas bubbles.

### 2.2.1 Laser Induced Plasma

The development of the laser (*Light Amplification by Stimulated Emission of Radiation*) at around 1960 lead to new spectroscopic techniques utilizing this new instrument [31]. In 1964 the first optically induced breakdown in a gas was reported by Maker, Terhune and Savage [32]. Following such observations, experiments were carried out to determine the mechanics leading to a generation of a plasma and measure the involved parameters like threshold power density, wavelength, focal diameter, pressure, pulse length, or involved material. In the 1970s much of laser plasma research showed up in russian literature, and in 1974 the idea of using laser in the analysis of metal and alloys was introduced [33]. The research on plasmas goes hand in hand with the development of laser induced plasma breakdown spectroscopy (LIBS), which utilizes plasma emissions as analysis methods.

LIBS is used for environmental analysis and predestined for investigations on elemental composition. In 2000 there was a demonstration on LIBS on a NASA mars rover [34].

The generation of a practically totally ionized gas (plasma) is generated by two dominant photon absorption mechanisms. First, if free electrons gain kinetic energy from laser radiation (inverse Bremsstrahlung absorption) this leads to an ionization and excitation through collision with excited and ground-state neutrals [35]. There has to be an initial electron present in the focal region of the laser beam and it must gain greater energy than the ionization energy of the material.

The second mechanism is multiphoton ionization (MPI). Here, an ionization is caused by the simultaneous absorption of multiple photons. MPI is important at shorter wavelength ( $\lambda < 1 \mu\text{m}$ ) and for application of laser induced plasma breakdown detection [30, 36, 29]. Here, breakdown is initiated when a colloid is present in the focal region of the laser. It needs at least one atom to be ionized by multiphoton ionization [37] resulting in a multiplication of the electron by inverse bremsstrahlung [38] and generation of a plasma.

Both mechanisms require high laser irradiance, usually in excess of  $10^8 \text{ W/cm}^2$  (breakdown of solids has been observed at irradiances of about  $10^6 \text{ W/cm}^2$ ) [39].

After the pulse duration the plasma cools down and recombination with free electrons occurs. This results in a broad band radiation and is followed by line emission. The emission of atomic lines is element specific and this is employed in laser induced (plasma) breakdown spectroscopy (LIBS, or sometimes also LIPS). An schematic overview is given in *Figure 2.3* after [27, 40].

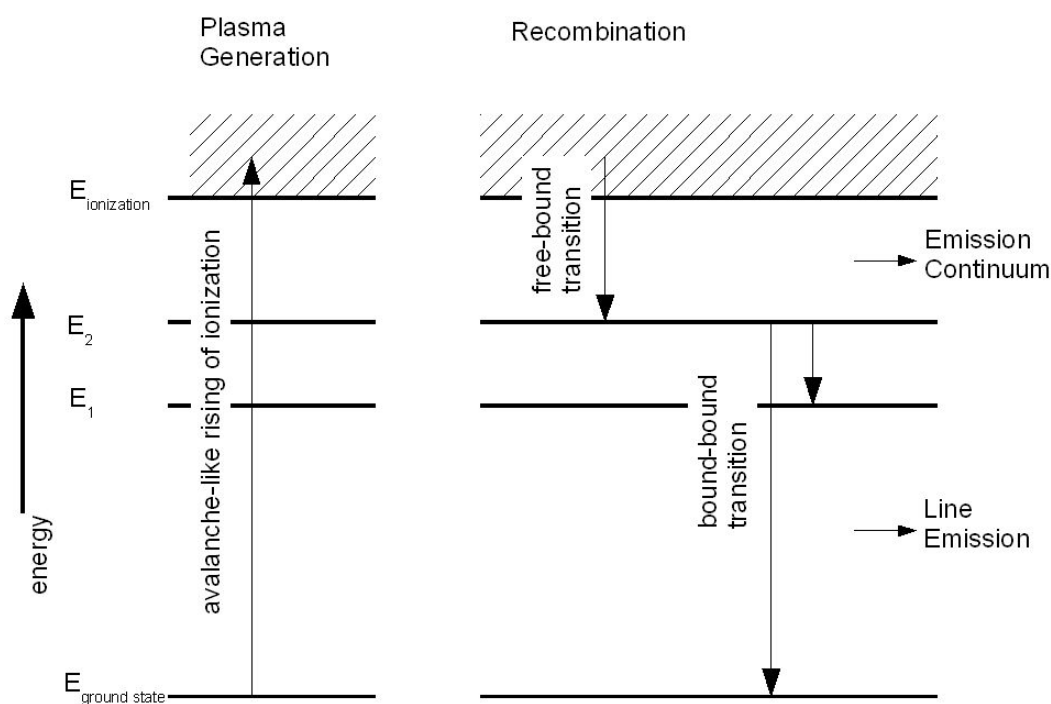


**Figure 2.3:** Schematic overview of plasma generation. During ionization, initial electrons absorb further photons from the laser beam and are accelerated. They knock out further electrons from the atoms and molecules and so an electron avalanche is produced. During generation the plasma heats up and the volume expands resulting in a shock wave. Following the laser pulse the plasma cools down by recombination and emission of radiation (optical signal). Schematic after [27, 40].

### 2.2.2 Determination of Breakdown Probability and Particle Concentration

A laser beam is focused into a liquid sample and the pulse energy is adjusted just below the breakdown threshold of the pure liquid. For particulate solid material in the focal region of the laser pulse, however, the breakdown threshold is then exceeded at the particle and a plasma is generated. The forming of a plasma results in the generation of a shock wave and the emission of radiation, so the breakdown event can be recorded by an acoustic and/or optical detector. These processes are shown in *Figure 2.4*.



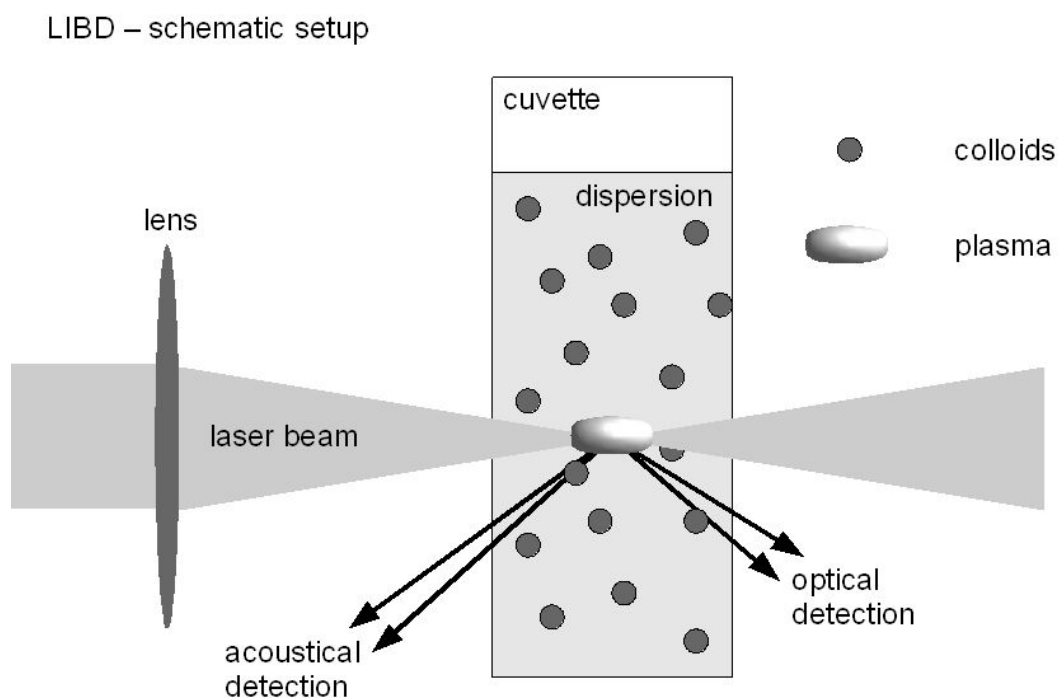


**Figure 2.4:** Schematic of LIBD processes. The incident pulsed laser beam is focused into a sample liquid containing colloids (nanosized solid material). Laser power is adjusted such that no breakdown occurs in the pure liquid, but if a colloid of the dispersion is in the focus of the laser beam a plasma is generated (due to lower threshold values of solid matter). The heating of the plasma leads to a volume expansion which generates an acoustic wave. After the pulse, recombination processes occur and accompanied by the emission of radiation. This can be used for optical monitoring of plasma events. According to [40].

For the calculation of breakdown probability (BP) several hundred of laser pulses are applied. Then, the breakdown probability is the number of breakdown events per number of laser pulses.

For determination of size and concentration of particles an optical detection of plasma events is required. Pictures of breakdown events synchronized with a laser pulse are taken and the location of the single events can be ascertained. Breakdown occurs not only at the focus but in a larger region where the breakdown threshold is exceeded. In the following this will be called "event zone". By stacking and superimposing all recorded pictures, this zone can be mapped. The extent of the event zone is used for the determination of mean diameter of the particulates.

The breakdown probability depends on the size and concentration of the particulates (and of the applied laser pulse energy) in contrast to the breakdown threshold, which only depends on the particle size. Therefore, the optical detection is required for determination of the particle size and together with the breakdown probability particle concentration measurements can be carried out.

**Estimation of Particle Size** The estimation of particle size can be done by means of an optical registration of breakdown events. By monitoring plasma events and superimposing a sufficient number of these pictures, a projection of the event zone in the x,z-plane can be achieved. This approach assumes that the probability of generating a plasma is based on the power density of the laser pulse at the location of the particle and on the number of weakly bound electrons in the particle. So, with increasing size of the particle an increasing number of these electrons are available. This results in a lower breakdown threshold for larger particles.

Therefore, by recording a sufficient number of plasmas, the extent of the event zone can be observed. The projection of this event zone is of an elliptic shape because the power density along the laser beam is higher than in the perpendicular direction. By monitoring the extent of the event zone along the laser beam (longest axis) size determinations can be carried out.

To evaluate breakdown probabilities and to analyze the distribution of breakdown events, the following equations are based on simplifications, e.g. a pure gaussian laser beam (TEM<sub>00</sub> mode) is assumed. Equations taken from Bundschuh et al. [40].

The minimum power density,  $I_{th}(P)$  for the particle dependent generation of a breakdown event is given by

$$I_{th}(P) = 4 \cdot E_0 \left[ \pi^2 \cdot \tau \cdot \omega_F^2 \left( 1 + 2 \left( \frac{z_{th}(P) \cdot \lambda}{\pi \cdot n \cdot \omega_F^2} \right)^2 \right) \right]^{-1} \quad (2.1)$$

- where  $E_0$  : laser pulse energy  
 $\lambda$  : laser wavelength  
 $\tau$  :  $1/e^2$  time of the laser pulse  
 $\omega_F$  :  $1/e^2$  radius of the power density located at the focal waist  
 $r, z$  : cylinder coordinates ((0,0) in the center of the focus)  
 $n$  : refractive index of the medium

Critical length,  $z_{th}(P)$ , and critical radius,  $r_{th}(P)$ , can be derived:

$$z_{th}(P) = \frac{\pi \cdot n \cdot \omega_F^2}{\lambda} \cdot \sqrt{\frac{2 \cdot E_0}{I_{th}(P) \cdot \pi^2 \cdot \tau \cdot \omega_F^2} - \frac{1}{2}} \quad (2.2)$$

and

$$r_{th}(P) = \frac{1}{\sqrt[4]{2}} \omega_F \sqrt[4]{\ln \frac{4E_0}{I_{th}(P) \pi^2 \tau \omega_F^2}} \quad (2.3)$$

It could be shown that the particle concentration has no influence on the extent of the event zone [10]. So, the assumption that the plasma breakdown threshold depends only on the size of particulate material (and the laser power density) can be used to some degree. Note, however, that the given equations are based on some simplifications, especially, they are valid for a pure Gaussian laser beam (for more details on the equations and mathematical background refer to [40]).

**Estimation of Particle Concentration** The breakdown probability depends on both, particle size and concentration. Therefore, optical measurement of breakdown events can be used for the calculation of breakdown probability and mean particle diameter as described above. Using the obtained information, particle concentrations can be determined. Higher concentration leads to a higher breakdown probability due to the fact that more particles per volume element exist. For calculation of unknown concentrations, a statistical analysis has to be carried out. Also, reference colloid suspensions could be produced for a comparison of samples diluted to different degrees.

To summarize the facts above, the breakdown probability can be measured by acoustic or optical detection. The optical detection has the advantage to monitor the spatial distribution of the measured events which is required for the determination of the mean particle diameter. The breakdown threshold is assumed to depend on size only, whereas the breakdown probability depends on the size and concentration of the particles. With the measured breakdown probability and the calculated size the particle concentration can be estimated.

Attempts have been made to use the method in conjunction with a laser induced breakdown spectroscopy (LIBS) systems. Both methods are based on the same principle but for LIBS the emission from the produced plasma has to be spectrally dispersed in a spectrograph and recorded by an intensified CCD camera. This has the additional advantage of element analysis and identification and some attempts have been made to join these two methods [41].

## 2.3 Biological and Chemical Foundations

### 2.3.1 Colloids in an Aqueous Environment

The scientific branch of colloidal chemistry is contributed to *Thomas Graham*, a Scottish chemist, who studied colloids in 1861. In 1857, *Faraday* investigated changes in color in a gold suspension and attributed these changes to scattering effects. This was confirmed

by Tyndall in 1869. Light is scattered in a colloidal system, in a solution this effect is not observed.

Commonly, dispersion is used as synonym for colloidal systems. Dispersions of solid material in liquids are called suspensions (e.g. blood, pigmented ink), dispersions of two not mixable liquids are called emulsions (e.g. milk, mayonnaise).

Colloids do not have a homogeneous composition, nor do they form a class of substances. The size of the dispersed colloidal particles ranges between one nanometer and one micrometer. Colloids can be categorized by their size or beside this as anorganic colloids, organic colloids or biocolloids.

Common methods for the quantification of colloids are *Photon Correlation Spectroscopy (PCS)*, *Electron Microscopy (REM/SEM)* or *Atomic Force Microscopy (AFM)*. Recently, *Laser Induced Breakdown Detection (LIBD)* has been introduced. PCS has the disadvantage of needing either relatively large particles ( $> 50$  nm) or high concentrations. Single-particle counters are based on light scattering by single particles, so colloids have to cross a light beam one after another where the generated flash of radiation is monitored [42, 21]. REM or SEM have the ability of element analysis in addition to size measurements, but due to fixation and sample preparation, the original suspension is destroyed. AFM has a resolution of atomic scale, but also requires relatively high concentrations. LIBD has the advantage of the detection of very small particulates at low concentrations.

In natural systems, particle size ranges from one nanometer to some micrometer [17]. Typical concentrations are  $10^2$  to  $10^{12}$  particles per cubic centimeter [43]. LIBD offers the possibility to quantificate colloids even at the low concentrations normally found in ground water [44, 45].

### 2.3.2 Pesticides

*"A pesticide is any substance or mixture of substances intended for preventing, destroying, repelling, or mitigating any pest. Pests can be insects, mice and other animals, unwanted plants (weeds), fungi, or microorganisms like bacteria and viruses. Though often misunderstood to refer only to insecticides, the term pesticide also applies to herbicides, fungicides, and various other substances used to control pests. Under United States law, a pesticide is also any substance or mixture of substances intended for use as a plant regulator, defoliant, or desiccant."* defined by the United States Environmental Protection Agency (EPA) [46, 47].

They are often referred to by the type of pest they are designed for as herbicides, insecticides, fungicides, and many other kinds. These pesticides are related because of the type of pest they address. Herbicides are used to kill plants that grow where they are not

wanted, insecticides to control insects and fungicides to control fungi. Pesticides also include substances like plant growth regulators, which alter the expected growth of plants (normally, fertilizers and other nutrients are excluded).

As the human population grew and agriculture spread mankind was looking for ways to protect their crops. Chemical compounds such as sulfur were used to kill or repel insects in the years BC. In the 1400s toxic substances like arsenic, lead, and mercury were used as pesticides. In the 1920s farmers started looking for less toxic substances when an increasing number of human poisoning and fatalities began to show and abandoned the toxic metal compounds. In the 1600s nicotine was used as insecticide and in the mid-1800s two more natural pesticides were applied. All these substances are mainly natural compounds and are referred to as *first generation pesticides*. These are historically used pesticides and include inorganic compounds like arsenic, lead or mercury and chemicals from plants like nicotine, pyrethrum or rotenone.

In 1939 *Paul Mueller* discovered the insecticidal properties of dichloro-diphenyl-trichloroethane (DDT), a chemical known since 1874. He was awarded *The Nobel Prize in Physiology or Medicine* in 1948 "for his discovery of the high efficiency of DDT as a contact poison against several arthropods" (medical application to fight typhus by killing lice during World War II). DDT is a synthetic chemical belonging to the group of organochlorines and was the first so-called *second generation pesticide*. As pesticide it was toxic to a wide range of insects and seemed to have a low toxicity to mammals. It is persistent and insoluble in water, meaning that it does not have to be applied often and it did not be washed off by rain. DDT was also inexpensive and easy to apply. All these advantages resulted in an increased crop yield and a quick spreading over the globe.

DDT was also used in non-agriculture applications. One example is the above given application to delouse soldiers in World War II and another example the spraying to control mosquitoes in residential areas in the United States until the 1960s.

In 1962 *Rachel Carson* (a scientist) published her best selling book "*Silent Spring*", which, in retrospect, could be seen as a first step in an environmental movement. She reported the dying of insect and worm eating birds in areas where pesticides

have been sprayed aerially, hence the title "*Silent Spring*". Following studies and research demonstrated that the low concentrations of pesticides in a body of water accumulates in

location	concentration
DDT in lake water	0.02 mg/kg
→ uptake by plankton	5.0 mg/kg
→ non-predatory fish	40 – 100 mg/kg in fatty tissue
(→ predatory fish	80 – 2500 mg/kg in fatty tissue)
→ fish eating birds	1600 mg/kg in fatty tissue

**Table 2.1:** Example of biomagnification. Increase of pesticide (DDT) concentration in lake water in the food chain [48].

organisms tissue (Bioconcentration; DDT for example accumulates in fat tissue) and concentrations increase in the food chain (Biomagnification; e.g. in *Table 2.1* for a pesticide (DDT) in lake water (taken from [48])). The high concentrations are not directly lethal to predatory birds (way up in the food chain) for example but impair their reproduction. DDE (a metabolite of DDT) is responsible for thinning of eggshells, thus they crack easier during incubation leading to the near extinction of bald eagles and brown pelicans. Metabolites of DDT also appeared in fatty tissue of Eskimos (far from any application) indicating that, due to its persistence, it has been transported long distances.

In 2001 *Stockholm Convention on Persistent Organic Pollutants* (POP) under the *United Nations Environmental Programme* (UNEP) was signed, which bans the use of POP chemicals, including DDT. The use of DDT was banned in many countries since the early 1970s but it was (and may be) the principal insecticide used in malaria control. Therefore the convention give conditions for governments to be exempted from the ban but established the goal of a complete elimination of DDT production and use, once alternatives have become available [49].

Today, new pesticides have to undergo extensive testing and strong regulations are in place to protect the environment and population. In most countries the production, selling or usage of a pesticide must be approved by an government agency (this leads to higher research and development costs for new pesticides so new chemicals are developed only for crops with large markets such as wheat, corn, or soybeans). In the U.S. the Environmental Protection Agency (EPA) is responsible for regulating the production and use of pesticides under the Federal Insecticide, Fungicide, and Rodenticide Act (FIFRA). Despite this regimentations, the usage of pesticides increases worldwide, so the usage of these substances should be supervised very closely.

Herbicides form a large group of pesticides which are used to kill plants. Selective herbicides prevent specific plants from growing in areas where they are not wanted while leaving the desired plant (relatively) unharmed. Nonselective or total herbicides are used to kill all plant material in the desired area (e.g. on railroad tracks). Herbicides can be classified by their mode of action, chemical family or by the type of plant they are designed for. Classification by their mode of action is done by HRAC (Herbicide Resistance Action Committee). Some widely known herbicides include *Atrazine* (a Photosystem II (PSII) inhibitor) or *Diuron* (also PSII inhibitor) which are not for sale any longer (in Germany) but where the components can be found in many environmental compartments, especially in the groundwater or wells.

Insecticides are used to kill insects and protect the crop. Often, the term pesticide is used as synonym for insecticide, but the modern understanding includes all the other substances mentioned above. DDT, which was mentioned in the short historical overview, and Lindan belong to the group of organochlorine insecticides. They do not kill insects directly but aim at specific interaction in the target organism. DDT for example opens sodium channels

in the nerve cells. Another large group are the organophosphates. These compounds are acetylcholinesterase inhibitors, killing the insects by disrupting nervous impulses. Similar agents were used in chemical warfare (such as sarin or VX) and work in the same way. As another class of pesticides, pyrethroid pesticides have been developed. These insecticides are similar to the natural compound pyrethrum. Their toxicity is much lower than that of the organophosphates and they are not very persistent.

Pesticide can be found in nearly every environmental compartment such as river and lakes of in food. These residues, even at low concentration have an impact on plant and animal life. This also reflects on the health of humans due to the intake via the foodchain. Modern pesticides and new pesticide development aims at the design of agents which are less persistent in the environment. An ideal pesticide would kill only the target pest, harm no other species, will disappear or break down into something harmless after use, do not cause genetic resistance in the target organism and is inexpensive. Unfortunately, even the modern pesticides do not meet all of these criteria and a lot of pesticides do not even come close [1].





# Chapter 3

## Material and Methods

This Chapter gives an overview about the used material. This includes chemicals as well as mechanical components and experimental setups. The first two sections introduce the used laser systems for laser induced fluorescence measurements and laser induced breakdown detection. Schematic setups are shown for each system and technical data is given. In the following section the method of laser induced fluorescence is detailed and two easy to handle techniques are introduced. In the final section of this chapter the materials and chemicals used are described, these include fluorescing particles, colloidal substances and pesticides. Additionally, extracts from the material safety data sheets of the pesticides can be found in *Appendix A*.

### 3.1 Laser Induced Fluorescence

#### 3.1.1 Nitrogen Laser System for Fast Optical Assessment

The nitrogen laser system (for a schematic setup refer to *Figure 3.1*) consists of a nitrogen laser (MSG 801 SD, LTB, Berlin, Germany) which is also equipped with a dye laser unit (UDL 200, module for the nitrogen laser). The dye laser is pumped by the nitrogen laser and consists of a cuvette (containing the dye as active material) and a mirror and grating as resonator. The nitrogen laser operates at a wavelength of  $\lambda = 337 \text{ nm}$ , the dye laser can be tuned to nearly every wavelength in the VIS (VIS = visible spectral region) and near UV (UV = ultraviolet). Depending on the dye, the laser radiation can be tuned in a spectral range of about 30 nm per dye. Radiation from either laser can be coupled into optical fibers and directed to the sample. For excitation, a Y-shaped fiber was used and fluorescence was recorded with another fiber (diameter: 600  $\mu\text{m}$ ).

For scanning experiments, the excitation fiber was extended by a lens system, which focused the beam onto the sample. The sample was located on a sample-holder which had an xy-table underneath operated by micrometer screws. With the help of this sample-holder the sample could be moved and thus scanning could be achieved with a spatial resolution of about  $10\ \mu\text{m}$ . The micrometer screws had to be operated manually. The focused laser beam had a diameter of about  $50\ \mu\text{m}$  to  $100\ \mu\text{m}$ .

The detection of the fluorescence radiation is conducted via an optical fiber to a spectrometer (MS 125, L.O.T.-Oriol GmbH, Darmstadt, Germany) and is recorded with a CCD-camera (InstaSpec IV, L.O.T.-Oriol GmbH, Darmstadt, Germany). The CCD-camera was set to  $-20\ ^\circ\text{C}$  by piezo-electrical cooling to improve signal-to-noise ratio. The CCD-chip consists of  $1024\ \text{pixel} \times 128\ \text{pixel}$ , where the pixel in one column are combined by hardware binning. The spectrometer has a fixed grating with  $150\ \text{lines/mm}$  which can map a spectral region of about  $500\ \text{nm}$  onto the CCD-chip. This leads to a resolution of about  $0.5\ \text{nm/pixel}$ .

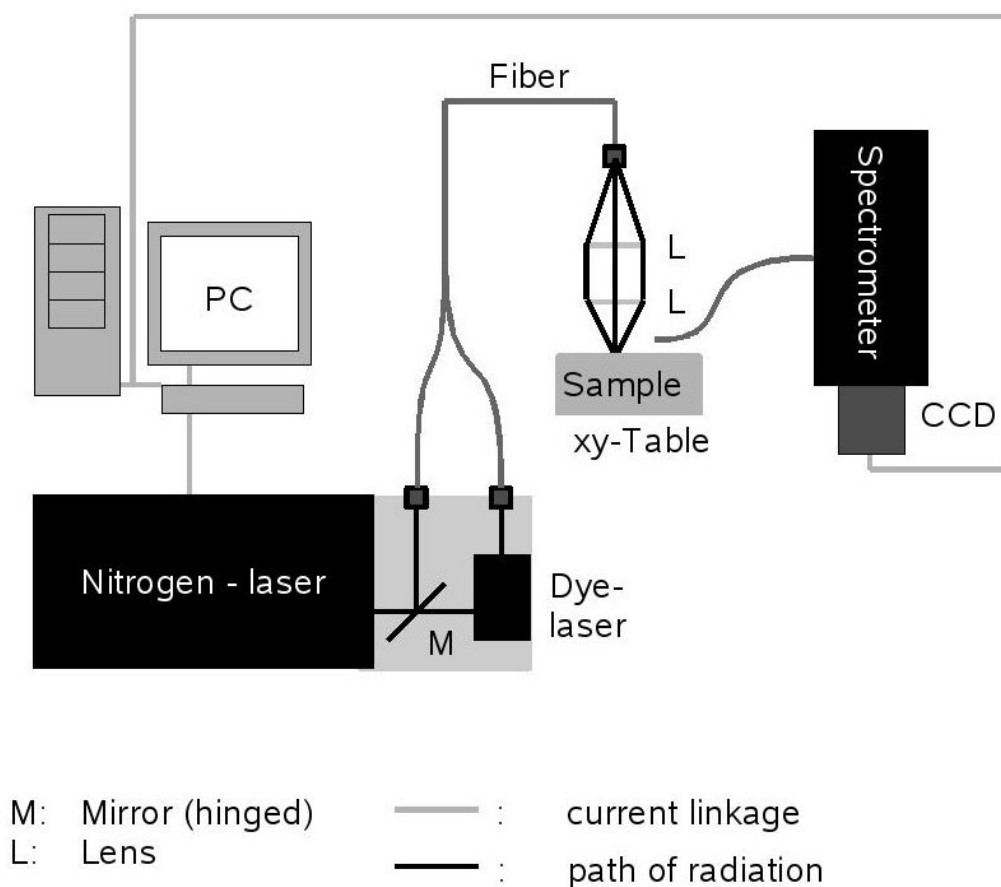


**Figure 3.1:** Schematic setup of the nitrogen laser system. The mirror, M, can be switched for using either the dye laser unit or for direct irradiation with the nitrogen laser.

The nitrogen laser was primarily used in the experiments for an optical detection of pesticide coverage on plant surfaces. It has the additional advantage of being movable (not bound to a laboratory) which will be important in view of a field application. For measurements of feasibility this is not actually needed, but it may become necessary for further applications. The dye laser unit was only used for auxiliary measurements, since the used fluorescence tracer material shows strong fluorescence when excited with the nitrogen laser. The advantage is the selective excitation of specific tracer material. Wavelength can be adjusted by manually rotating a micrometer screw. Some test measurements were carried out, but, as mentioned above, fluorescence tracer material was used which showed a strong fluorescence when excited with the nitrogen laser. Also, the pulse energy of the dye laser was about a tenth of the pulse energy of the nitrogen laser.

Nitrogen Laser System	
company	MSG 801 SD, Lasertechnik Berlin, Berlin, Germany
wavelength	337.1 nm
bandwidth	0.1 nm
pulse energy	ca. 400 $\mu$ J
pulse duration	500 ps
dye laser unit	UDL 200 (module for the nitrogen laser)
bandwidth	1 nm
pulse energy	ca. 40 $\mu$ J

**Table 3.1:** Technical data of the nitrogen laser system used for the measurements described in *Chapter 4*.

In *Table 3.1* technical data for the nitrogen laser system and the dye laser unit is compiled. The dye laser unit is a module for the system and, therefore, is also manufactured by *Lasertechnik Berlin*. For technical data of the detection unit, refer to *Table 3.2*.

Detection Unit		
type	MS 125	InstaSpec IV
	L.O.T.-Oriel GmbH	L.O.T.-Oriel GmbH
	Darmstadt, Germany	Darmstadt, Germany
array size	1024 pixel × 128 pixel	
focal length	125 mm	
entry slit	variable per insert	
grating	150 lines/mm	
visible spectral region	ca. 500 nm	
resolution	0.5 nm	

**Table 3.2:** Technical data of the detection unit of the nitrogen-laser system.

### 3.1.2 Nd:YAG Laser System for Time Resolved Measurements

The Nd:YAG laser system (schematic setup refer to *Figure 3.2*) consists of a Q-switched (Q-switch = quality-switch) Nd:YAG laser (Nd:YAG = neodymium-doped yttrium aluminium garnet,  $\text{Nd:Y}_3\text{Al}_5\text{O}_{12}$ ; Compact Laser 501 DNS 910, BMI, France), which is a solid state laser with a crystal as active material. In pulsed operation, Q-switching leads to a maximum of population inversion when releasing the pulse into the cavity and generates a pulse of a pulse energy of about 900 mJ with a pulse duration of about 6 ns. The Nd:YAG system emits laser radiation at a wavelength of  $\lambda = 1064 \text{ nm}$  which is in the IR (IR = infrared) spectral region. Internally, the system is frequency-doubled and -tripled using two KDP crystals (KDP = potassium dihydrogen phosphate,  $\text{KH}_2\text{PO}_4$ ) which are temperature controlled to  $35 \text{ }^\circ\text{C}$  in order to stabilize phase-matching by counteracting heating due to operation. For technical data of the KDP crystals refer to *Table 3.3*.

Non-linear Crystals		
crystal	KDP (potassium dihydrogen phosphate)	BBO ( $\beta$ -barium borate)
formula	$\text{KH}_2\text{PO}_4$	$\beta\text{-BaB}_2\text{O}_4$
usable wavelength	260 nm – 650 nm	220 nm – 295 nm
damage threshold	$0.5 \text{ GW/cm}^2$	$5 \text{ GW/cm}^2$
efficiency	ca. 7 %	ca. 8 %

**Table 3.3:** Technical data of the frequency doubling and -tripling crystals used in the Nd:YAG laser system.

The chassis also houses a dye laser unit, with is pumped by the frequency tripled Nd:YAG laser at a wavelength of  $\lambda = 355$  nm. The dye laser was not used in the experiments but the frequency mixing KDP crystal was still in the path of the laser beam, as well as a mirror (80 % reflection at  $\lambda = 355$  nm and anti-reflectant at  $\lambda = 1064$  nm and  $\lambda = 532$  nm) which directs the beam into the dye laser unit. Outside the housing radiation of  $\lambda = 1064$  nm,  $\lambda = 512$  nm and  $\lambda = 355$  nm is available due to this construction. In *Table 3.4* technical data of the Nd:YAG laser is composed.

Nd:YAG Laser System	
Company	Compact Laser 501 DNS 910, BMI, France
Type	Quality-switched Nd:YAG laser
Wavelength	1064 nm
SHG, THG	internal KDP crystals
Pulse energy	900 mJ at 1064 nm 400 mJ at 532 nm 200 mJ at 355 nm
Pulse duration	ca. 6 ns
Bandwidth	ca. 1 cm <sup>-1</sup>
Repetition rate	10 Hz

**Table 3.4:** Technical data of the Nd:YAG laser system used for the measurements described in *Chapter 4*.

After leaving the housing a separation unit is placed in the path of radiation, separating the base wavelength of  $\lambda = 1064$  nm and the second harmonic using a HR mirror (HR = highly reflective) optimized for reflection of  $\lambda = 532$  nm (at forty five degrees to the beam). This also takes care of most of the radiation at a wavelength of  $\lambda = 355$  nm. After the separator the beam passes another HR mirror (also optimized at  $\lambda = 532$  nm) and a telescope consisting of two lenses. The telescope reduces the beam diameter of about 9 mm to approximately 2 mm. After that, the beam passes a frequency doubling BBO crystal (BBO =  $\beta$ -barium borate,  $\beta$ -BaB<sub>2</sub>O<sub>4</sub>) resulting in an UV radiation of  $\lambda = 266$  nm which was used for excitation. This is directed by a HR mirror (optimized to reflect radiation of a wavelength of  $\lambda = 266$  nm) onto the sample, which is positioned on an xy-table.

Fluorescence is collected by an optical fiber (UV-transparent, diameter = 600  $\mu$ m) and coupled into a spectrometer (Chromex 500, Chromex, Albuquerque, USA). The spectrometer has a turret containing three gratings (150 lines/mm, 600 lines/mm and 1800 lines/mm) which can be selected by a controlling computer. For most experiments the grating with 150 lines/mm was used, which maps a spectral region of about 165 nm onto the CCD chip. The controlling computer can also move the position in a way, that the desired wavelength region is mapped onto the CCD camera.

Detection Unit		
type	Chromex 500 Chromex Albuquerque, USA	ICCD-576 G/RB Spectroscopy Instruments Erwitte, Germany
array size		576 pixel × 384 pixel
pixel size		23 μm × 23 μm
temp. resolution		<5 ns
focal length	500 mm	
entry slit	10 μm – 2000 μm	
gratings	grating 1: 1800 lines/mm, grating 2: 600 lines/mm, grating 3: 150 lines/mm	
visible spectral region	grating 1: 15 nm, grating 2: 40 nm, grating 3: 160 nm	
resolution	grating 1: <0.1 nm, grating 2: 0.25 nm, grating 3: 1.0 nm	

**Table 3.5:** Technical data of the detection unit of the Nd:YAG system.

As detection unit an ICCD camera (ICCD = intensified charged-coupled device; ICCD-576 G/RB, SI, Erwitte, Germany) was used. The camera has a micro-channel plate (MCP) working as intensifier, which is also used as electronic shutter (by reversing the polarity of acceleration voltage). With this kind of shutter, exposure times of up to 5 ns can be achieved. Temperature was set to -45 °C by piezo-electrical cooling. Therefore, a water circulation is needed to transport excess heat and rinsing with nitrogen is also necessary in order prevent condensation. The CCD detector was in the 576 pixel × 384 pixel format. Technical data of the detection system is collected in *Table 3.5*. Due to the requirements of water and nitrogen supply and the power unit for the laser, this setup is laboratory based and not mobile.

For time resolved fluorescence measurements an exact timing of the components in the setup (releasing the Q-switch and opening the shutter of the CCD camera) is required. For this requirement the system employs a delay generator (DG535, Stanford Research Systems, USA), which is also used for a gradual shifting of the 5 ns exposure window and thus recording a wave-time matrix (WTM). This can be used to calculate the fluorescence life time (exponential decay of the excited state by emitting radiation in the form of fluorescence).

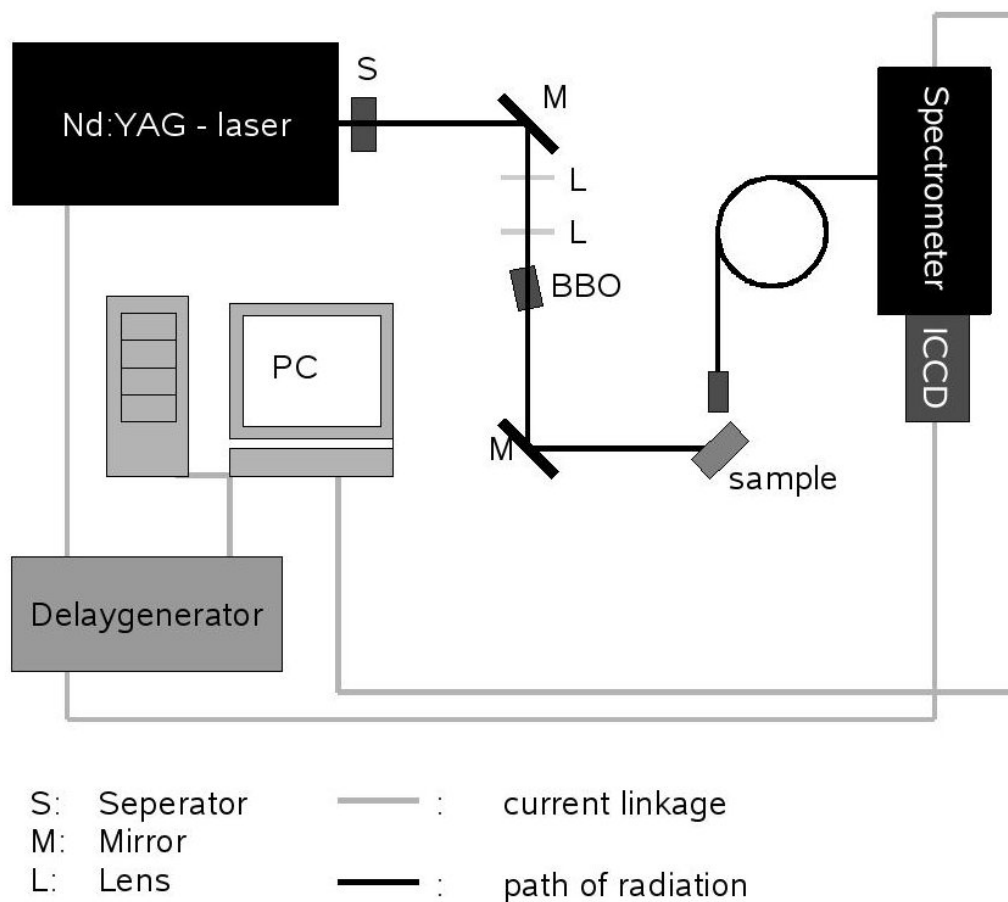


**Figure 3.2:** Setup of the Nd:YAG-laser system used for time resolved measurements. The emission of the Nd:YAG laser is internally frequency doubled, after passing a separator, the radiation of  $\lambda = 532$  nm is frequency doubled again (by a BBO crystal), resulting in radiation used in these experiments of  $\lambda = 266$  nm.

The entire system is controlled by a computer running the enclosed software *Winspec 1.6.3* which has a build-in programming language used to address the various components of the setup and for programming routines to achieve some automation of the measuring process (e.g. for time resolved measurements). The software is also used for recording the resulting spectra.

## 3.2 Laser Induced Breakdown Detection

### 3.2.1 Nd:YAG-Laser System for Plasma Breakdown Induction

The Nd:YAG laser system (schematic setup refer to *Figure 3.3*) used for laser induced plasma breakdown detection consists of a Nd:YAG laser (Spectra-Physics Laser Division (Newport Corporation), Mountain View, USA) which also has internal modules for SHG (SHG = second harmonic generation) and THG (THG = third harmonic generation). The investigations had to share the laser radiation with two other experiments and employed the frequency doubled radiation of a wavelength of  $\lambda = 532$  nm (because of the THG unit, the beam could also consist of fractions of the radiation of  $\lambda = 355$  nm and of the laser radiation of  $\lambda = 1024$  nm). Passing two HR mirrors the beam is directed through an iris and then focused by a lens.

The iris was used for adjusting the laser pulse energy, since the build in potentiometer of the laser power supply could not be set exact and in fine enough steps. Additionally, it was very sensitive to slight rotations, so another means of controlling laser power had to be used. One disadvantage of using the iris is the simultaneous alteration of the beam diameter (and also the beam profile by cutting of the edges). Typical values in the experiments described in *Chapter 4* employ a diameter of about 3 mm at maximum, whereas the laser beam diameter upon leaving the housing is about 9 mm.

The samples were prepared in a quartz glass cuvette which was placed with the focus of the laser beam inside and preferably near the entry side (in order to keep loss from scattering as low as possible) of the cell. The cuvette was also slightly rotated in order to keep possible back reflection between the glass-sides from interfering with the experiment. For a schematic setup of the laser plasma breakdown detection setup refer to *Figure 3.3*.



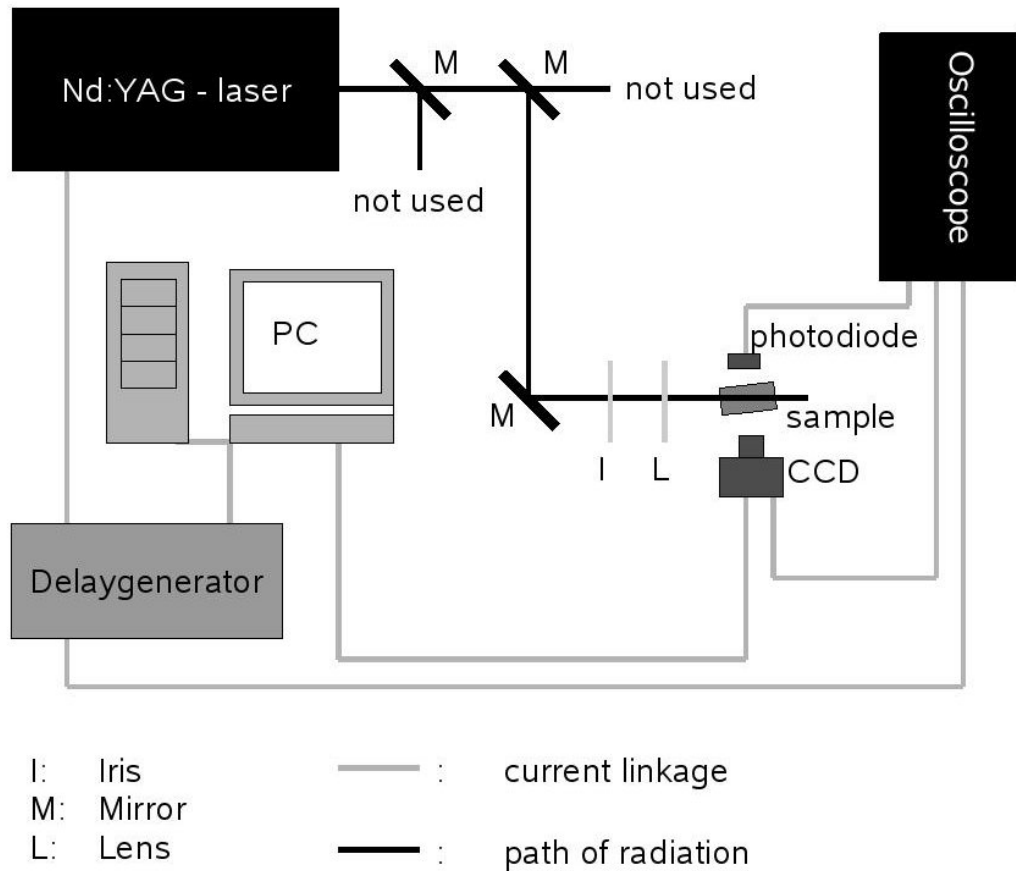


**Figure 3.3:** Setup of the Nd:YAG laser system used for laser induced breakdown detection of colloids or fine particulate material in liquids. The parts of the laser beams marked as "not used" were part of other experimental setups.

A color CCD-camera was placed perpendicular to the laser beam to monitor plasma events. Resolution was set to  $800 \text{ pixel} \times 600 \text{ pixel}$  and a green bandpass filter was inserted to cut off scattered radiation from the laser beam. A photo diode was also put in a perpendicular position to the incident beam. It was connected to an oscilloscope and CCD-camera in order to synchronize recording of events and laser pulse. Recording was done by taking pictures of plasma events repeatedly (at the repetition rate of the laser, typically at 1.6 Hz or 3.3 Hz). Pictures were stored on a personal computer in a compressed jpg-format and this data was evaluated by a self written *MatLab*-program.

### 3.3 Fluorescence Measurements

For a fast optical assessment of pesticide coverage on leaves, fluorescence imaging methods were employed. First, a droplet of water was applied to the surface of a leaf and investigated under a fluorescence microscope. This yields information about the dissolution of a *Rhodamine 6G* crystallite, by adding such a particulate to the water droplet and monitoring fluorescence over time. As a simple and low-cost system, a leaf was covered with a layer of *Rhodamine 6G* and droplets of pesticide were applied to the surface. The prepared leaf was irradiated with an UV lamp and pictures were taken with a CCD-camera.

#### 3.3.1 Direct CCD Imaging under UV Irradiation

Clean Bench	CCD Camera
self made	Canon
	PowerShot A60
UV-C	2.0 Megapixel
	3.0 optical zoom
	2.5 digital zoom

**Table 3.6:** Technical data of the clean-bench (UV-lamp) and CCD camera used for the measurements described in Chapter 4.

The idea of a very simple and cost effective imaging setup leads to the usage of a commercially available CCD camera (Canon A60, 2 Megapixel) as detection unit. For excitation, radiation in the UV was required. For this purpose a clean bench was used. The clean bench has a UV-C lamp for sterile working and this lamp was used as excitation source. Leaves were coated with a *Rhodamine 6G* layer and droplets of pesticides were put on different places on the leaf surface. One half of the leaf was left without *Rhodamine 6G* coating to be used as reference and droplets were applied

symmetrically to both sides.

This leaf was then placed under the UV lamp of the clean bench and emission in the visible was acquired using an RGB camera. The method is fine for mapping of pesticides, it yields location and extent of coverage, but no spectral information is acquired. Without spectral data, a compound identification cannot be carried out.

Technical data for the instrumentation can be derived from Table 3.6. For more detailed information and measurements utilizing this simple setup refer to Section 4.1.5.2.

#### 3.3.2 Fluorescence Microscope

A fluorescence microscope (Zeiss Universal, Carl Zeiss AG, Germany) was used for imaging of a droplet of distilled water on a leaf surface. Excitation was carried out by a xenon lamp (XBO 75W/2, Osram GmbH, Munich, Germany) and by inserting a band-pass filter excitation has its maximum at about  $\lambda_{excitation} = 400$  nm. An area on the leaf

surface of about  $2 \text{ mm} \times 3 \text{ mm}$  was investigated for fluorescence imaging using an objective with a  $8 \times$  magnification. In the detection pathway another filter was employed, which separates excitation from fluorescence emission. Detection was carried out by a color CCD-camera (Satisec Sat-11 SP) and pictures were processed in a computer.

Fluorescence Microscope	CCD Camera
Carl Zeiss AG	Satisec
Zeiss Universal	Sat-11 SP
$8 \times$	

**Table 3.7:** Technical data of the fluorescence microscope and CCD camera used for the measurements described in *Chapter 4*.

For the measurements, *Rhodamine 6G* crystals were applied to the droplet of distilled water and a time series of pictures was stored monitoring the dissolution of the solid particulates by their fluorescence emission (refer to *Section 4.1.3*).

Technical data for the fluorescence microscope and CCD camera are summed up in *Table 3.7*. The microscope was in part self assembled, therefore, device type and brand given in *Table 3.7* only refers to the chassis and some of the components.

## 3.4 Material and Chemicals

In this part an overview about the chemicals and other material used in the experiments is given. Among these are different solvents and the chemicals also include several dyes and other fluorescing particles used as tracer material. Information about the sample pesticides is presented in this part.

### 3.4.1 Solvents

In the measurements different solvents were used, the most common are presented in this part. Distilled water is the most widely used solvent being used for some of the dyes and for the pesticides. In short, also ethanol, methanol and acetone are introduced.

**Distilled Water:** Distilled water or to be more precise bi-distilled water (two times distilled water, for convenience the term "*distilled water*" will be used) is the most common solvent. In this thesis it was used as solvent for the pesticides. In field application tap water would be used, but in order to avoid additional unknown parameters and to eliminate possible fluorescence signatures stemming from substances in tap water (e.g. from humic substances) distilled water was used. There are no special fluorescence or absorption properties in the investigated wavelength region (from  $\lambda = 250 \text{ nm} - 800 \text{ nm}$ ). Distilled water was also used for cleaning and flushing of glass vessels and various containers.

**Acetone:** Acetone was used as solvent for the fluorescing tracer material. Especially for the application of *Rhodamine 6G* as aerosols on leaves the fast evaporation of this substance was utilized. It does not show fluorescence in the investigated spectral region but absorption and scattering occur in the UV up to about  $\lambda = 340$  nm.

**Methanol:** Methanol is very similar to ethanol in respect to their optical properties. The photometer measurements show a nearly identical spectrum, where no absorption bands can be observed in the near UV- or visible spectral region. Methanol is the major solvent for the laser dyes like *Rhodamine 6G*. For use of the dyes as active medium in a dye laser most are solved in methanol.

**Ethanol:** Ethanol and methanol are very similar as mentioned in the methanol entry. The absorption of both substances is nearly identical, there are only minimal displacements in wavelength. Ethanol, however, is in pure and in denatured form obtainable, were the denatured form shows an additional maximum at about  $\lambda = 273$  nm in the photometer measurements. In the pure ethanol this peak is missing, therefore it is likely to originate from the substance in the denatured alcohol.

The absorption measurements of the solvents were carried out using a two beam photometer (Uvikon Spectrophotometer 922, Kontron Instruments, Herts, UK). As reference, the spectrum of an empty quartz glass cuvette is also measured. In the VIS region all solvents are transparent and show transmission of nearly on hundred percent.

### 3.4.2 Fluorescing Particulates

In the experiments described in *Chapter 4* changes in fluorescence properties of a tracer material added to a pesticide solution were investigated in order to give an assessment of pesticide coverage on leaves. As fluorescing tracer material several dyes were tested as well fluorescing nanoparticles and some biological marker substances. The dyes were all manufactured for used as active material in dye laser systems, so they are designed for high efficiency and fluorescence yield. For the purpose of using them as laser dyes, they are usually solved in methanol (for most dyes used in dye lasers working in the visible region). Nanoparticles were also tested as fluorescence marker, but have the distinct disadvantage of being very cost intensive. They often need special solvents like toluene and disintegrate when exposed to oxygen. For the purpose of a fast optical detection of pesticide coverage, the dyes were preferred over the nanoparticles because of the mentioned disadvantages.

### Dyes for Allocating Pesticides

In this section, chemical and physical properties of the used dyes are summarized. All used dyes are manufactured for the use as laser dyes, therefore they were first solved in methanol according to the manufacturers instructions for the use in a nitrogen pumped dye laser. The dyes to be used in the experiments should show high fluorescence intensity which agrees best with rhodamines. They should also be soluble in distilled water because the solvent should have as little impact on the plant surface as possible.

Dye	CAS	appearance	formula	mol. weight
Rhodamine 6G	989-38-8	red, crystalline solid	C <sub>28</sub> H <sub>31</sub> N <sub>2</sub> O <sub>3</sub> Cl	479.02 u
Rhodamine 101	64339-18-0	red, crystalline solid	C <sub>32</sub> H <sub>31</sub> N <sub>2</sub> O <sub>7</sub> Cl	591.06 u
Coumarin 120	26093-31-2	yellow, crystalline solid	C <sub>10</sub> H <sub>9</sub> NO <sub>2</sub>	175.19 u
Coumarin 307	55804-66-5	yellow, crystalline solid	C <sub>13</sub> H <sub>12</sub> NO <sub>2</sub> F <sub>3</sub>	271.24 u

**Table 3.8:** Technical data of the used dyes (Source: Lambdachrome Laser Dyes [50])

In *Table 3.8* the dyes are presented. All dyes were ordered from *Lambda Physik* (Berlin, Germany). Dyes were prepared in concentrations for an excitation utilizing the nitrogen laser at  $\lambda_{excitation} = 337$  nm. For usage in a dye laser, *Rhodamine 6G* should be tunable around  $\lambda = 590$  nm, *Rhodamine 101* around  $\lambda = 640$  nm, *Coumarin 120* around  $\lambda = 440$  nm and *Coumarin 307* around  $\lambda = 500$  nm. In the same spectral region, their fluorescence signals could be found.

### Fluorescing Nanoparticles

In a first approach for using fluorescing tracer material for the detection of coverage and investigating changes in fluorescence properties, fluorescing nanoparticles were used. Two different particulates were tested for the application, *CdTe* and *CdSe*. *CdTe* was provided by chemistry department of the University of Hamburg, these particles are in aqueous solution. *CdSe* nanoparticles are obtained from *evident Technologies* (ED-C10-TOL-0545, CdSe Core TOPO EviDots, evident Technologies, New York, USA) and were solved in toluene.

*CdTe* has the advantage of being in aqueous solution, making it much easier to handle and to apply to the target surface.

*CdSe* is solved in toluene, which is very volatile. Additionally, the particulates are destroyed quickly when in contact with oxygen for some time.

With both kinds of nanoparticles the fluorescence signal is very strong. They are much more expensive than the laser dyes, therefore the dyes were given precedence.

### 3.4.3 Pesticides and their Matrix

In this project several pesticides, to be more precise nine herbicides and three insecticides, were used (refer to *Table 3.9*). All of these pesticides were in the original composition which could be bought and were mixed with the recommended amount of water (in all these experiments distilled water was used instead of tap water and if a concentration range was given, the highest concentration was used). With the exception of *E 605 forte* all pesticides were available for sale in Germany at that point and special thanks goes to the *Pflanzenschutzamt Hannover* which provided the herbicides and also to the *Institute of plant protection and plant disease* (University of Hannover) for providing the insecticides.

In *Table 3.9* the mode of action after HRAC (*Herbicide Resistance Action Committee*) is given for herbicides (the first nine products in *Table 3.9*) the remaining agents are insecticides (these are acetylcholinesterase inhibitors, which interrupt nervous impulses by binding to cholinesterases).

Trade Name	Active Ingredient	Mode of Action
<i>Patoran FL</i>	Metobromuron	inhibition of Photosynthesis at PSII
<i>Roundup UltraMax</i>	Glyphosate	inhibition of EPSP synthase
<i>Duplosan DP</i>	Dichlorprop-P	synthetic auxins (action like indoleacetic acid)
<i>Goltix 700SC</i>	Metamitron	inhibition of Photosynthesis at PSII
<i>Arelon flüssig</i>	Isoproturon	inhibition of Photosynthesis at PSII
<i>Centium 36 CS</i>	Clomazone	bleaching: inhibition of carotenoid biosynthesis
<i>Lexus</i>	Flupyr-sulfuron Methyl	inhibition of acetolactate synthase (ALS)
<i>Reglone</i>	Deiquat	PSI electron diversion
<i>Gesatop 50</i>	Simazine	inhibition of photosynthesis at PSII
<i>Tamaron</i>	Methamidophos	acetylcholinesterase inhibitor
<i>Metasystox</i>	Oxydemeton-methyl	acetylcholinesterase inhibitor
<i>E 605 forte</i>	Parathion	acetylcholinesterase inhibitor

**Table 3.9:** Used Pesticides with trade name, active ingredient and mode of action (after HRAC for herbicides). The first nine agents given are herbicides, the last three are insecticides. *E 605 forte* is the only product not allowed to use anymore, the rest is commercially available (in Germany). *Arelon flüssig* is also available from a different company under the name of *Tolkan Flo* but these are otherwise identical.

In *Appendix A* information taken from the material safety data sheet (MSDS) of the pesticides is presented. This is an extract from the data sheet available by the manufacturer. Concerning the herbicides this information includes only part *01 – Identification of the substance/preparation and of the company*, *02 – Composition / information on ingredients* and *09 – Physical and chemical properties*. For more information please refer to the manufacturer (products may only be available in Germany, so material safety data sheets (material safety data sheet = Sicherheitsdatenblatt (German)) may also be available in German only).





# Chapter 4

## Results and Discussion

In this part experiments will be shown dealing with the detection of pesticides. The aim in the first part "*Optical Assessment of Pesticide Coverage*" (Section 4.1) was to provide a mapping of pesticide coverage on leaves and to achieve an fast optical assessment. Therefore, fluorescence properties of chosen pesticides were investigated and experiments were carried out using fluorescence tracer material to overcome problems of weak autofluorescence and influence of matrix effects possibly steaming from the biological material. The investigations did not simply utilize the fluorescence of the marker substance but target at changes in fluorescence properties. These changes include quenching of the intensity or shifts in fluorescence wavelength or lifetime due to interaction with the marker substance. With this it is not only possible to map the covered area but also to differentiate between pesticides and to discriminate pesticides from water.

In the second part "*Quantification of Pesticide Colloidal Suspension*" (Section 4.2) the question of quantification of pesticide colloids in suspension was addressed. Most pesticides or their active components are not easily dissoluble in water, therefore it comes to the formation of colloids. These colloids typically have diameters in the range of nanometer up to a few micrometer and so are hard to detect. In this part Laser Induced Breakdown Detection (LIBD) is utilized for colloid detection and quantification. LIBD has the ability to detect very small particles at low concentrations and is therefore predestined for the task at hand. In the experiments an automated evaluation of data was used, which in addition to the breakdown probability could also estimate the area of breakdown events. This made it possible to quantificate higher concentrations of the sample substance (even at one hundred percent breakdown probability concentrations could be differentiated).

## 4.1 Optical Assessment of Pesticide Coverage

The experiments in this part were done primarily by utilizing a nitrogen laser with an excitation wavelength of  $\lambda_{excitation} = 337 \text{ nm}$  (refer to *Section 3.1.1*). Fluorescence can be induced by UV-radiation to a wide variety of substances and biological material such as the fluorescence of chlorophyll in the leaves or the auto-fluorescence of the pesticides. Additional experiments were carried out using the fourth harmonic of an Nd:YAG laser system with an excitation wavelength of  $\lambda_{excitation} = 266 \text{ nm}$  (refer to *Section 3.1.2*).

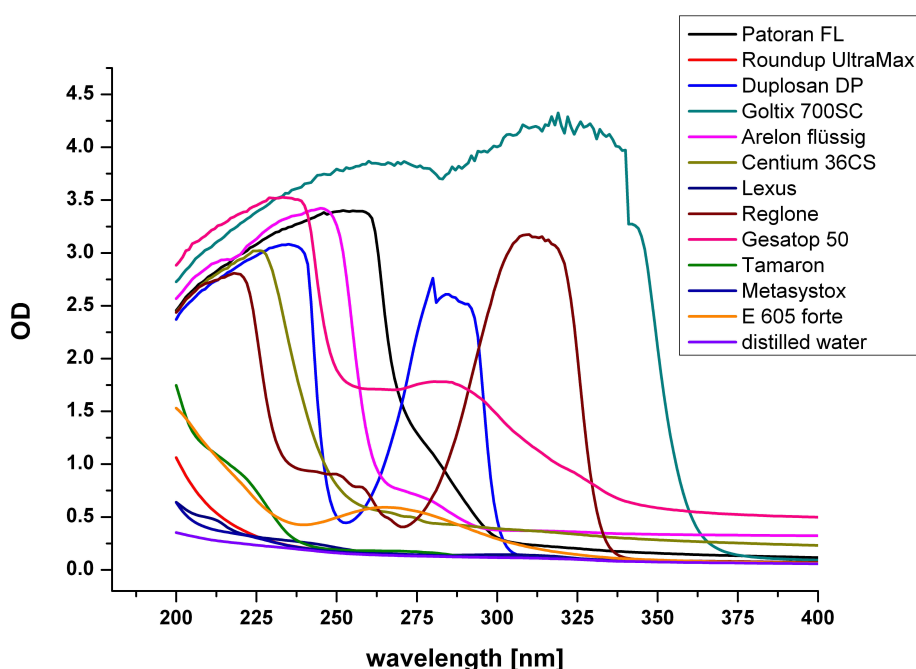


**Figure 4.1:** Absorption measurements of the chosen pesticides recorded by a two beam photometer. Optical density (OD) of the sample pesticides is given for each wavelength between 200 nm and 800 nm in steps of 1 nm. Scan speed was set to 200 nm/min. In the graph only the spectral region in the UV up to 400 nm is shown, at higher wavelength the extinction is nearly constant without any special properties. Also, OD for *Goltix 700SC* exceeds the reliable measuring region of the photometer with its large optical densities values.

*Figure 4.1* shows the absorption measurements of the sample pesticides recorded by a two beam photometer. The pesticides were all solved in distilled water but were otherwise prepared after manufacturers instructions for field application. The extinction spectra were recorded in a spectral region from 200 nm to 800 nm in scan steps of 1 nm and at a scanning speed of 200 nm/min. In *Figure 4.1* only the spectral region of interest between 200 nm and 400 nm is shown. At greater wavelength (above 400 nm) the extinction remains nearly constant and without any special properties. Measurements of optical

densities greater than three give no reliable data due to the detection limit of the photo diode in the photometer. Some of the pesticides come close to this limit or exceed this value, most notably *Goltix 700SC*. With *Goltix 700SC* there is also a leap observable in the graph at about 340 nm. This occurs due to a change in lamps in the photometer, which uses a lamp for the visible (VIS) spectral region and a special lamp for irradiation in the UV.

These sample pesticides will then be applied to biological surfaces such as leaves mimicking field spray application. This application will be carried out in two steps. First, a carrier material will be used as artificial homogeneous surface. As carrier material a cover slip was used and droplets were applied by a pipette. On this glass carrier material, the application of droplets containing pesticides or the fluorescence markers was tested, where the chief objective was the investigation of the application of the fluorescing marker material on the surface. In a second step this procedure was transferred to a leaf, which has a more inhomogeneous surface than the cover slip.

### 4.1.1 Auto-Fluorescence Spectra of Particulate Dyes on Surfaces

Many pesticides show a weak and broad auto-fluorescence but, mostly, this emission is not sufficient for analysis of samples on a green plant due to the strong fluorescence signatures stemming from chlorophyll and other compounds in the plant. Therefore, the fluorescence of particulate dyes was investigated and changes in fluorescence properties were used for the detection of pesticides. Therefore, fluorescence spectra of the different particulate dyes are investigated on the carrier material, glass in form of a cover slip, and on a leaf of *Hedera helix* as biological surface. This serves also the purpose of investigating different solvents for the fluorescence markers and to test a homogeneous application of these substances.

#### 4.1.1.1 Fluorescence of Particulate Dyes on a Glass Surface

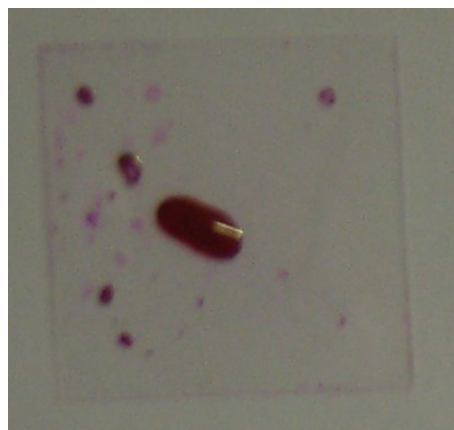
The glass surface of a cover slip was used as carrier material in these experiments. Investigations on parameters like application of droplets with a pipette, drying of droplets, or an uniform coverage of the fluorescence tracer material on the surface were in the foreground. Additionally, fluorescence signatures of the sample dyes are to be investigated and compared to results obtained from the substances in a cuvette.

Initial experiments were conducted testing several dyes, namely *Coumarin 102*, *Coumarin 120*, *Coumarin 307*, *Rhodamine 101* and *Rhodamine 6G*. These were solved in methanol and applied to the surface of the cover slip. Then fluorescence measurements were carried out as can be seen in *Figure 4.3*. Due to the solvent these

droplets did not stay in the form of a droplet, but propagate over the cover slip forming a uniform layer on the surface to a more or lesser degree. The most homogeneous layer (as judged by eye) was achieved using *Rhodamine 101*, while most of the other dyes did not form a layer at all (refer to *Figure 4.2*).



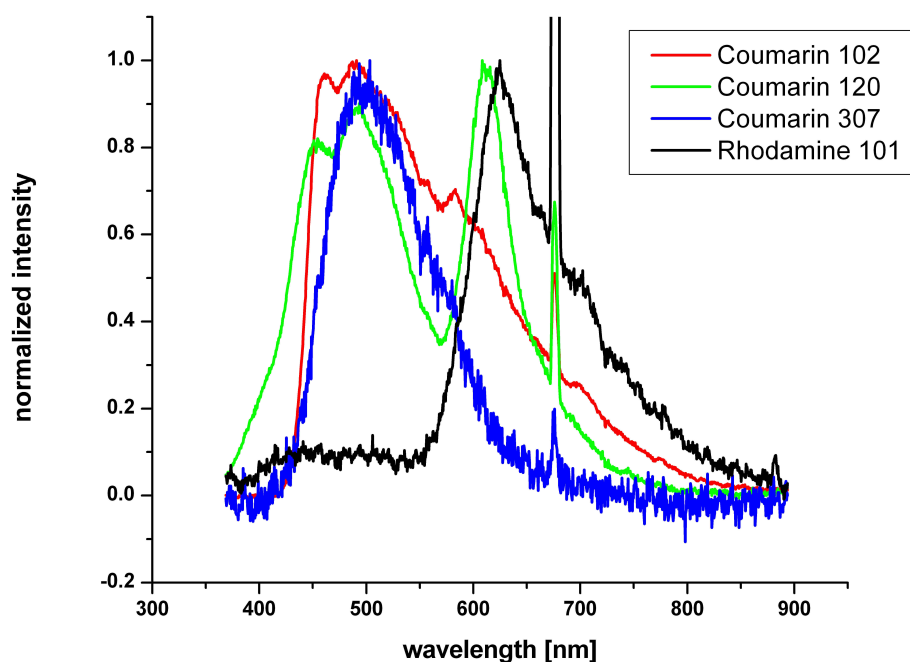
(a) *Rhodamine 101* solved in methanol applied to the surface of the glass carrier material.



(b) *Rhodamine 6G* solved in methanol applied to the surface of the glass carrier material.

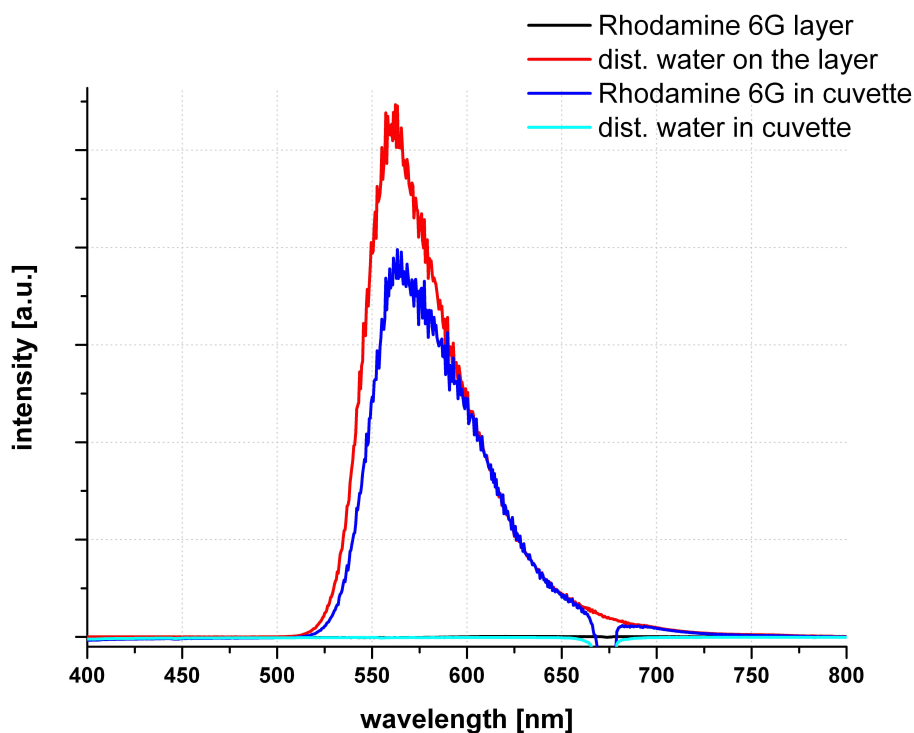
**Figure 4.2:** Layer of *Rhodamine 101* and *Rhodamine 6G* on the surface of the glass carrier material. Droplets were applied to the surface and the dry layer was formed quickly.

In *Figure 4.2* pictures of *Rhodamine 101* and *Rhodamine 6G* layer on a cover slip are shown. The dyes were solved in methanol which evaporated very fast. *Rhodamine 6G* did not form a good layer, but on the surface of a leaf, this dye provides a uniform coating.



**Figure 4.3:** Comparison of different particulate dyes on the surface of a glass carrier material (a cover slip). Excitation was done by a nitrogen laser ( $\lambda_{excitation} = 337$  nm) and fluorescence emission was normalized to the maximum. The peak observable at  $\lambda = 674$  nm is due to the second order Rayleigh scattered laser beam (effect of the grating used in the spectrometer).

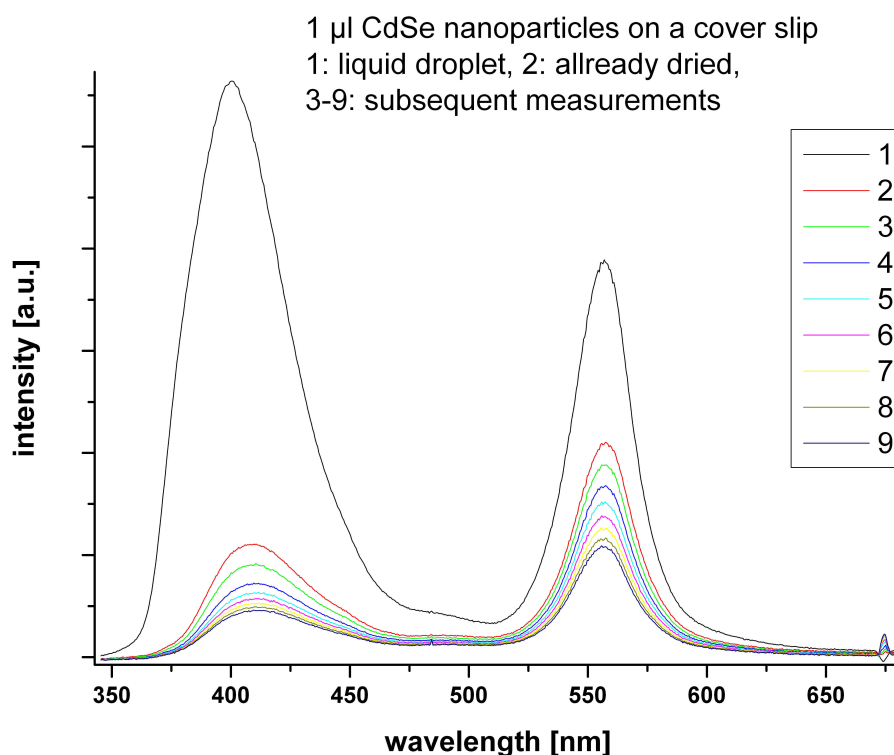
A comparison of the fluorescent dye *Rhodamine 6G* solved in distilled water and measured in a cuvette and the same dye applied as layer to the carrier material is shown in *Figure 4.4*. The dry layer of *Rhodamine 6G* exhibits no fluorescence signal, therefore, a droplet of distilled water was applied. The dye dissolves in the droplet and a strong fluorescence signal could be observed. In comparison, the dye was measured in a cuvette.



**Figure 4.4:** Comparison of the dye *Rhodamine 6G* (solved in distilled water) on the surface of a glass carrier material (a cover slip) and solved in a cuvette. Excitation was done by a nitrogen laser ( $\lambda_{excitation} = 337$  nm). A droplet of distilled water was added to the layer, since the dry marker did not fluoresce. The material dissolved in the water and a strong fluorescence signal could be observed.

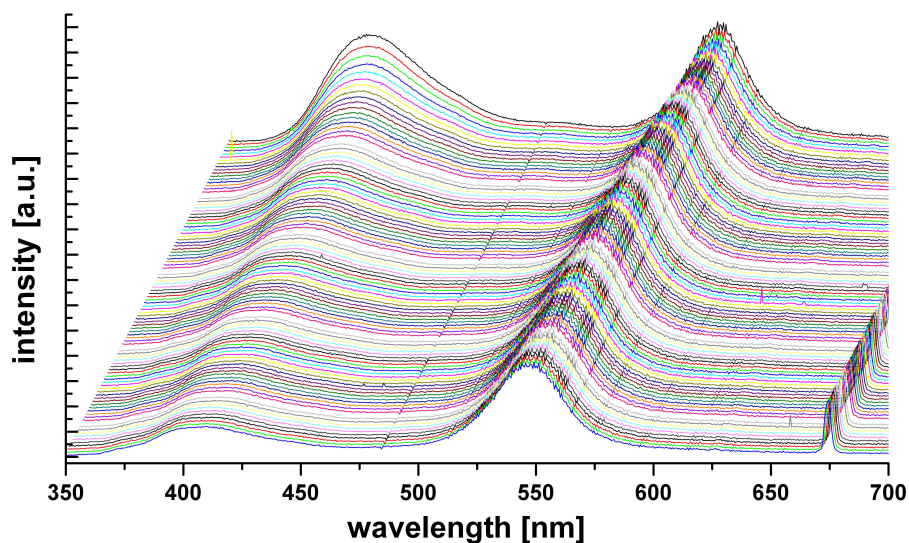
**Fluorescence of Nanoparticles on a Glass Surface** In addition to the particulate dyes nanoparticles were investigated for the use as fluorescence tracer material. Sample nanoparticles for this purpose were *Cadmium Tellurium (CdTe)* and *Cadmium Selenium (CdSe)*. *CdTe* was in an aqueous solution whereas *CdSe* was solved in toluene. The *CdTe* nanoparticles were easier to handle, mostly due to the use of distilled water as solvent in contrast to toluene for the *CdSe* nanoparticles. Both kinds of particles exhibit strong fluorescence signals but were also insusceptible to spectral shifts. Therefore a fluorescent dye was used in the later experiments, were changes in fluorescence properties of the tracer material in presence of the sample pesticides were investigated. From an economic point of view the nanoparticles are also second choice due to the much higher expenses. Nevertheless, in the following some results of the measurements using nanoparticles are presented. In a first approach, investigations of changes in fluorescence properties of nanoparticles were carried out when applied with chosen pesticides or the active ingredients of pesticides.

Figure 4.5 shows fluorescence measurements of *CdSe* nanoparticles on the glass carrier material. The first graph (1) in the figure refers to the liquid nanoparticle solution in its solvent toluene, accounting for its much higher fluorescence intensity. In the second graph (2) this droplet has dried up (toluene is highly volatile) and all the subsequent measurements are done on the dried droplet but in the same spot. The figure also indicates that some bleaching effects occur when irradiating the dried nanoparticles, since the fluorescence intensity decreases with each subsequent measurement.



**Figure 4.5:** Investigation of *CdSe* nanoparticles as fluorescence tracer on a glass carrier material. *CdSe* nanoparticles were solved in toluene, therefore only the first measurement could be carried out on the liquid droplet. All subsequent measurements were done on the dried droplet but in the same place.

The peak at the longer wavelength at about  $\lambda = 553$  nm was stable in regard to fluorescence intensity during repeated measurements, the shorter wavelength peak at about  $\lambda = 410$  nm, however, decreased with consecutive irradiation. This behavior was analyzed in the following experiment (Figure 4.6) where a series of experiments were recorded over time and plotted in a waterfall diagram. This diagram shows consecutive measurements, which were carried out one right after the other.



**Figure 4.6:** Waterfall diagram of *CdSe* nanoparticles on glass carrier material. A series of measurements was recorded over time in order to test for bleaching effects. The first measurement is shown in the back of the diagram and the last one is in the forefront.

To illustrate the decrease in fluorescence intensity a cut along the time axis is presented in *Figure 4.7*.  $\lambda_1$  accounts for the lower wavelength peak at  $\lambda_1 = 410$  nm and  $\lambda_2$  for the longer wavelength peak at  $\lambda_2 = 553$  nm. Each measurement in *Figure 4.6* was done by accumulating one hundred fluorescence spectra (ca. 10 s per measurement) and these investigations were carried out on the same spot on the cover slip and one right after the other. As shown before (*Figure 4.5*) toluene evaporates very quickly, therefore these experiments were done on an already dry droplet.



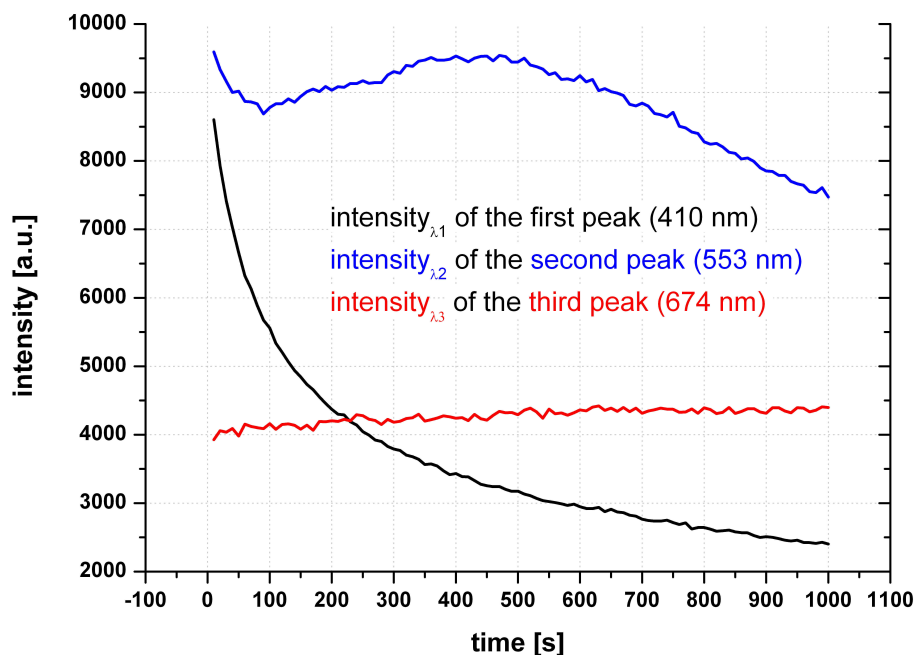
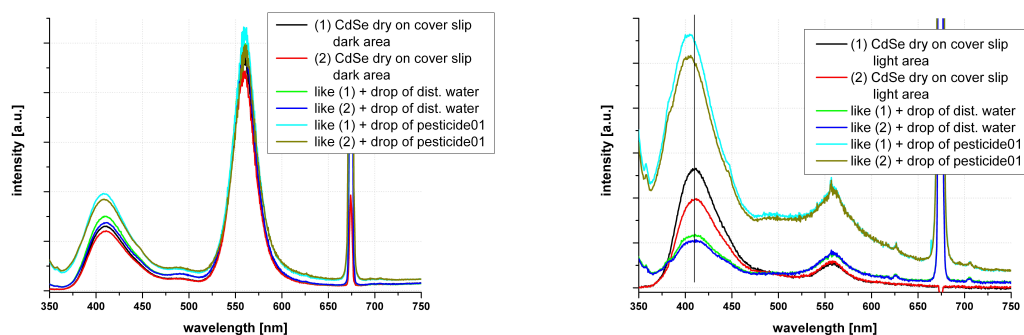


**Figure 4.7:** Cuts along the time axis of *Figure 4.6*. The intensities of the two peaks at  $\lambda_1 = 410$  nm and  $\lambda_2 = 553$  nm are plotted over time and for comparison the Rayleigh scattering at  $\lambda_3 = 674$  nm.

*Figure 4.7* shows the intensities of the two observable fluorescence maxima at  $\lambda_1 = 410$  nm and  $\lambda_2 = 553$  nm over time. It can clearly be seen that the lower wavelength peak bleaches with each consecutive measurement whereas the longer wavelength peak is more or less unaffected. For comparison the Rayleigh scattering peak at  $\lambda_3 = 674$  nm is also included which shows an almost constant intensity.

The intensity of the two fluorescence peaks in relation to each other pointed at the possibility to estimate a layer thickness of the applied nanoparticles. In *Figure 4.8* CdSe nanoparticles on the glass carrier material are shown. *Figure 4.8(a)* illustrates a dark area (thick layer) of dried particles in comparison with a light area (thin layer) also of dried particles (*Figure 4.8(b)*). On both layers distilled water and some pesticide samples were applied.



(a) *CdSe* nanoparticles on glass carrier material, measurement on the thick layer area. A drop of dist. water and *Patoran FL* is also applied.

(b) *CdSe* nanoparticles on glass carrier material, measurement on the thin layer area. A drop of dist. water and *Patoran FL* is also applied.

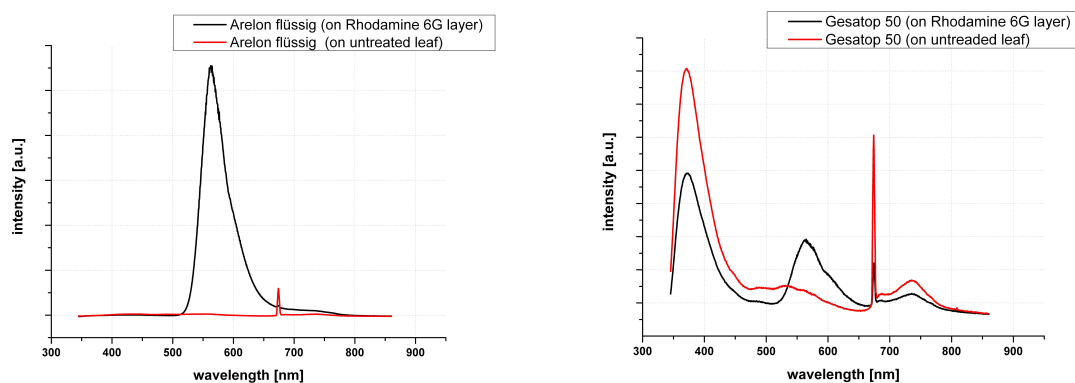
**Figure 4.8:** Layer of *CdSe* nanoparticles on glass carrier material and fluorescence measurements on the thick (*Figure 4.8(a)*) and the thin (*Figure 4.8(b)*) layer areas. Nanoparticles were measured after drying, with a droplet (1  $\mu\text{L}$ ) of distilled water, and with a droplet (1  $\mu\text{L}$ ) of *Patoran FL* applied to the layer.

The layer was created by applying a droplet of the *CdSe* nanoparticles, let it dry, and than apply another droplet to the same spot. This was repeated several times in order to create different layer thicknesses. These layers were then used in the measurements shown in *Figure 4.8*.

In the following experiments the particulate dyes was given precedence over the nanoparticles due to their easier handling, availability, and lower expenses. Also, the fluorescence properties of the tested nanoparticles was not or only marginal influenced in presence of the chosen pesticides.

#### 4.1.1.2 Fluorescence of Particulate Dyes on a Leaf Surface

Following the experiments of the fluorescent dyes applied to a artificial surface (the glass cover slip as carrier material) these experiments were transferred to a biological surface. As biological sample the leaves of ivy (*Hedera helix*) were chosen. This evergreen plant has the advantage of being available during all seasons and is easy to handle. For these experiments, the leaves were detached from the plant. Additionally, parts of the leaves were cut out in order to position them properly in the setup.



(a) Fluorescence spectra of *Arelon flüssig* applied to an untreated leaf and to a leaf coated with a *Rhodamine 6G* layer.

(b) Fluorescence spectra of *Gesatop 50* applied to an untreated leaf and to a leaf coated with a *Rhodamine 6G* layer.

**Figure 4.9:** Fluorescence spectra of *Arelon flüssig* and *Gesatop 50* applied to the surface of a leaf. Both pesticides are applied to an untreated leaf surface and to a surface coated with a *Rhodamine 6G* layer (*Rhodamine 6G* was dissolved in methanol). The nitrogen laser at  $\lambda_{excitation} = 337$  nm was used for fluorescence excitation.

Figure 4.9 shows measurements on the surface of an ivy leaf. Two example pesticides, *Arelon flüssig* and *Gesatop 50*, were applied to the surface of an untreated leaf and to a leaf coated with a *Rhodamine 6G* layer. The *Rhodamine 6G* layer can not be detected by itself, but after applying a liquid droplet its fluorescence is observable at about  $\lambda = 560$  nm. It can also be seen that *Arelon flüssig* can not be detected on a leaf surface on its own, but the auto-fluorescence of *Gesatop 50* is strong enough for detection of this herbicide.

Layer formation behavior of the solved fluorescing dyes on the surface of a leaf was different from coating a glass surface. The leaf itself had a more uneven surface which is also crisscrossed by veins. To avoid the alteration of physiological parameters or to minimize the impact on the leaf, cutting out parts of the surface is done as little as possible. Therefore, handling of the leaf was more difficult in respect to proper placement in the experimental setup, but it should not interfere much with processes in the leaf, e.g. photosynthetic processes. With the experiments on the glass carrier material, *Rhodamine 101* solved in methanol formed the most homogeneous layer which was also relatively easy to achieve. On the surface of an ivy leaf, however, it turned out to not forming a layer at all. Despite extensive testing the creation of a layer does not seem possible. Additionally, the dye solutions tend to accumulate in the veins which were topological dips on the leaf surface.

From the measurements on the surface of a leaf, *Rhodamine 6G* turned out to form a uniform layer. Experiments were carried out to use the fluorescing dyes with different

solvents, important being methanol, distilled water, and acetone. Distilled water should be the least hazardous solvent for biological material, but it takes a long time to dry. Methanol and acetone evaporate more quickly, therefore aiding the formation of a uniform dry layer. The solubility of the dyes was best in methanol and not very good in distilled water or acetone, but it was possible to solve them in all solvents.

In the follow up experiments investigating fluorescence properties of the fluorescence marker influenced by the chosen pesticides *Rhodamine 6G* was used as fluorescent label. As shown in the experiments above, layer formation on the leaf was nearly uniform, and it was available in larger amounts at relatively low cost, especially when compared to the fluorescing nanoparticles. Additionally, the toxicity of the used chemical marker should be taken into account when suggesting any practical application or use in the environment.

The fluorescent dye *Rhodamine 6G* was applied to the surface in form of a micro-droplet as described above in this section. These droplets of 0.5  $\mu\text{L}$  or 1  $\mu\text{L}$  were placed by a pipette and provide a thin layer on the leaf after drying. Another procedure was the application of dye as aerosols. The dye solution in acetone was atomized and the distance of the atomizer to the leaf surface was set in a way, that all the solvent evaporates and only dry solid aerosols reach the plant. This application results in a very thin layer not visible to the eye.

## 4.1.2 Auto-Fluorescence Spectra of Pesticide Droplets on Surfaces

Concerning the chosen pesticides, similar experiments were conducted as with the fluorescent labeling agents. In *Figure 4.1* at the beginning of this part (page 38) absorption spectra of the sample pesticides are given. These spectra were recorded with the pesticides solved in distilled water and measured in a cuvette. For simulating the spraying practice, these substances have to be applied to a biological surface. This is done by the application of droplets using a pipette. As with the fluorescing particulates described in *Section 4.1.1*, in a first step, the pesticides are applied to the artificial surface of a cover slip. The scientific findings are then transferred, in a second step, to the application of pesticides on a leaf as biological surface.

### 4.1.2.1 Fluorescence of Pesticide Droplet on a Glass Surface

Prior to applying the pesticides to a leaf surface, experiments on a cover slip as carrier material were carried out. The commercially available trade units of these substances were prepared in water according to the manufacturers instructions. The one alteration to standard application was the usage of distilled water instead of tap water. These pesticides were applied in droplets of 1  $\mu\text{L}$  to the glass surface of the cover slip using a pipette. For

excitation the nitrogen laser was used at  $\lambda_{excitation} = 337$  nm (for experimental setup refer to *Chapter 3*).

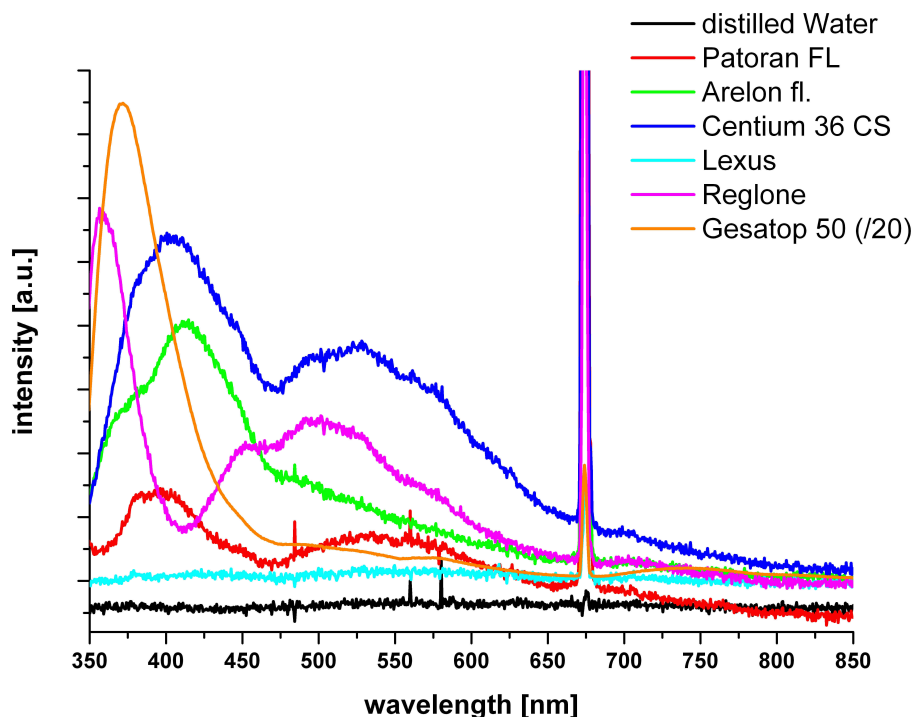


**Figure 4.10:** Auto-fluorescence of the sample pesticides. Pesticides were solved in distilled water and were applied to a glass surface as a droplet of 1  $\mu$ L. Fluorescence excitation was carried out using a nitrogen laser at  $\lambda_{excitation} = 337$  nm. The fluorescence intensity of *Gesatop 50* is divided by twenty for better comparison with the other pesticides.

Most of the sample pesticides display a weak auto fluorescence as presented in *Figure 4.10*. The intensities of *Gesatop 50* are divided by twenty for better representation of the fluorescence data, although it is the notable exception among the samples. *Gesatop 50* displayed a high auto-fluorescence which may be used for a direct detection of this pesticide on a surface. Even the signal of the other substances may be strong enough for a detection on the carrier material, but on a biological surface such as a leaf, the fluorescence signals would be hardly distinguishable from background signals, e.g. the fluorescence of chlorophyll or other bio-emitters.

Because of the usually weak auto-fluorescence and the relatively strong background signals of a natural surface, monitoring of an added fluorophore, a labeling agent like a fluorescent dye, was used in the presented experiments in order to obtain a more precise and reliable assessment of pesticide coverage. As fluorescence tracer, particulate dyes

were investigated (refer to *Section 4.1.1*) and the effect of the sample pesticides on the fluorescence signals of these marker substances was analyzed.

In the following measurements *Rhodamine 101* was used on a glass surface. *Rhodamine 101* was chosen due to the formation of a homogeneous dry layer on this substrate as described in *Section 4.1.1*. Active ingredients of pesticides were applied to a glass surfaces coated with a *Rhodamine 101* layer (*Rhodamine 101* was solved in methanol in these experiments). Active ingredients of pesticides were solved in distilled water and a droplet was applied to the glass surface with a pipette. These droplets stayed in a half spherical form due to the surface tension of water and were measured while still wet. A droplet of distilled water was added for reference and as comparison to the pesticide containing droplet. A choice of these experiments is shown in *Figure 4.11*. The inside-graph is a magnification of the peak area for better visualization. In the magnification, slight spectral shifts can be observed.

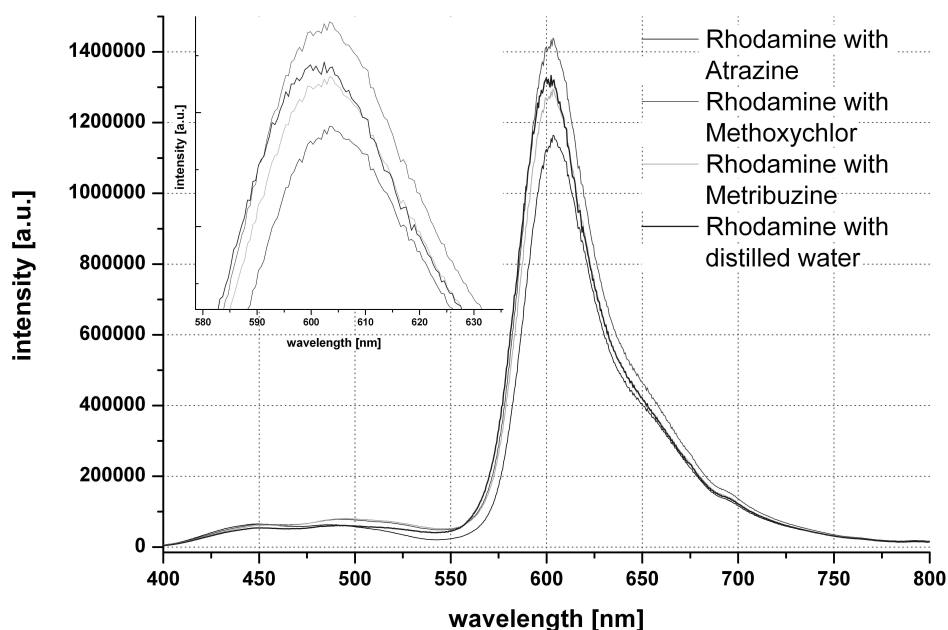


**Figure 4.11:** Pesticide active ingredients solved in distilled water and applied to glass carrier material coated with a *Rhodamine 101* layer. For comparison there is also a measurement with a droplet of distilled water. Measurements of the applied droplets were carried out while they were still wet, this is the reason for the relatively high intensities.

Following the experiments with *Rhodamine 101*, additional measurements with the fluorescence tracer material in conjunction with pesticides were carried out. Here, *Rhodamine 6G* was used as fluorescent marker. One droplet (1  $\mu\text{L}$ ) of the fluorescence tracer solved in distilled water and one droplet (1  $\mu\text{L}$ ) of the pesticide solution were applied on the same

spot on the cover slip. While both droplets were still wet, fluorescence measurements were carried out. The results of these experiments are shown in *Figure 4.12*.

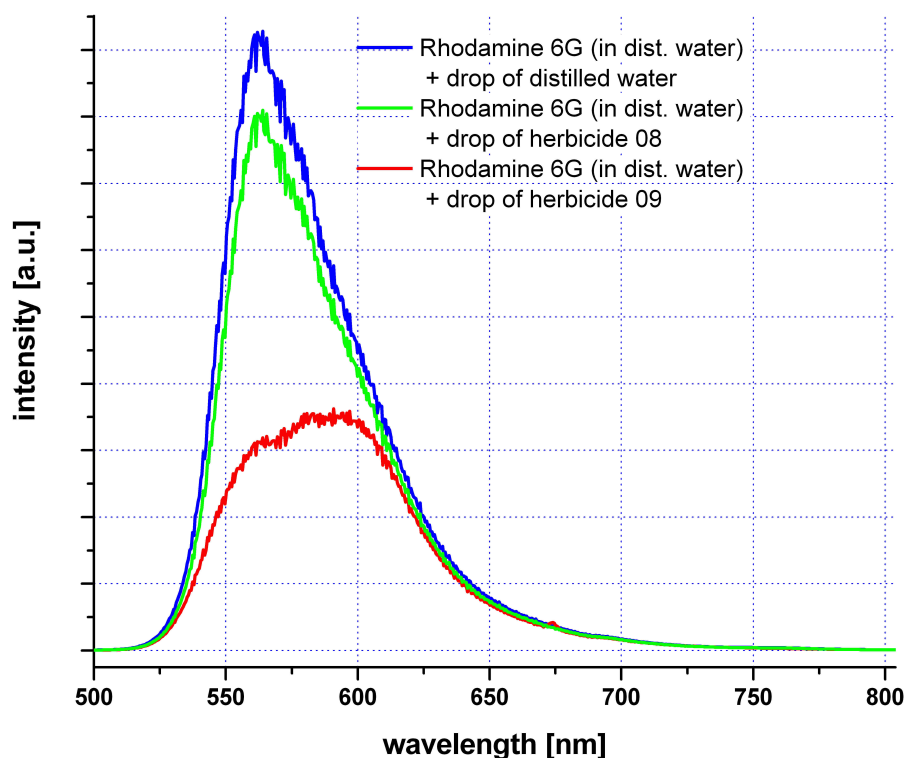


**Figure 4.12:** Fluorescence of the pesticides on the surface of the glass carrier material. A droplet of a pesticide and a drop of *Rhodamine 6G* were applied on the same spot on the cover slip (1  $\mu\text{L}$  each) and measured while wet.

Additionally, cover slips were prepared with a layer of *Rhodamine 6G* solved in methanol. The methanol evaporates more quickly than distilled water and leaves a more uniform layer (refer to *Section 4.1.1*). Although not as homogeneously as the layer formation with *Rhodamine 101*, *Rhodamine 6G* was still an adequate alternative. In contrast to *Figure 4.12* a droplet (1  $\mu\text{L}$ ) of pesticide was applied to the dry layer of the fluorescent labeling material. The dye particulates dissolve in the distilled water of the pesticide solution and fluorescence emission was investigated. Results are shown in *Figure 4.13*. In comparison to the application of pesticide droplets on such a layer, the fluorescence signal of a droplet of *Rhodamine 6G* solved in distilled water and a droplet of distilled water applied to the same spot (compare also with *Figure 4.12*) is displayed.

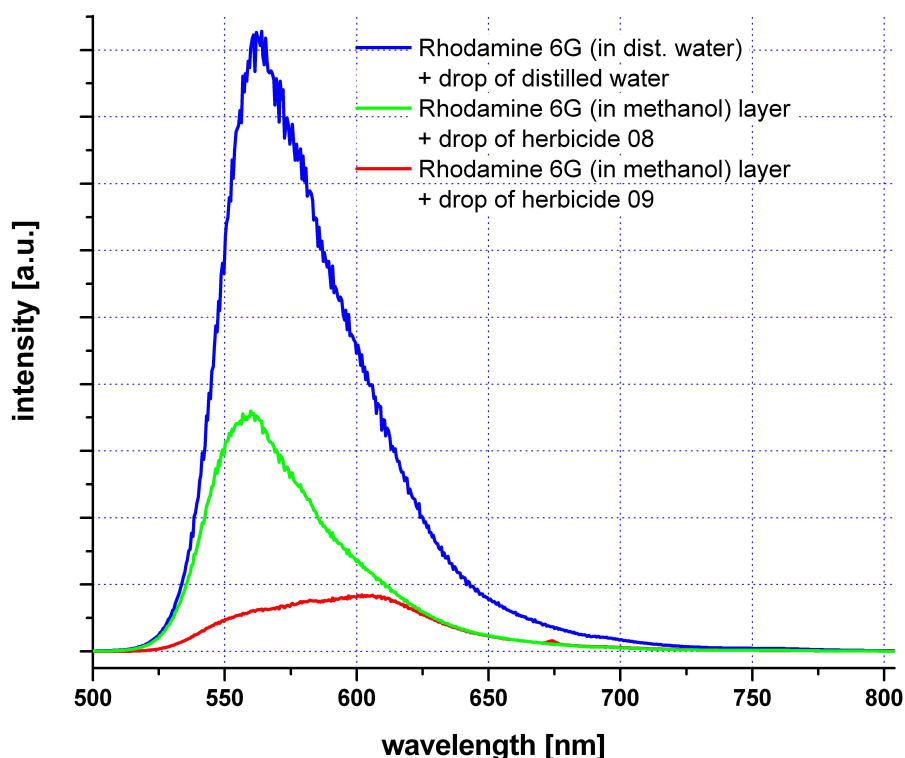


**Figure 4.13:** Fluorescence of the pesticides on the surface of the glass carrier material. The cover slip was coated with a layer of *Rhodamine 6G* solved in methanol. After drying of the layer, a drop containing a pesticide (1  $\mu\text{L}$  each) was applied. For comparison a drop of *Rhodamine 6G* solved in distilled water and a drop of distilled water applied to the same spot is also displayed (compare *Figure 4.12*).

A spectral shift in the fluorescence emission of *Gesatop 50* can be observed in *Figure 4.12* as well as in *Figure 4.13*. The effect of pesticides on the fluorescence of *Rhodamine 6G* was investigated more extensively and results will be shown in *Section 4.1.4*.

#### 4.1.2.2 Fluorescence of Pesticide Droplet on a Leaf Surface

After testing the pesticides on an artificial surface, these substances were applied to a natural surface, to that of an ivy leaf. Similar investigations have been carried out with the fluorescence marker (refer to *Section 4.1.1*), but in that part the formation of a homogeneous layer and application of the substances was of interest. The pesticide solutions were designed for an application on leaves and they are optimized to penetrate the cuticula of the leaves in order to get the active ingredient to its place of action. Nevertheless, effects on fluorescence signatures of the labeling agent could already be observed (refer to *Section*



4.1.2), which may be caused by interactions of the pesticide solutions with the particulate dyes.

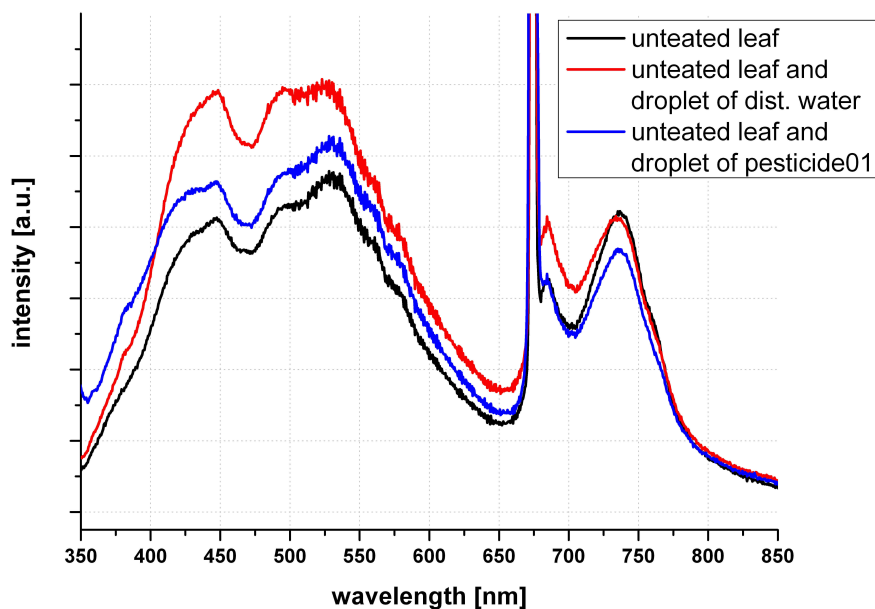


**Figure 4.14:** Fluorescence of an untreated leaf compared to the same leaf, where a droplet of distilled water was added. Additionally, a drop of pesticide solution was applied to the untreated surface. Droplets were 1  $\mu\text{L}$  and applied by a pipette.

In *Figure 4.14* the fluorescence spectrum of an untreated ivy leaf (*Hedera helix*) is shown, and, in addition, one drop of distilled water and one drop of *Patoran FL* were added to the surface (1  $\mu\text{L}$  each). The peak at  $\lambda = 674$  nm, again, results from the usage of a grating in the spectrometer (second order of Rayleigh scattered laser radiation). The maxima at  $\lambda = 680$  nm and  $\lambda = 730$  nm are contributed to chlorophyll fluorescence. The emission at  $\lambda = 680$  nm is accredited to chlorophyll-a fluorescence originating from the photosystem II and emission at  $\lambda = 730$  nm is also accredited to chlorophyll-a fluorescence but originating from photosystem I (for reference refer to [51, 52]). The broad fluorescence emission around  $\lambda = 450$  nm and  $\lambda = 530$  nm is ascribed to other substances in the plant cells or in the cell walls (e.g. ferulic acid [53]). As shown in the figure, there is nearly no difference between the three graphs and the auto-fluorescence of the pesticide is hidden in the fluorescence signals steaming from the leaf.

Additionally, the pesticide droplets were investigated when applied to a leaf surface coated with a *Rhodamine 6G* layer. As in the experiments before, droplets of 1  $\mu\text{L}$  were applied and measurements were carried out when the droplets were still wet. Then, the measurements were repeated with the dried droplets. The results of the investigations of two sample pesticides are shown in *Figure 4.15*.

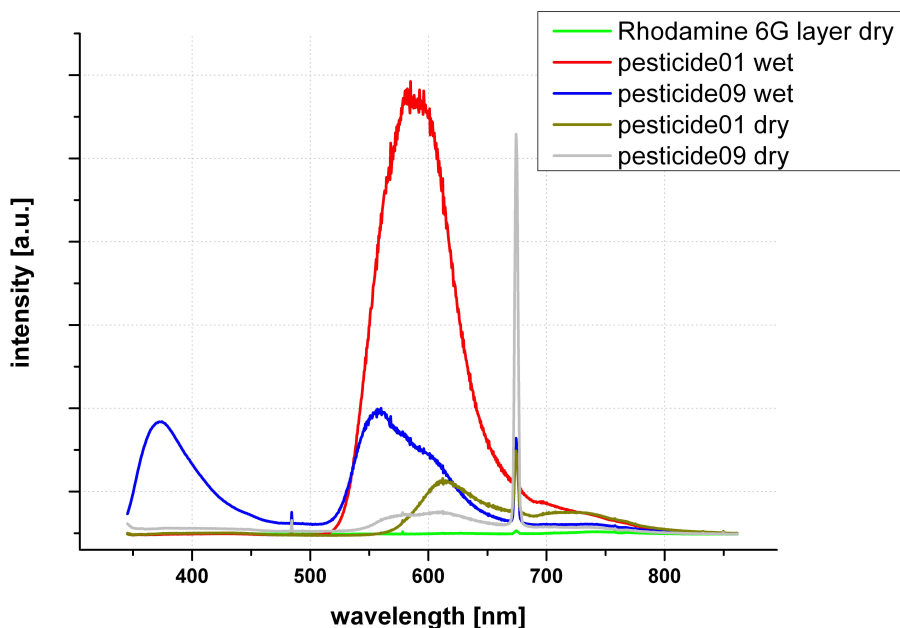


**Figure 4.15:** Fluorescence of a leaf with a dry *Rhodamine 6G* layer compared to the same leaf, where droplets (1  $\mu\text{L}$  each) of two sample pesticides (*Patoran FL* and *Gesatop 50*) were added. Additionally, these droplets were measured when they have dried.

*Rhodamine 6G* solved in methanol was applied to an ivy leaf (*Hedera helix*) and a layer of this fluorescent dye was created. Then a droplet (1  $\mu\text{L}$ ) of *Patoran FL* and one droplet (1  $\mu\text{L}$ ) of *Gesatop 50* were applied to the surface. Dye particulates dissolve in the distilled water and generating a strong fluorescence signal when excited as displayed in *Figure 4.15*. The leaf with the *Rhodamine 6G* layer was also investigated. Background signals from the surface were very small in comparison to the emission of fluorescing particles, therefore, they did not distort the results. *Gesatop 50* exhibited the highest auto-fluorescence of the chosen pesticides and can be detected directly on the surface. An interesting aspect is the relatively strong fluorescence signals steaming from the dried droplets. With both pesticides, a fluorescence signal could be detected which is approximately at the spectral position of the *Rhodamine 6G* in dissolved form. This is investigated further in *Section 4.1.4*.

### 4.1.3 Dissolution of Dye Micro-Crystals in Droplets

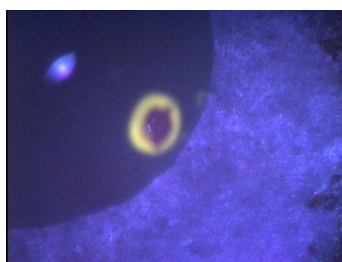
When a droplet of distilled water or a droplet containing a pesticide were added to the above described layer of the fluorescent dye, strong fluorescence signals of these labeling substances could be observed due to dissolution of the particulates in the liquid.

Therefore, the dissolution process of the *Rhodamine 6G* crystallite dye was investigated and experiments were carried out using a fluorescence microscope (refer to *Chapter 3*). A ivy leaf was placed under the microscope and excited with radiation around  $\lambda_{excitation} = 400$  nm. Emission was recorded by a color video camera which was set to take single pictures in a time series. The area visible in *Figure 4.16* is about  $3 \text{ mm} \times 2 \text{ mm}$  and, due to an emission filter, the surface of the leaf appears blueish.

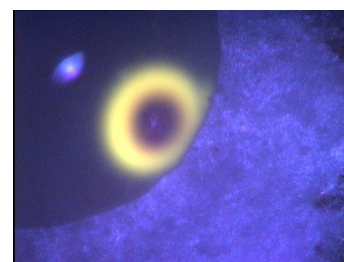
A droplet of distilled water (about  $0.5 \mu\text{L}$ ) and a *Rhodamine 6G* crystallite was applied to the surface of the ivy leaf. The water droplet and the *Rhodamine 6G* crystallite were not in contact in the beginning of the measurement (refer to *Figure 4.16(a)*). The droplet of distilled water appears dark and the crystallite as dark red spot (marked by the red circle in *Figure 4.16(a)*). To observe the dissolution of the *Rhodamine 6G* crystallite, it was moved into the droplet and a time series of pictures was taken.



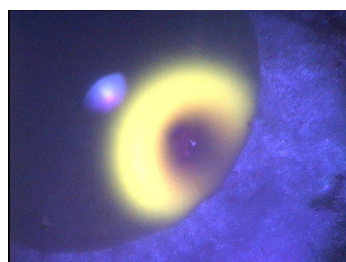
(a) Droplet of distilled water and a *Rhodamine 6G* crystallite (marked by the red circle) on the surface of an ivy leaf.



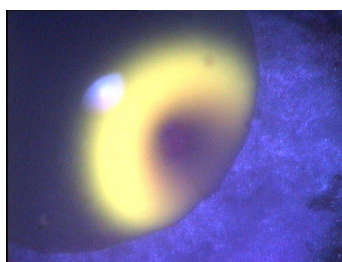
(b) The crystallite has been moved into the droplet. Recording is now started over time ( $t = 0$  s).



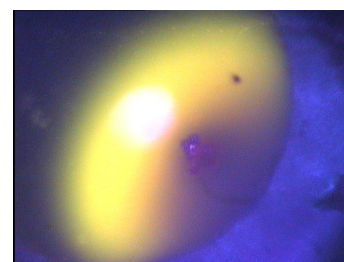
(c) Droplet of distilled water containing the *Rhodamine 6G* crystallite ( $t = 12$  s).



(d) Droplet of distilled water containing the *Rhodamine 6G* crystallite ( $t = 34$  s).



(e) Droplet of distilled water containing the *Rhodamine 6G* crystallite ( $t = 77$  s).

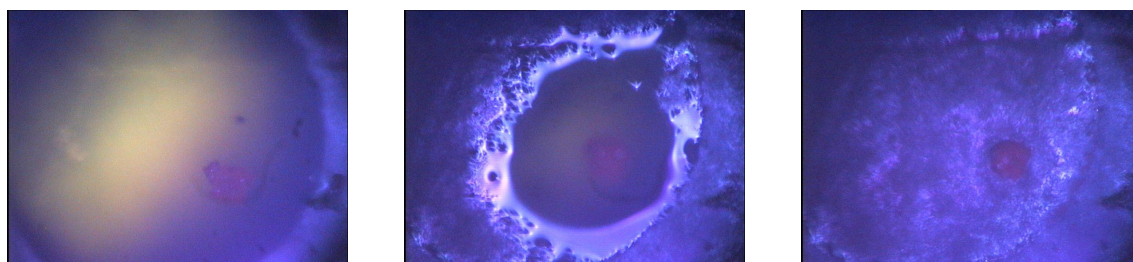


(f) Droplet of distilled water containing the *Rhodamine 6G* crystallite ( $t = 232$  s).

**Figure 4.16:** Images of a fluorescence microscope monitoring the dissolution of a *Rhodamine 6G* crystallite (diameter of ca.  $50 \mu\text{m}$ ) in a droplet of distilled water on the surface of an ivy leaf. The excitation maximum was at  $\lambda_{excitation} = 400$  nm and emission in the range of  $500 \text{ nm}$  to  $600 \text{ nm}$ . *Figure 4.16(a)*: The location of the crystallite is indicated by the red circle and it is not in contact with the droplet. *Figure 4.16(b) – Figure 4.16(f)*: The droplet was moved into the droplet and a time sequence of *Rhodamine 6G* fluorescence during dissolution were recorded.

In *Figure 4.16* the *Rhodamine 6G* crystal (size ca. 50  $\mu\text{m}$  in diameter) was moved into the droplet of distilled water (still separated in *Figure 4.16(a)*) and the dissolution of the crystallite was observed over time (*Figure 4.16(b)* – *Figure 4.16(f)*). In the water *Rhodamine 6G* shows a strong fluorescence signal and it can be seen that the distribution of the fluorescent marker within the droplet spreads and fills the whole droplet. The fluorescing ring observed in *Figure 4.16(b)* – *Figure 4.16(f)* stems from dissolved *Rhodamine 6G* around a still undissolved *Rhodamine 6G* crystallite. After a short time the whole droplet can easily be observed due to the strong fluorescence of dissolved *Rhodamine 6G* in the distilled water (refer to *Figure 4.17(a)*).

In *Figure 4.16(f)* the still undissolved remainder of the *Rhodamine 6G* crystal can be seen. Due to heating caused by the excitation light source, the droplet dried after some time leaving the undissolved part of the crystallite on the surface. In *Figure 4.17* a picture right before the drying process is shown (*Figure 4.17(a)*) which is taken about 10 min after moving the dye crystallite into the droplet. Then the drying process started and *Figure 4.17(b)* shows the droplet in the middle of this process. Finally, the droplet has dried (*Figure 4.17(c)*) and the undissolved remainder of the *Rhodamine 6G* crystallite can be observed.



(a) Droplet of distilled water containing the *Rhodamine 6G* crystallite ( $t = 630$  s after *Figure 4.16(b)*).

(b) Droplet of distilled water containing the *Rhodamine 6G* crystallite in the middle of the drying process ( $t = 760$  s).

(c) Droplet of distilled water dried and the undissolved remainder of the *Rhodamine 6G* crystallite ( $t = 836$  s).

**Figure 4.17:** Images of a fluorescence microscope monitoring the dissolution of a *Rhodamine 6G* crystallite (diameter of ca. 50  $\mu\text{m}$ ) in a droplet of distilled water on the surface of an ivy leaf as in *Figure 4.16*. *Figure 4.17(a)*: The location of the crystallite can be observed and this photo is taken shortly before the drying process started. *Figure 4.17(b)*: The droplet during the drying process. *Figure 4.17(c)*: Finally, the dried droplet and the undissolved remainder of the *Rhodamine 6G* crystallite. The form of the droplet can still be seen by the layer of *Rhodamine 6G* which is thicker at the rim of the droplet.

In *Figure 4.17(c)* the area of the droplet of distilled water can be seen weakly by the layer of *Rhodamine 6G* on the leaf surface. This layer looks a little different than the remaining surface of the leaf and at the rim of the dried droplet *Rhodamine 6G* has accumulated at higher concentrations.

#### 4.1.4 Effects of Pesticides on *Rhodamine 6G* Fluorescence

Since the auto-fluorescence of many pesticides is rather weak and often covered by emitters in the plant, the investigation of fluorescence properties of a labeling agent in presence of the pesticides is suggested. Promising results could be obtained by using *Rhodamine 6G* (for details refer to *Chapter 3*) as fluorescing agent. A sample leaf was first exposed to *Rhodamine 6G* solid aerosols until covered by this micro- and nanoparticulates. Then, pesticides were applied as droplets emulating field spray application. The dry *Rhodamine 6G* crystallites exhibit a weak emission, but when a droplet of distilled water is applied, the crystallites dissolve and a strong fluorescence signal could be detected (refer to *Section 4.1.3*). In presence of a given pesticide there are several effects to be observed. These are initiated either by the active ingredient of the pesticide itself or they stem from an organic matrix which is added to the retail version of a given pesticide in order to enhance the solubility of the active substance and to help the migration into the plant. These effects include spectral shifts in the fluorescence wavelength of the tracer substance, quenching or enhancement of the fluorescence intensity and changes in fluorescence decay time. Investigations of these effects can be found in this section.

##### 4.1.4.1 Effects of Pesticides on Fluorescence Intensities

A parameter affected by the presence of pesticides is the intensity of the fluorescing marker material. To make quantitative statements using changes in fluorescence intensity presents more difficulties than the use of wavelength shifts, because of variations in laser power, heterogeneity in the biological material and heterogeneity in the applied droplet. Additionally, there are optical effects like quenching or reabsorption which cause an increase or decrease in signal intensity. Furthermore, the transparency of the investigated pesticides was inhomogeneous, ranging from transparent to opaque and their color ranging from milky white to brown. Absorption bands were investigated in *Figure 4.1.A*. A substantial increase of fluorescence intensity of the tracer material in contrast to its dry emission is readily observed, and caused by dissolution of the particles in the applied micro-droplets as described above.

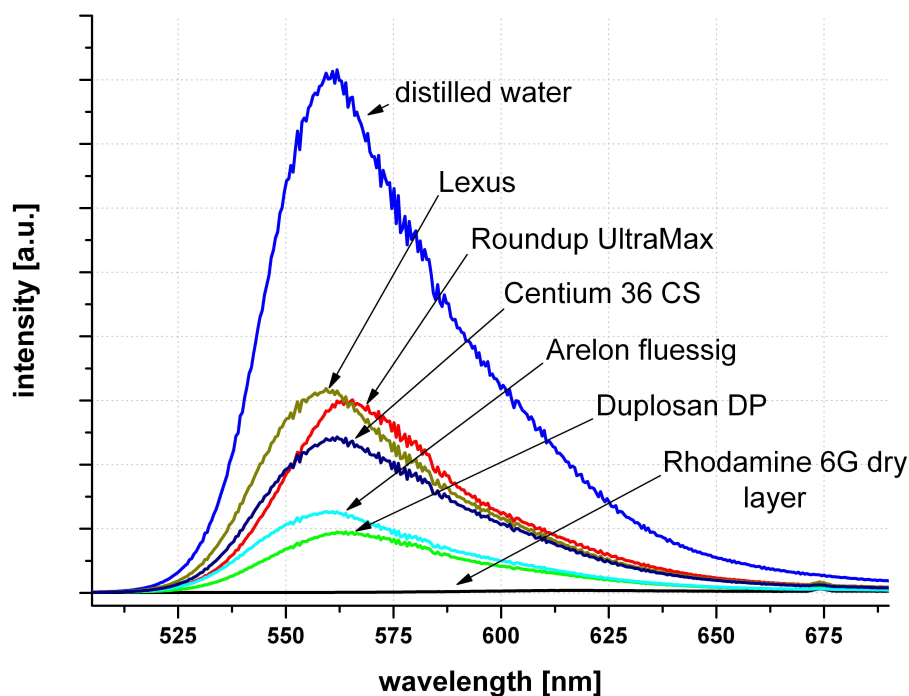


**Figure 4.18:** Fluorescence intensity of the particulate dye *Rhodamine 6G* as a layer on the surface of an ivy leaf (*Hedera helix*). A drop (1  $\mu\text{L}$ ) of distilled water was added as reference as well as droplets (1  $\mu\text{L}$  each) of a sample pesticide. In addition, the fluorescence of the dry *Rhodamine 6G* layer is also shown. For excitation a nitrogen laser at  $\lambda_{\text{excitation}} = 337 \text{ nm}$  was used.

In *Figure 4.18* the fluorescence intensities of a *Rhodamine 6G* coated leaf with a micro-droplet of pesticide is shown. As reference measurements on the dry *Rhodamine 6G* layer and of a droplet of distilled water are presented. Compared to the solid state emission of the *Rhodamine 6G* particulates there is a great increase in fluorescence intensity in the pesticide samples and in the distilled water. This is mainly due to dissolution of the *Rhodamine 6G* crystallites in the solvent (distilled water). Also, an material specific fluorescence quenching in comparison to the pure water sample could be observed, resulting from interactions of the particulate dye molecules with the components in the pesticide droplet. Additionally, the pesticide auto-fluorescence may be affected by the presence of the dye molecules resulting in a contribution to the overall effect.

In comparison to *Figure 4.18* the sample pesticides were applied to the surface of the glass carrier material. The cover slip was coated with a *Rhodamine 6G* layer and the sample pesticides were applied in micro-drops on the dry layer. The experiment is shown in *Figure 4.19* whereby the same pesticides were used.

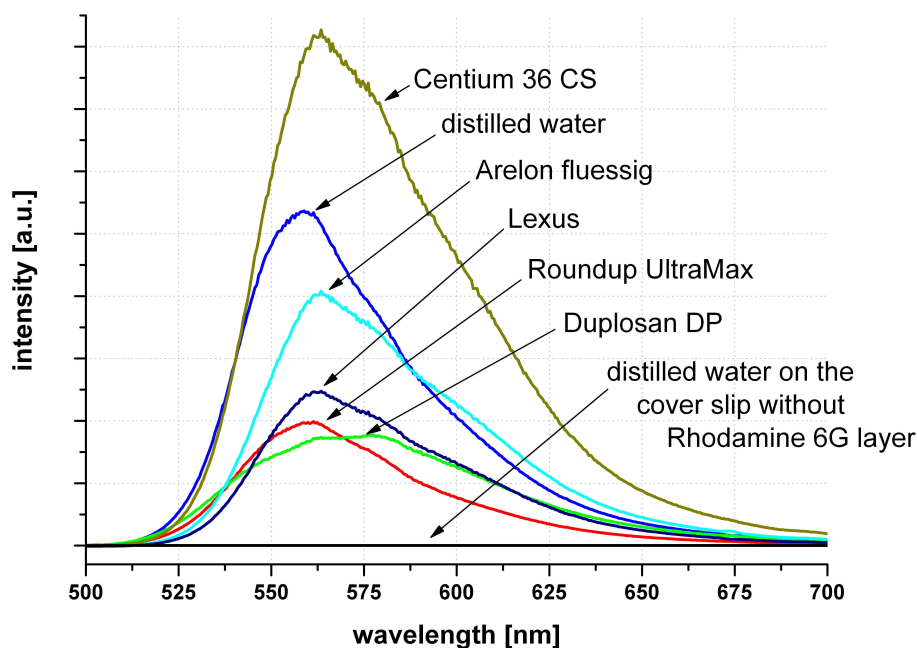


**Figure 4.19:** Fluorescence intensity of the particulate dye *Rhodamine 6G* as a layer on the surface of a cover slip. A drop (1  $\mu\text{L}$ ) of distilled water was added as reference and droplets (1  $\mu\text{L}$  each) of a sample pesticide. In addition, the fluorescence of a micro-droplet on the cover slip without a *Rhodamine 6G* layer is shown.

As can be observed in *Figure 4.18* the emission of the dry *Rhodamine 6G* treated leaf surface is very weak, and the distilled water droplet has the highest fluorescence intensity. This is because it contains no quenching compounds, which may be present in the matrix of the pesticide emulsion. Additionally, a shift in fluorescence wavelength can be observed with several of the pesticides under investigation and this will be addressed in the following section. Spectral shifts can also be observed in *Figure 4.19* but on the glass surface the fluorescence signals are different from the ones on the biological surface. *Centium 36 CS* exhibits an increased fluorescence intensity when compared to the distilled water droplet.

#### 4.1.4.2 Analysis of Spectral Shifts

As could already be observed in the previous sections, a spectral shift (in the fluorescence signal of the labeling dye) occurs when a droplet containing a pesticide is added to a surface coated with the fluorescence marker *Rhodamine 6G* (as a dry layer). Fluorescence emission of a drop of distilled water was used as reference in these experiments, meaning that spectral shifts are measured in relation to the emission of such a distilled

water micro-droplet. The sample pesticides were also solved in distilled water, indicating that wavelength shifts are results of the interaction of the pesticide active ingredient or its surfactants with the particulate dyes.

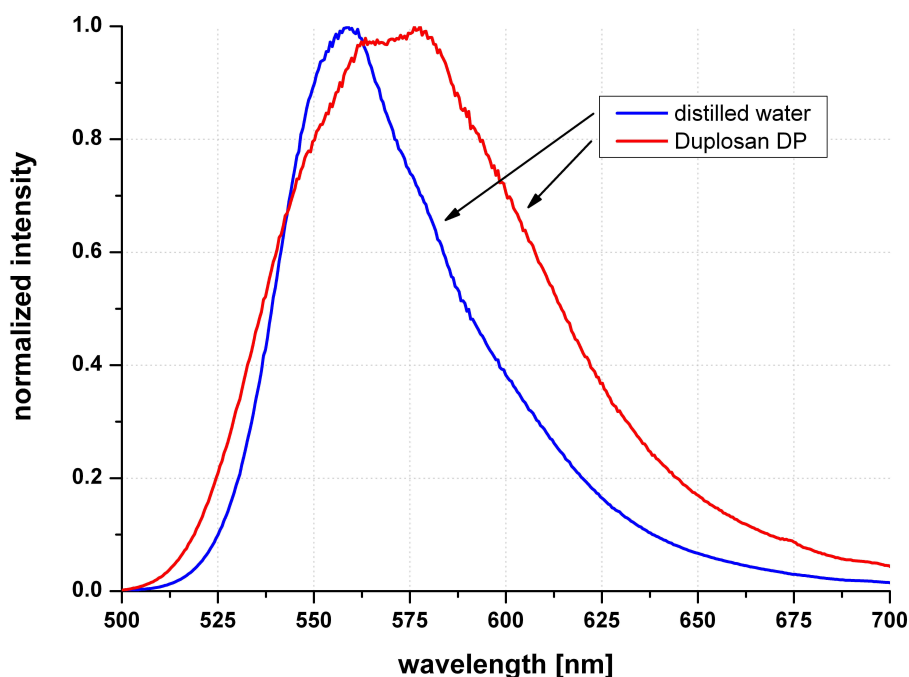


**Figure 4.20:** Shift in *Rhodamine 6G* fluorescence wavelength due to the interaction of the dye with a droplet containing the pesticide *Duplosan DP*. The fluorescence of a droplet of distilled water was used as reference and is also shown in this figure. Both spectra were normalized to emphasize the spectral shift of *Rhodamine 6G* in the pesticide containing droplet.

In order to emphasize spectral shifts, fluorescence spectra of *Duplosan DP* and distilled water were normalized as shown in *Figure 4.20*. Both, the pesticide droplet and a droplet of distilled water (1  $\mu\text{L}$  each) were applied to a leaf surface prepared with *Rhodamine 6G* dry layer. As seen in *Figure 4.20* the pesticide containing droplet can clearly be distinguished from the droplet of pure distilled water by a spectral shift in the *Rhodamine 6G* fluorescence.

The appearance of wavelength shifts in presence of a pesticide allowed a differentiation between a droplet of pure distilled water and a droplet containing such a pesticide. Moreover, further experiments indicated that the quantity of the wavelength shift depends on the concentration of the pesticide.

To analyze a concentration dependent wavelength shift, fluorescence spectra of *Rhodamine 6G* were recorded. The concentration of *Rhodamine 6G* was kept constant



(at trace level). A sample pesticide, *Arelon flüssig*, was applied at different concentrations. Spectral shifts were measured against the *Rhodamine 6G* fluorescence in distilled water (pesticide concentration of zero). In *Figure 4.21* this concentration dependent measurement is displayed, showing the quantity of the spectral shift as function of *Arelon flüssig* concentration.

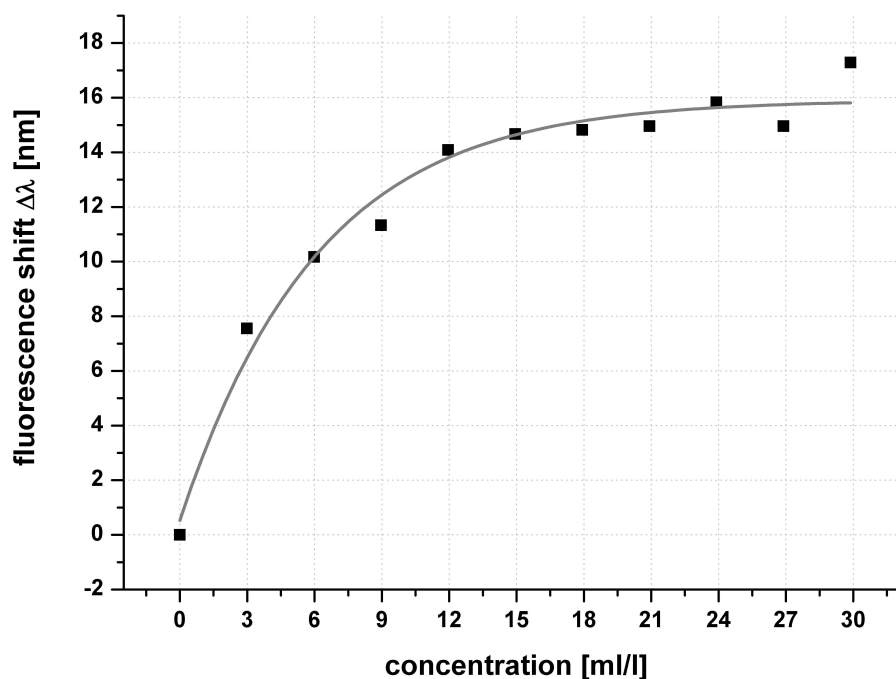


**Figure 4.21:** Spectral shift of the *Rhodamine 6G* fluorescence due to interaction with a droplet containing the pesticide *Arelon flüssig* at different concentrations. A concentration of zero is to be understood as distilled water without the pesticide. This was used as reference.

In *Figure 4.21* a pesticide concentration of zero indicates the measurement of distilled water and the spectral shifts at higher concentrations are measured in relation to this fluorescence signal originating in the dissolved *Rhodamine 6G* crystallites. The pesticide concentration for field application is about 30 mL/L for *Arelon flüssig* in water which is the highest concentration in *Figure 4.21*. This concentration was diluted several times using distilled water and *Rhodamine 6G* fluorescence maxima were recorded for each concentration. As shown in *Figure 4.21*, *Arelon flüssig* can be detected at low concentrations. A wavelength shift can be observed and its quantity is increasing with increased concentration of the pesticide until a plateau is reached (at about 15 mg/L for *Arelon flüssig*). This indicates that the shift can be used for analytical purposes, since the spectral shift is at its maximum value for concentration used in agricultural applications.

Such a shift in the fluorescence wavelength of the marker material could not be observed with all of the chosen pesticide samples (e.g. *Roundup UltraMax* as shown in *Figure 4.22*). With some, there is no shift or the quantity of the shift is very small (in the order of one nanometer or even less). Therefore, these pesticides can not be differentiated from distilled water. Also, very small shifts did not lead to assured results due to the heterogeneity of the biological material.

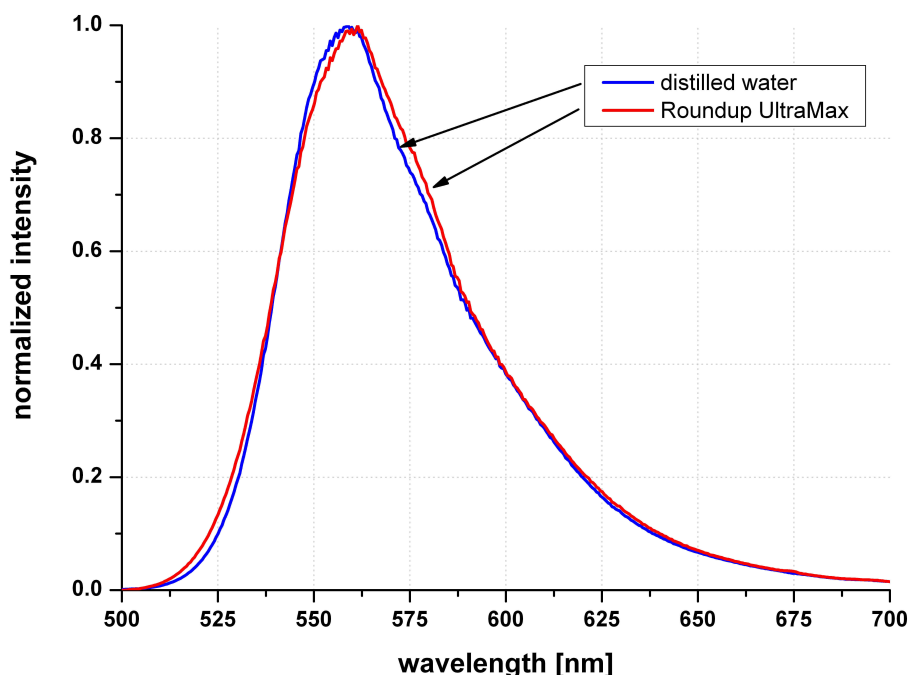


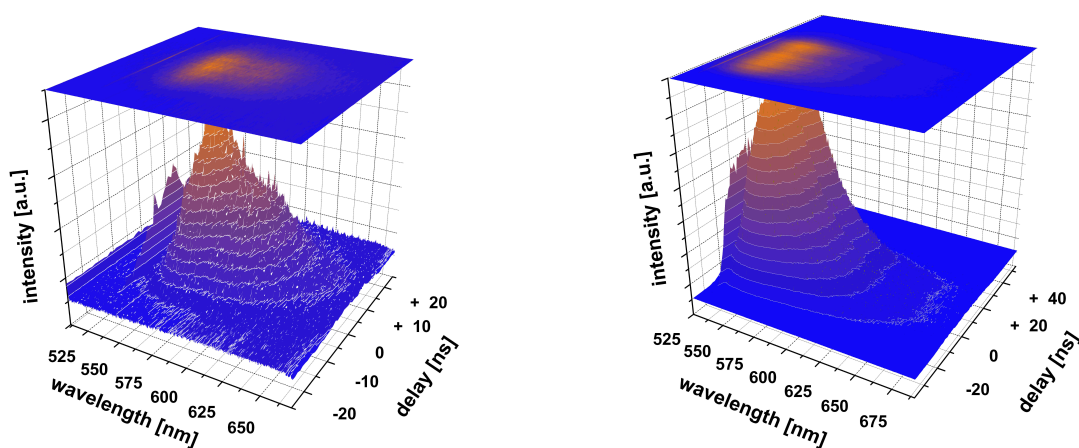
**Figure 4.22:** Shift in *Rhodamine 6G* fluorescence wavelength due to the interaction of the dye with a droplet containing the pesticide *Roundup UltraMax*. *Roundup UltraMax* is an example for a pesticide showing no spectral shift in comparison to the distilled water micro-droplet.

*Figure 4.22* shows the pesticide *Roundup UltraMax* in comparison to distilled water. *Roundup UltraMax* is an example of a pesticide showing no wavelength shift, or only in a very small quantity.

#### 4.1.4.3 Investigation of Fluorescence Decay Times

In addition to spectral shifts in the fluorescence wavelength of the marker substance, fluorescence decay times of this tracer material in presence of the sample pesticides were investigated. Time resolved measurements require more sophisticated components such as a delay generator and a gateable camera. For the analysis of fluorescence decay times,

the Nd:YAG laser system (for experimental setup refer to *Section 3.1.2*) was employed using a frequency quadrupled Nd:YAG laser beam ( $\lambda_{excitation} = 266$  nm) as excitation source. In addition to the fluorescence lifetime of *Rhodamine 6G* the decay times of the sample pesticides auto-fluorescence was recorded. This additional information, combined with the spectral data, may be used for a better compound identification.



(a) Time resolved fluorescence spectrum of *Rhodamine 6G* solved in distilled water in a cuvette.

(b) Time resolved fluorescence spectrum of *Rhodamine 6G* solved in distilled water applied to the surface of a leaf (*Hedera helix*).

**Figure 4.23:** Time resolved fluorescence spectra of *Rhodamine 6G* dissolved in distilled water. Measurements were done in (a) a cuvette and (b) on the surface of an ivy (*Hedera helix*) leaf. The experiments were done using the Nd:YAG-setup and for excitation the frequency quadrupled Nd:YAG laser emission was utilized at  $\lambda_{excitation} = 266$  nm.

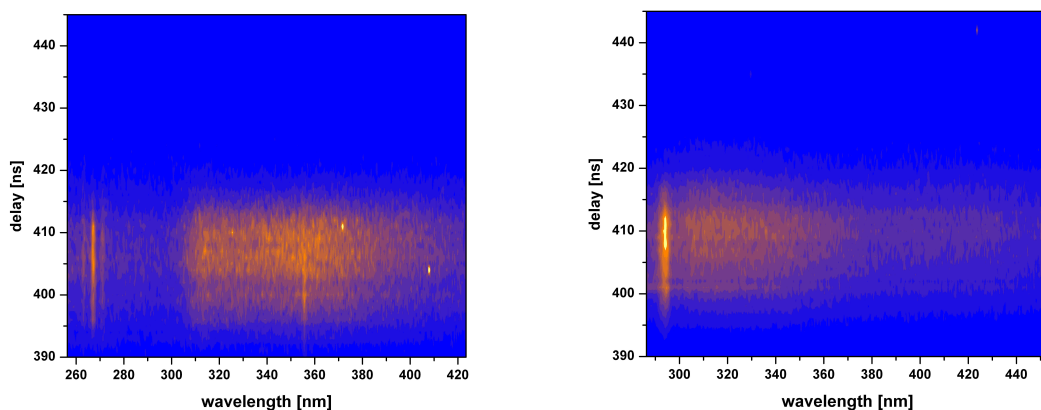
*Figure 4.23* shows the time resolved fluorescence spectra of the tracer material *Rhodamine 6G* solved in distilled water. In *Figure 4.23(a)* the experiment was carried out with the sample in a cuvette and in *Figure 4.23(b)* a droplet of the sample liquid was applied to the surface of an ivy leaf (*Hedera helix*) for comparison. As can be observed in *Figure 4.23*, the fluorescence life time is in same order of magnitude as the laser pulse duration and an application to the leaf surface did not alter fluorescence properties.

For a better identification of the compounds the fluorescence decay times of the pesticides were analyzed. As mentioned above this provides another property of the pesticide under investigation and in conjunction with the spectral data this may lead to a more precise compound identification. *Figure 4.24 (a)–(h)* provide time resolved measurements of the sample pesticides auto-fluorescence (from the nine sample pesticides, *Goltix 700SC* is omitted because no fluorescence signal could be observed when exciting with the Nd:YAG laser).

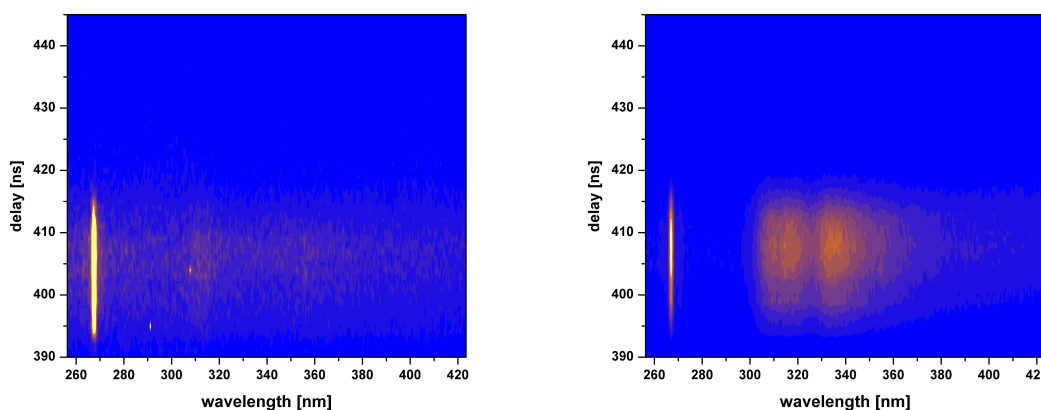
Contour plots of the time resolved auto-fluorescence spectra are given in the figures, and excitation was accomplished by the frequency quadrupled Nd:YAG laser at

$\lambda_{excitation} = 266$  nm. These time resolved measurements were carried out with the pesticide solution in a cuvette and fluorescence was monitored perpendicular to the incident laser beam as indicated by the diagram of the setup in *Section 3.1.2* (*Figure 3.2* on page 27).

The peak at  $\lambda = 266$  nm in *Figure 4.24* (a)–(h) results from Rayleigh scattering of the excitation radiation.



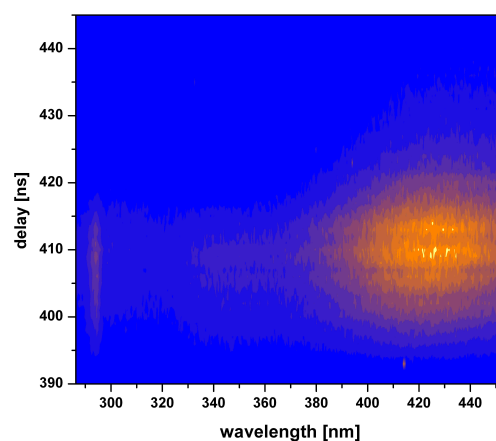
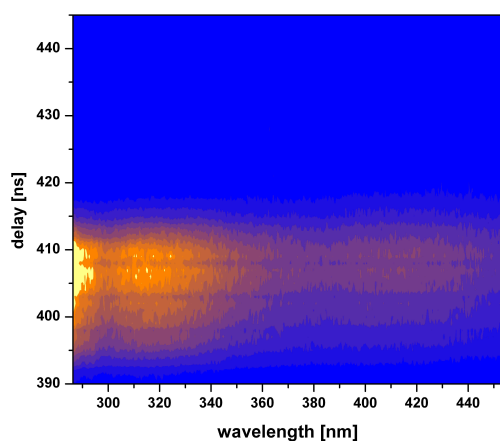
(a) Time resolved fluorescence spectrum of *Patoran FL*. (b) Time resolved fluorescence spectrum of *Roundup UltraMax*. Attention to a change in displayed spectral region.



(c) Time resolved fluorescence spectrum of *Du-plosan DP*. (d) Time resolved fluorescence spectrum of *Arelon flüssig*.

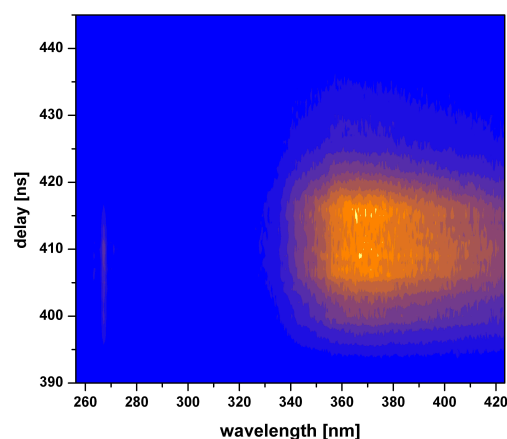
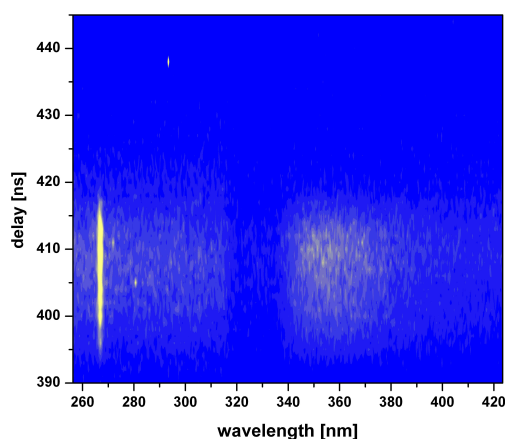
**Figure 4.24:** (a)–(d): Time resolved fluorescence spectra of the sample pesticides (refer to (e)–(h) for the second part of the sample pesticides, *Goltix 700SC* is omitted in these figures). Excitation was carried out using the fourth harmonic ( $\lambda_{excitation} = 266$  nm) of the Nd:YAG laser system. In (b) and (f) the Raman line of water can be observed at about  $\lambda = 293$  nm.

The peak at about  $\lambda = 293$  nm (notable in *Figure 4.24 (b) and (f)*) corresponds to the Raman scattering of the incident laser radiation in water (attention to a change in scaling in *Figure 4.24 (b), (e), and (f)*). The Raman signal of water can be found at a shift of ca.  $3400\text{ cm}^{-1}$  to the incident radiation, therefore, the Raman band was expected at about  $\lambda = 292$  nm which agreed very well with the measurement. It is noticeable that *Arelon flüssig (Figure 4.24(d))* showed two fluorescence maxima at about  $\lambda = 315$  nm and  $\lambda = 335$  nm.



(e) Time resolved fluorescence spectrum of *Centium 36 CS*. Attention to a change in displayed spectral region.

(f) Time resolved fluorescence spectrum of *Lexus*. Attention to a change in displayed spectral region.



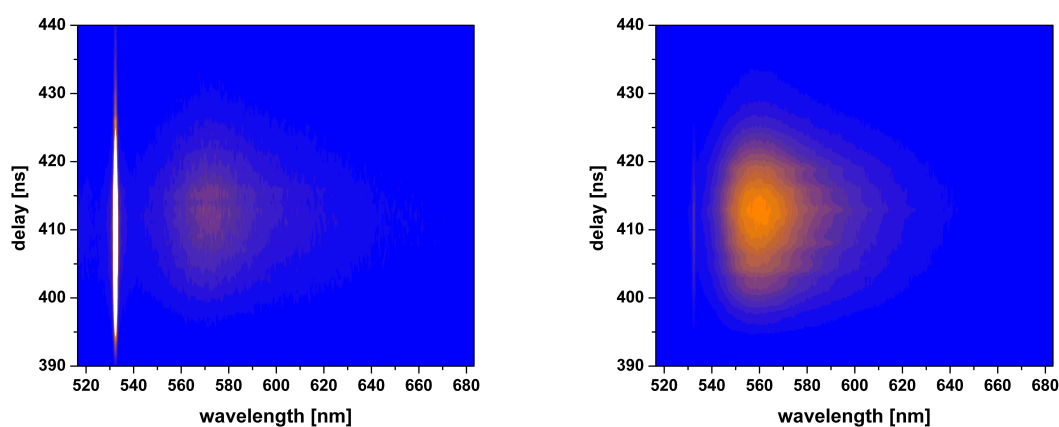
(g) Time resolved fluorescence spectrum of *Re-glone*.

(h) Time resolved fluorescence spectrum of *Gesatop 50*.

**Figure 4.24:** (e)–(h): Time resolved fluorescence spectra of the sample pesticides (refer to (a)–(d) for the first part of the sample pesticides). Excitation was carried out using the fourth harmonic ( $\lambda_{excitation} = 266$  nm) of a Nd:YAG laser system. In subfigure (f) the Raman line of water can be observed at about  $\lambda = 293$  nm. Attention to a change in displayed spectral region in (e) and (f).

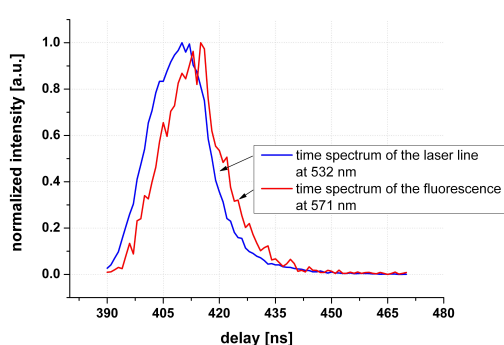
Figure 4.24 (e) to (h) are displayed in a second part of Figure 4.24. Here, the contour-plots of the time resolved auto-fluorescence of the remaining four sample pesticides are shown. The figure have been split in two parts for better representation of the data.

In comparison to the pesticides in a cuvette, a sample leaf (*Hedera helix*) was put on a stage which is movable in x- and y- direction. For the investigation the particulate dye *Rhodamine 6G* was added to the pesticides and a droplet of the resulting solution was applied to a leaf surface. Additionally, these experiments aim at the investigation of the influence of pesticides on the *Rhodamine 6G* decay time.

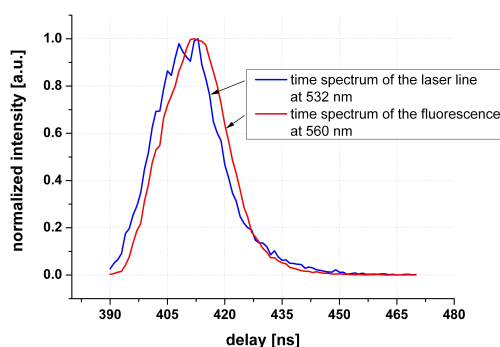


(a) Time resolved fluorescence spectrum of *Rhodamine 6G* solved in *Arelon flüssig* and applied to a leaf surface as droplet.

(b) Time resolved fluorescence spectrum of *Rhodamine 6G* solved in distilled water and applied to a leaf surface as droplet.



(c) Spectra along the time axis of (a) at  $\lambda = 532$  nm and  $\lambda = 571$  nm.



(d) Spectra along the time axis of (b) at  $\lambda = 532$  nm and  $\lambda = 560$  nm.

**Figure 4.25:** Time resolved fluorescence spectra of 200  $\mu\text{L}$  *Rhodamine 6G* solution (1.63 g/L) in (a) *Arelon flüssig* and in (b) distilled water. The solutions were applied to the surface of an ivy sample leaf (*Hedera helix*) and excitation was accomplished by the fourth harmonic of a Nd:YAG laser. Subfigures (c) and (d) are taken from the time resolved measurements at the laser line (at  $\lambda = 532$  nm) and at the fluorescence maximum (at  $\lambda = 571$  nm and  $\lambda = 560$  nm respectively).

Results of the experiments on a leaf surface are shown in *Figure 4.25* where the *Rhodamine 6G* fluorescence is displayed. Subfigure (a) illustrates the measurement of the pesticide containing droplet and in subfigure (b) a droplet of distilled water is displayed.

In *Figure 4.25* (c) and (d) no change in fluorescence decay times of the tracer could be observed in presence of the pesticide (both subfigures are taken from the time resolved measurements in subfigure (a) and (b) respectively). Furthermore, the decay time of the fluorescence tracer in the same timescale as the pulse length of the laser. Therefore, the fluorescence life time could not be easily read off the graph.

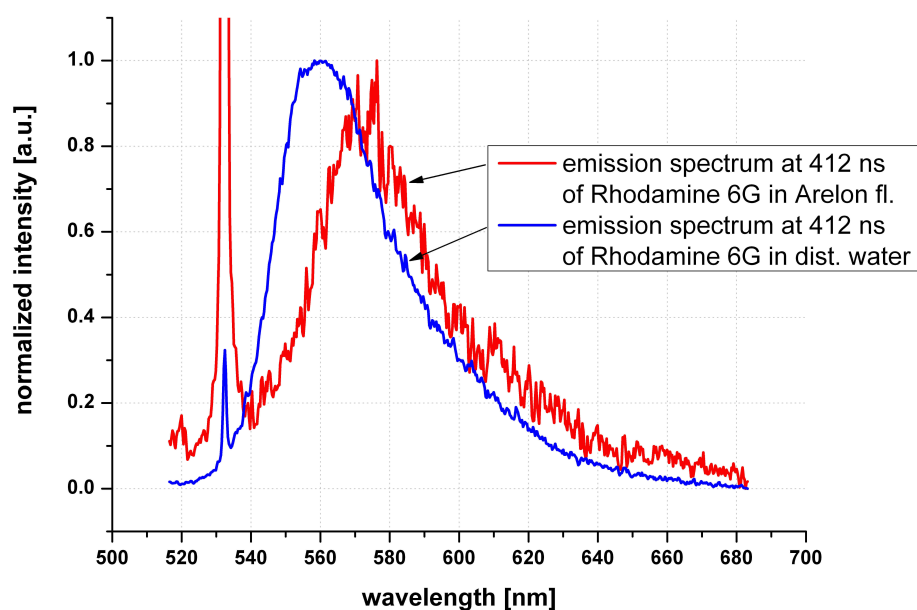


**Figure 4.26:** Emission spectra of *Rhodamine 6G* in *Arelon flüssig* and in distilled water on a leaf surface. Spectra are cuts from *Figure 4.25* (a) and (b) at a delay of  $t = 412$  ns.

The spectral shift is illustrated in *Figure 4.26*, where the emission spectra taken from *Figure 4.25* (a) and (b) at a delay of  $t = 412$  ns are presented. For comparison the presented spectra are normalized to the *Rhodamine 6G* fluorescence emission maximum.

Although spectral shifts could be measured (*Figure 4.26* and refer to *Section 4.1.4*) in presence of the pesticides, the properties of fluorescence life times seemed to be unaltered. This holds true for all pesticides under investigation, therefore the fluorescence life time  $\tau$  could not be used as an indicator for mapping droplets on a leaf surface. From a practical point of view, the recording of fluorescence decay spectra for a field application is also very problematic due to the more sophisticated and normally laboratory based equipment necessary.

On the other hand the time resolved measurement of the pesticide auto-fluorescence could be used for better characterization of a given pesticide. Therefore, this measurements can be used to retrieve additional information like the fluorescence life time  $\tau$ .

### 4.1.5 Obtaining Imaging Data of Pesticide Coverage on Leaves

In *Section 4.1.4* it was shown that spectral data provides enough information to detect a given pesticide on the surface of a leaf. These experiments were done at single measuring points, therefore, some kind of imaging became necessary for the assessment of coverage. In order to provide such data, experimental methods, a scanning technique and direct imaging, were examined and these investigations are presented in the following.

#### 4.1.5.1 Scanning Data

As shown in the previous section, the spectral shift of the *Rhodamine 6G* fluorescence can be used to monitor the presence of pesticides in a droplet and a droplet containing such a substance can be differentiated from a droplet of pure distilled water. The investigations of spectral shifts in the fluorescence wavelength suggests that these could be used to achieve mapping of pesticide coverage on a leaf surface. Therefore, a droplet containing a pesticide was applied to a sample leaf (*Hedera helix*) surface pretreated with a coating of *Rhodamine 6G*. The leaf was fixed on a stage, which could be moved in the horizontal plane, and irradiated from above with the laser beam. The laser radiation was focused by a lens system to the surface of the leaf in order to minimize the irradiated area. The stage was movable using micro-meter screws, which results in a lateral resolution of about 10  $\mu\text{m}$ .

The scanning experiments were conducted by focusing the laser beam on the leaf surface, recording a fluorescence emission spectrum and then moving the stage to the next position with the micro-meter screws. Thus, the focused laser beam was effectively moved in a line over the droplet (which was applied to the leaf surface) and at each measuring step a fluorescence spectrum was recorded. This results in a graph which shows the extend of the droplet. These measurements were carried out with a wet droplet and with a dried droplet. The wet droplet has the distinct disadvantage that it dried during the measurements, especially when irradiated by the focused laser beam. When the droplet has dried, however, the fluorescence intensity was much lower (as seen in *Figure 4.9* on page 47), but the signal could be detected nonetheless.



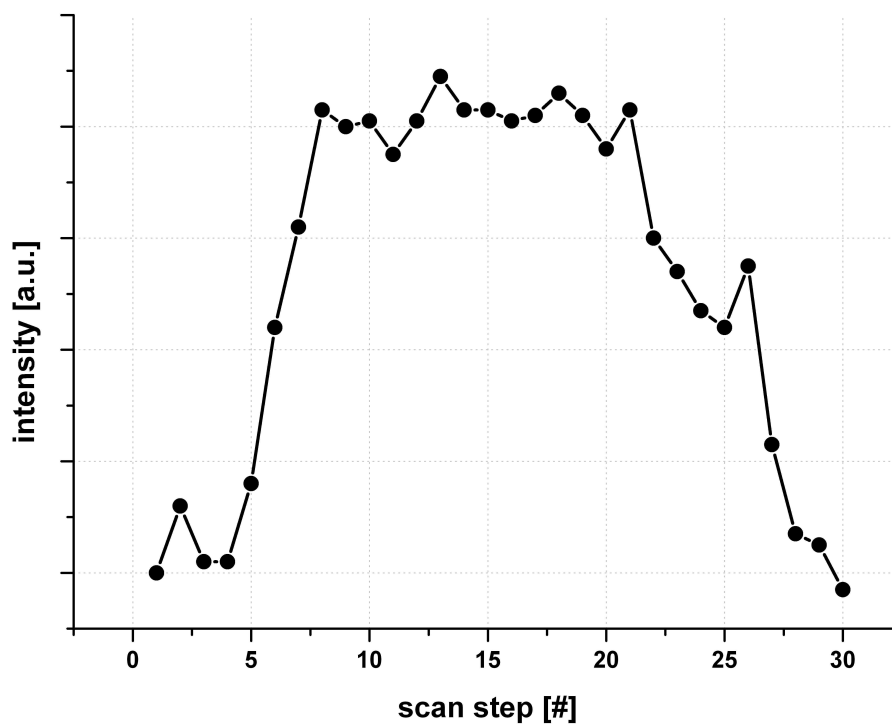


**Figure 4.27:** Scanning in a line over a droplet of pesticide applied to the surface of a *Rhodamine 6G* coated ivy leaf. Fluorescence spectra are recorded at each scanning step using a focused nitrogen laser beam as excitation source. The *Rhodamine 6G* fluorescence intensity at  $\lambda = 562$  nm is plotted against the position of the laser focus.

Fluorescence spectra were recorded in *Figure 4.27* and the *Rhodamine 6G* fluorescence intensity is plotted against the position of the laser focus. Scan steps were 0.125 mm and the graph shows that the droplet has a diameter of about 3 mm. For better illustration a three dimensional plot (*Figure 4.28*) was also added. It shows the full spectral information at every scan step, therefore, the graph in *Figure 4.27* is a cut along the scan axis at the position of the *Rhodamine 6G* fluorescence peak. With the three dimensional presentation, compound identification is also possible. Spectral shift can be detected, since these experiments provide the full fluorescence spectra at each measuring point.

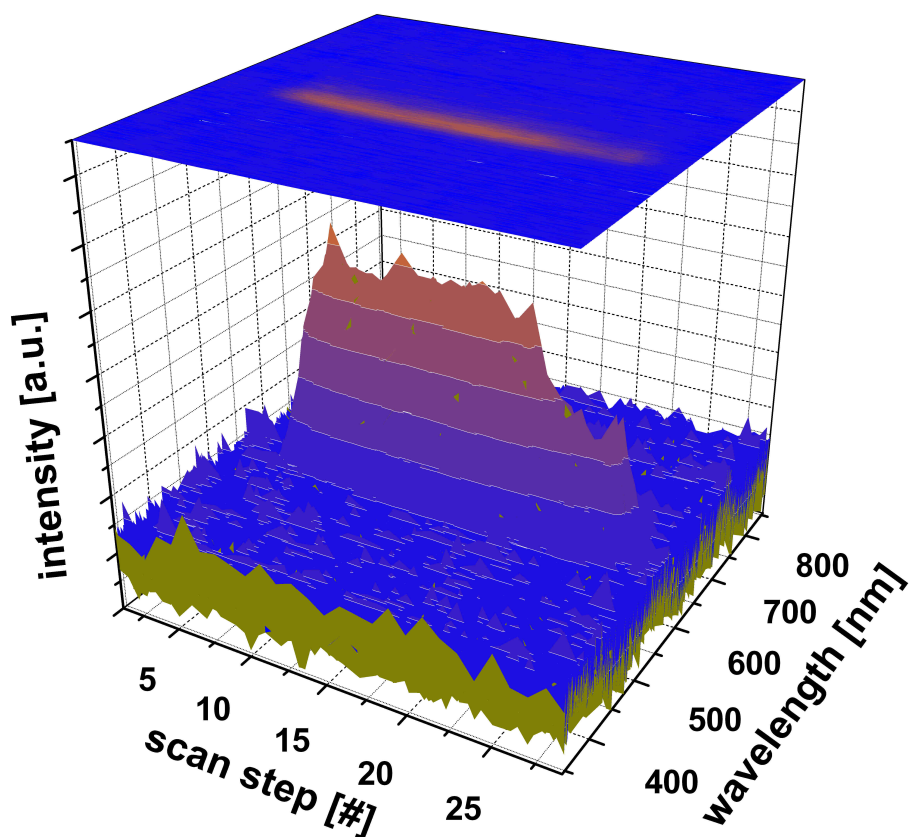


**Figure 4.28:** Scanning over a droplet containing *Roundup UltraMax* on a *Rhodamine 6G* coated ivy leaf. Full fluorescence spectra are shown at each scanning step over the droplet. *Figure 4.27* represents a cut through the wavelength axis at  $\lambda = 562$  nm.

This scanning experiments showed that the position of the droplet can be assessed on the leaf surface. This works even when the droplet has dried, which should be much easier to handle for field application. In an practical application some sample leaves could be taken and prepared with a layer of the fluorescence tracer material. The coverage of a pesticide spraying could then be monitored. Here, the feasibility of the proposed methods was shown, for any practical application, field experiments will have to be carried out.

#### 4.1.5.2 Imaging Data

As described in the above section, scanning over a droplet and determining its size can be done by recording the fluorescence intensity of the fluorescence tracer material (*Rhodamine 6G*) at every scan step. Due to interactions with a given pesticide, changes in fluorescence properties, such as wavelength shifts, can be monitored and used for identification of the pesticides and can also be utilized to assess coverage. The scanning process

can be done in lines and, thus, be used as an imaging tool which provides accurate and detailed results concerning the fluorescence parameter in question. Disadvantages being the time consumption of the process and that the sample leaf has to be fixed on a stage in order to carry out the scanning. Therefore, other imaging techniques were examined also in the view of field applicability.

**UV Lamp and CCD Camera as Low Cost Imaging System:** A simple and cost effective fluorescence imaging system consists of a UV lamp as excitation source and direct fluorescence detection using a CCD camera. As sample setup an UV-C lamp (taken from a clean bench) was used for irradiation of the ivy sample leaf. The leaf was coated with a layer of *Rhodamine 6G* on one half and left untreated on the other half. Then the sample pesticides were applied as droplets to both sides. Fluorescence emission was recorded by taking a picture with a commercially available digital camera (*Canon PowerShot A60*) as CCD detector.



**Figure 4.29:** Fluorescence image of an ivy leaf (*Hedera helix*) recorded by a digital camera. The right half of the leaf was pretreated with a *Rhodamine 6G* layer, the left side was left untreated. On both sides droplets containing the sample pesticides were applied (not visible on the left side). Irradiation was done using an UV-C lamp and the fluorescence of the dye dissolved in the droplets can be observed on the right side while on the left side (not pretreated with *Rhodamine 6G*) there is no notable emission.

In *Figure 4.29* an ivy leaf was taken and the right half was prepared with a layer of *Rhodamine 6G* while the left half was left untreated. Then droplets of pesticides were applied to the surface in a way that one was on the *Rhodamine 6G* treated side and one on the untreated side. The leaf was put under an UV-C lamp and a photo was taken with the digital camera. As can be seen, the droplets are clearly visible on the *Rhodamine 6G* treated side by the strong fluorescence signal of the dissolved dye, whereas the droplets on the untreated side are barely visible (therefore, only half shown). These strong signals stemming from the *Rhodamine 6G* micro-crystals dissolving in the water contained in the pesticide droplets.

For the purpose of mapping the droplet distribution on the leaf surface, this simple setup satisfies the requirements. The extent and location of the applied droplets can be determined. However, no spectral information is supplied in these measurements, therefore, an identification of the compounds contained in the droplets is not possible. Also, droplets of pesticides can not be discriminated from droplets of distilled water.

## 4.2 Quantification of Pesticide Colloidal Suspension

Typically, the retail version of the chosen pesticides comes with the active component and with surfactants or other substances in an emulsion. This emulsion helps the active component to be solved in water and to get to its place of action once applied. The solubility of the active component itself is usually very low, therefore, water with pesticide reaching the soil is likely to contain these active components. Due to their low solubility in water they are likely to form colloids which may not be detected by water standard chemical analysis due to their small size (smaller than  $0.45\ \mu\text{m}$ ). Furthermore, these colloids are likely to be existent in low concentrations.

### 4.2.1 Breakdown Probability Detection

For the purpose of the detection of small colloids in water and for the detection of these substances at low concentrations, a laser induced breakdown detection (LIBD) setup (refer to *Chapter 3*) was used. Employing this method a focused laser beam is used for plasma generation and breakdown events are recorded by a digital video camera (e.g. in *Figure 4.30*).

In the example measurement (*Figure 4.30*) the laser beam propagates from left to right (the picture was rotated after the measurements, therefore, the laser beam runs from bottom to top in the figure). Pulse energy is adjusted to such a value that the plasma breakdown threshold in the sample is exceeded and emission of plasma events (in the form of yellow and reddish circles) can be observed (multiple events were recorded in in this figure, because the laser power is set to a high value).

Recapitulating the description given in *Chapter 3*, the laser pulse energy is adjusted just below the plasma breakdown threshold of the sample liquid, distilled water in this case. Thus, no emission will be observed in the pure liquid, but when investigating a colloidal suspension, the presence of the solid particulates will cause a plasma generation when entering the focal region (due to their lower plasma breakdown threshold value).

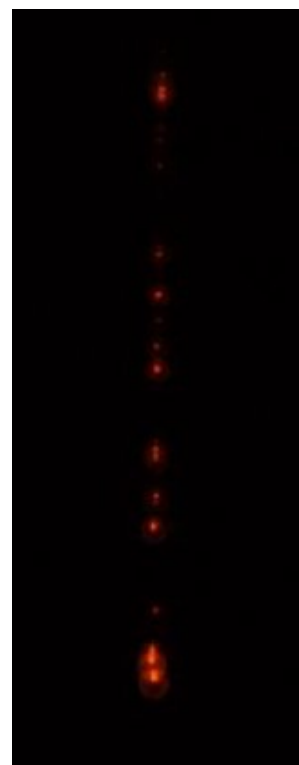


**Figure 4.30:** Picture taken by the digital camera. Here, multiple events are shown in the path of the laser beam (the laser beam runs from bottom to top).

These experiments were carried out using a pulsed laser system and a detection of events was done at every pulse. This registration of pulses results in a breakdown probability, which is the number of observed plasma events per number of laser pulses. Furthermore, the optical measurement of plasma emission allows the registration of the position of the events in relation to the laser focus. By superimposing a lot of these pictures a region can be determined where plasma ignition is possible and from the extent of this region together with the breakdown probability the particle size can be determined.

In the example shown in *Figure 4.30* plasma events of varying intensities could be observed ranging from strong events to a very weak emission of radiation. For the calculation of breakdown probability the number of laser pulses initiating plasma events per total number of pulses is determined. At every laser pulse a picture was taken and, therefore, all pictures containing visible events are counted. Here lies the difficulty, since the counting of visible events is done by hand (judging events by eye). Some events are so weak, that they only became visible after processing the picture. The judgment by human eye would not register such weak events, thus, underestimating the breakdown probability. Also, the data may not be comparable since the content of very weak events may vary from series to series.

An assortment of these different events is shown in *Figure 4.31*. These images are cutouts of  $80 \text{ pixel} \times 80 \text{ pixel}$  taken from the recorded photos (A recorded picture was  $800 \text{ pixel} \times 600 \text{ pixel}$  in size and stored in the *jpg*-format). *Figure 4.31 (a) – (e)* illustrates plasma emission intensity in descending order and in *(f)* a picture without event is shown for comparison.

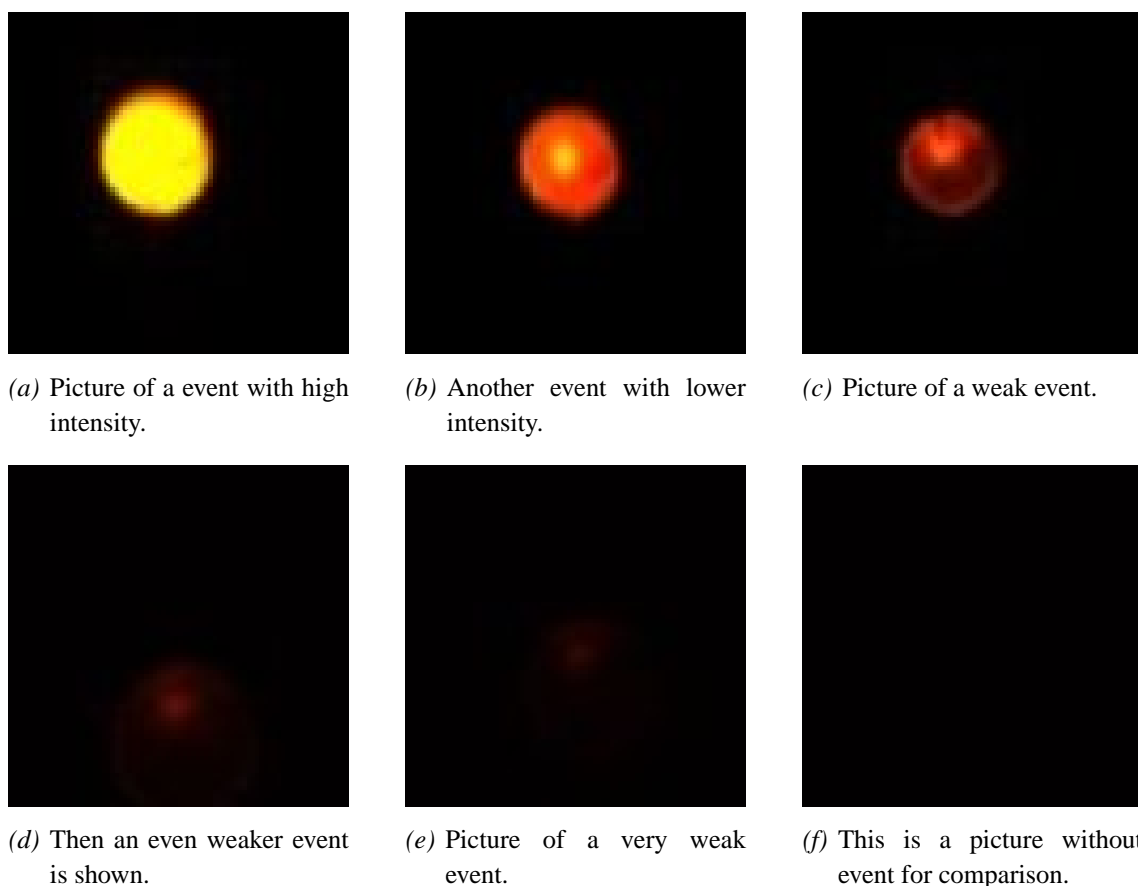


**Figure 4.31:** Cutouts of pictures taken by the camera. Event intensity is descending through *Figure 4.31 (a) – (e)* and in *Figure 4.31(f)* a picture without event is shown for comparison.

As already mentioned before, determination of breakdown probability bears the difficulty of defining an emission as plasma event. Counting pictures containing events in *Figure 4.31*, when done by the human eye, would result in counting the events in the subfigures (a) – (c). In (d) and (e) events are likely not to be registered, especially when taking the whole picture into account not only a small part. To achieve a measure of independence from the observer, a computer program was used later on for automated data analysis (refer to *Section 4.2.2*, but in principle, this yields similar difficulties in defining an event).

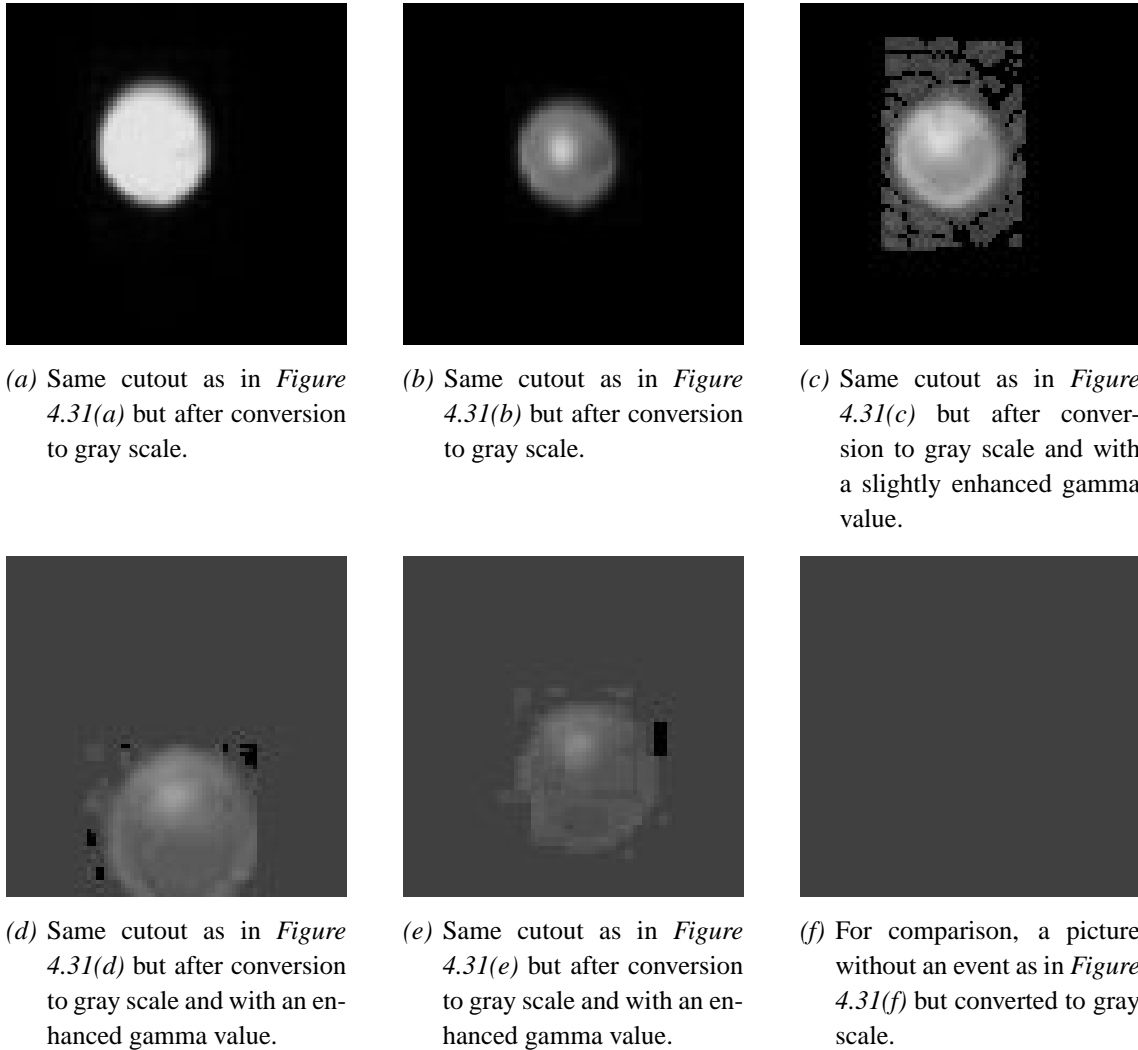


**Figure 4.32:** Cutouts of pictures taken by the camera. *Figure 4.32 (a) – (f)* correspond to *Figure 4.31 (a) – (f)* but here the pictures are processed. All figures were converted to gray scale and subfigures (c) – (f) also have an enhanced gamma value to show events clearly visible.

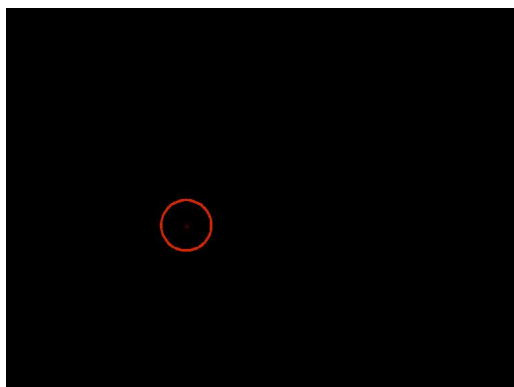
In order to get a more accurate count of plasma events and, thus, breakdown probability, the photos are processed by enhancing the gamma value, contrast, and brightness. *Figure 4.32* illustrates the same cutouts as *Figure 4.31* after conversion to gray scale. Additionally, the gamma value has been enhanced in subfigures (c) – (f).

To illustrate the difficulty of defining a threshold value for the counting of events the following pictures are shown. In contrast to the cutouts above, the whole pictures of  $800 \text{ pixel} \times 600 \text{ pixel}$  as recorded are shown in *Figure 4.33*.

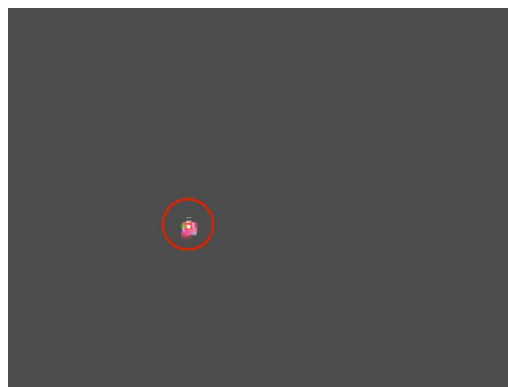
In *Figure 4.33* a very weak event is presented. Here, the processing of the picture became necessary in order to correctly recognize a plasma event. Like in the cutouts above, the pictures had to be processed by enhancing the gamma value, adjusting brightness, or



manipulating contrast. The event in this picture can barely be seen and is, therefore, marked by the red circle.



(a) Picture of an event as recorded by the camera. This event is very weak, so the judgment by hand is barely sufficient for counting breakdown events (The event can be seen in the middle of the red circle).



(b) Same picture as shown in subfigure (a). Here, contrast and brightness are adjusted to much higher values so that the event can be seen more clearly (The red circle marks the event the same as in subfigure (a)).

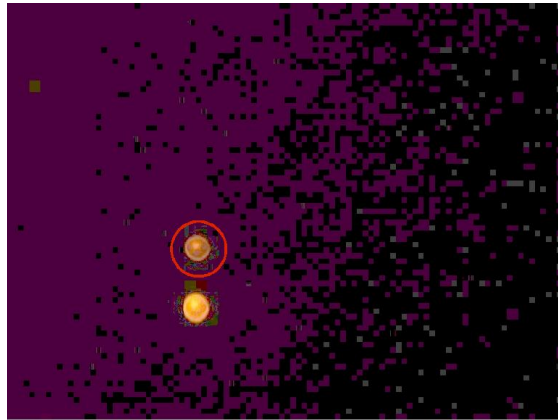
**Figure 4.33:** A recorded picture of a weak event is shown. *Figure 4.33(a)* shows the picture without post processing as recorded by the camera. In *Figure 4.33(b)* the same plasma event is shown but brightness and contrast were adjusted to illustrate the event more clearly.

A series of measurements contains several hundred pictures, therefore, it is a very time consuming process and a data analysis software is required. Refer to *Section 4.2.2* for evaluation of this data by a *MatLab* program. Additionally, the laser pulse can cause several particles in the focal region to generate a plasma (for discussion of multiple events refer to *Section 4.2.3.1*).

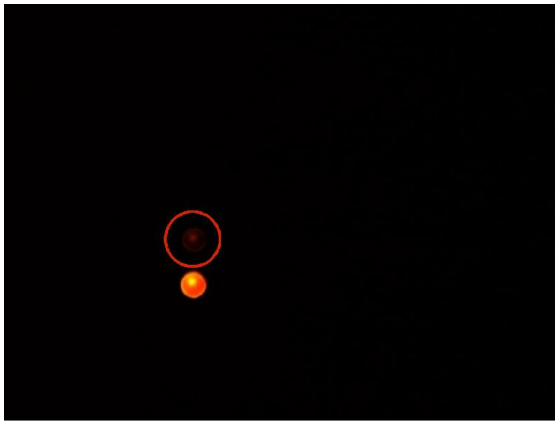
In the next figures there are two events in each picture for better comparability of their plasma emissions. One of these events shows a high intensity the other emission is much weaker (*Figure 4.34(a)*). In the second figure taken from the same experiment (*Figure 4.34(c)*), a strong signal is shown and also a very weak signal which can barely be seen by eye. *Figure 4.34(e)* shows weak and very weak signals. Additionally, in *Figure 4.34(b)*, *(d)*, and *(f)* corresponding pictures (to the subfigures *(a)*, *(c)* and *(e)*) with enhanced gamma value for highlighting the different events are shown.



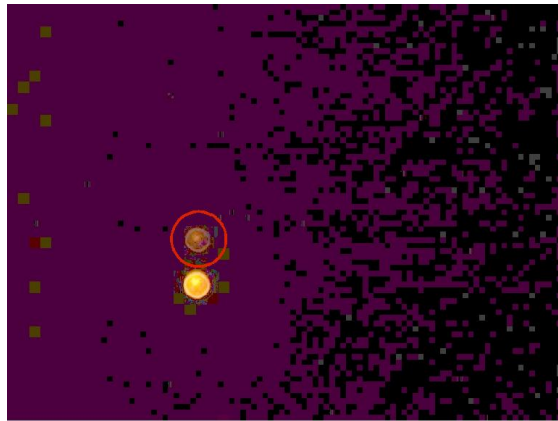
(a) Picture of a strong event and a weak event. An event of high intensity looks like the one shown here, but many events look like the weak event.



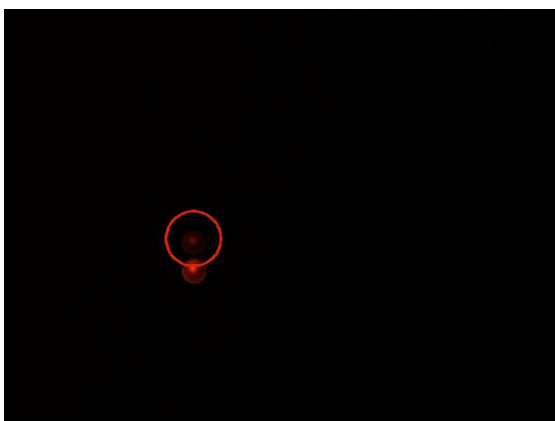
(b) Same picture as in (a) with enhanced gamma value. The weak event is shown more clearly.



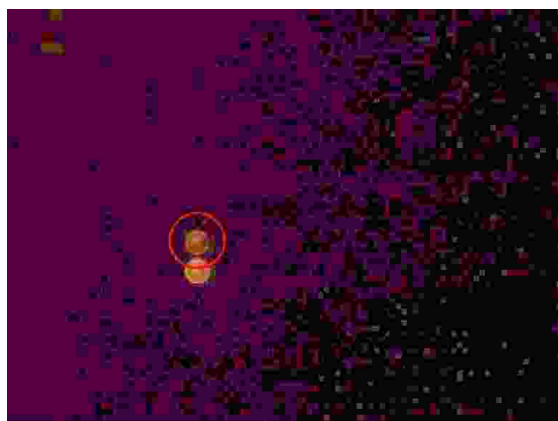
(c) Picture of a strong event and a very weak event. The very weak event is chosen to illustrate the different intensities observable.



(d) Same picture as in (c) with enhanced gamma value.



(e) Picture of a weak event and a very weak event. Here, also a very weak event is shown. There are also events which can not be observed by eye, therefore, a post processing of the pictures is necessary.



(f) Same picture as in (e) with enhanced gamma value. Here, also the weak event can be observed more clearly. In some pictures it's the only way to show these weak events.

**Figure 4.34:** Pictures taken by the camera with two events each ((a)–(f)). The event with lower intensity is marked by a red circle. The pictures in the right column ((b), (d) and (f)) are the corresponding pictures with enhanced gamma value ((a) corresponds to (b), (c) to (d) and (e) to (f)).

In *Figure 4.34(c)* and *(e)*, two events are shown, where one exhibits a weak plasma emission. When enhancing the gamma value in all the pictures, the breakdown probability would differ from a probability derived by using the unaltered records, depending on the number of weak events. In the gamma enhanced figures an inhomogeneous background could also be observed. The background signals are of higher intensity on the left hand side of the recorded pictures than on the right hand side. This can cause the recognition of false events when using an automated data evaluation (refer to *Section 4.2.2*).

In the first test measurements and in experiments to adjust parameters of the setup like the laser beam diameter or pulse energy, evaluation of the recorded pictures was done by visible detection (counting events by looking at the pictures). Due to the problem of correctly counting all events and recognizing them as such (as shown in the above sample pictures), results for breakdown probability were likely to be underestimated.

#### 4.2.1.1 Breakdown Probability at Varying Colloid Concentrations

For a test of the LIBD setup, samples containing silica dioxide ( $\text{SiO}_2$ ) particles in different concentrations were prepared. Silica colloid powder was solved in distilled water and left in a sedimentation column. The first sample (*Sample09*) contained colloids of  $2\ \mu\text{m}$  size at a concentration of  $8.6 \cdot 10^7\ \text{cm}^{-3}$  and a second sample (*Sample10*) particulates of  $0.35\ \mu\text{m}$  in a concentration of  $2.0 \cdot 10^{10}\ \text{cm}^{-3}$ . Both sample colloidal suspensions were diluted several times and this series of different concentrations was used in the measurements.

Samples were prepared in a laboratory but no special clean room was used. Therefore, all samples could also be contaminated after production by particulates in the ambient air or by contamination in the distilled water (distilled water was used and not special ultra pure water). Additionally, when filled into the measuring cuvette, this cuvette did not have a cover and, furthermore, it was reused in the experiments and there may have been some residue of the previous measurement left.

In initial experiments the sample with the highest concentration was measured in comparison to distilled water in order to test the setup and investigating feasibility of the selected method. Beam power and diameter were adjusted to match the conditions required for carrying out the investigations. Changing the beam diameter was accomplished by using an iris aperture and pulse energy was monitored with the help of a power meter (refer to *Chapter 3*). A small beam diameter of about  $3\ \text{mm}$  was used in the experiments to minimize scattering in the sample before the focal area and slight variations in the diameter resulted also in an adjustment of pulse energy.

In the investigations, pulse energy was adjusted by the iris aperture, which leads to variations in beam diameter. Originally, the laser beam had a diameter of about  $9\ \text{mm}$  before the iris. After passing the iris, depending on the adjusted energy value, the beam diameter

varied from 2 mm to 3 mm (the power adjustment at the laser unit itself was not suited for slight variations needed in these experiments, therefore the iris was required).

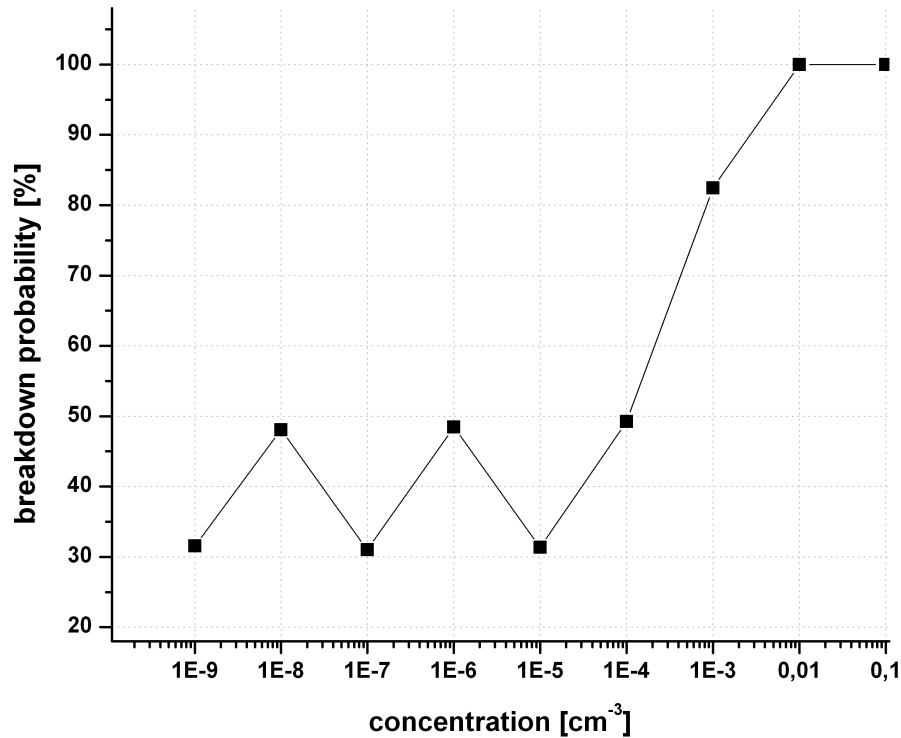


**Figure 4.35:** Breakdown probability in dependence of the concentration of *Sample 11*. Breakdown probability was calculated by counting visible events (see also *Figure 4.31* and *Figure 4.32*). All concentrations were measured at a fixed laser pulse energy.

In *Figure 4.35* the breakdown probability is shown over the concentration of the sample under investigation. Concentration is given in relation to the concentration of a given prepared sample. The prepared sample was diluted in several steps (ten times in each step) and for the resulting series of concentrations, breakdown probability was investigated. These measurements are shown in *Figure 4.35*.

A camera was coupled to the laser monitoring single pulses and store the resulting series of pictures on a computer. Due to filtering the pictures without plasma events appear black and events appear yellow to red (refer to *Figure 4.30* or *Figure 4.31*).

#### 4.2.1.2 Breakdown Probability at Varying Laser Power

Instead of measuring a series of different concentrations at a fixed laser power, the laser power was varied in these experiments at a fixed concentration. These investigations were

carried out for two different samples and for distilled water. The two samples were of different particle size, but chosen such that their concentration matches closely (*Sample09*, *Sample10* and distilled water are shown in *Figure 4.36*). Laser power was adjusted by the iris aperture, and this also means a change in beam diameter (affecting scattering, power density, etc.). At high laser power this results in a greater beam diameter, which in turn, leads to more scattering in the sample and thus produces unreliable results (breakdown threshold may not be reached at the focal region, if too much radiation is scattered). In these experiments the beam diameter was adjusted from as small as possible to about 3 mm (The diameter of the laser beam before the iris was about 9 mm).

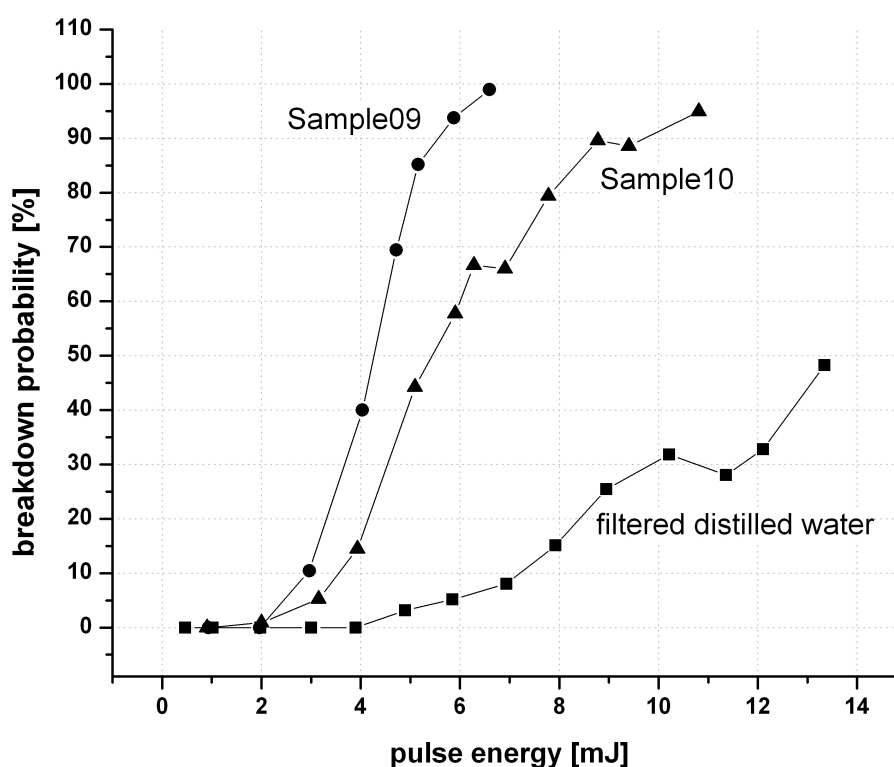


**Figure 4.36:** Breakdown probability of *Sample09* (Silica concentration of  $2.0 \cdot 10^5 \text{ cm}^{-3}$ ), *Sample10* (Silica concentration of  $8.6 \cdot 10^4 \text{ cm}^{-3}$ ) and filtered distilled water over pulse energy is shown. Pulse energy was measured using a power meter and adjusted by opening and closing an iris aperture. Influence due to changes in beam diameter (by opening the iris) are neglected at the pulse energy range in this experiment.

*Figure 4.36* shows the investigation of the breakdown probability in dependence of the adjusted laser pulse energy at the two samples (*Sample09* and *Sample10* as described above) and distilled water. The sample colloid suspensions can be differentiated by their breakdown probability and both can be distinguished from the distilled water. The distilled

water sample is measured as control and even at a laser pulse energy of about 14 mJ it exhibits a breakdown probability of approximately fifty percent. *Sample09* is in the shape of a *S*-curve and would reach one hundred percent breakdown probability at a pulse energy of about 7 mJ. *Sample10* also roughly resembles a *S*-shaped curve and here breakdown probability of one hundred percent would be reached at about 12 mJ pulse energy.

*Sample09* contains particulates of greater size (average diameter of 2.0  $\mu\text{m}$ ) than *Sample10* (average diameter of 0.35  $\mu\text{m}$ ) and bigger particulates have a lower plasma breakdown threshold (refer to *Section 2.2*). This can be observed in *Figure 4.36*. With increasing pulse energy, laser plasma breakdown probability also increases. The bigger particles (*Sample09*) require less energy for plasma generation. Thus, they would reach one hundred percent breakdown probability at lower pulse energy values than the smaller particles (*Sample10* at a nearly matching concentration), which would require higher pulse energy values for plasma generation.

In distilled water the breakdown probability also increases with increasing laser pulse energy, but even at the highest applied pulse energy (of ca. 14 mJ) a breakdown probability of about fifty percent was reached. This also agrees with the theory, since the method is based on the different breakdown threshold values for liquids and solids. Threshold values for liquids should be higher than for solids, therefore, the distilled water requires higher pulse energies for plasma generation. For detection of particulates, exactly this fact is used, and laser pulse energy is adjusted just below the threshold value in water, so that any solid particulate in the focal region would cause a plasma event and can be detected in this way (refer to *Section 2.2*).

### 4.2.2 Automated Data Evaluation

As already mentioned in the above sections, in the first test measurements evaluation of events was done by hand, meaning the judging of events in a recorded picture was done by looking at it by eye of the observer. This may result in a wrong estimation of breakdown probability due to hardly visible events (for examples refer to *Figure 4.31*) when the recorded pictures were not processed. After processing recognition of events became more reliable (refer to *Figure 4.32*) but was very time consuming, since such experiments are composed of many measurements containing several hundred pictures. Therefore, in order to obtain more reproducible results and investigate a great many data files, an automated evaluation of the recorded frames was desired.

For this purpose a *MatLab* algorithm was designed, which can find breakdown events in the pictures and estimate the area in pixel. As a short explanation, the pictures of events were converted to gray scale and then a filter was applied to even the background. In a next step an edge-finding algorithm was applied, which detected gradients in the color

(gray) value and thus outlined events. The edge was thickened in some steps and if they formed a closed outline the interior was filled. If such an area existed, this was counted as an event.

The *MatLab* algorithm was applied to the recorded pictures in order to find events and to calculate the breakdown probability. The automation in the evaluation of the data was necessary due to the large amount of recorded pictures and in order to achieve an independence of human judgment in the decision if there is an event or not.

Defining an event was still a problem because of errors in event recognition due to high background signals. This may lead to very small areas of a few square pixel which resulted in a wrong assessment of breakdown probability. To circumvent such errors, a threshold value had to be defined, separating area to count as an event from areas not counting as event. Defining such a threshold value also holds some difficulties.

#### **4.2.2.1 Counting Breakdown Events in Colloidal Suspension**

For counting breakdown events with help of the *MatLab* program as described in the introduction of this part (*Section 4.2.2*), it was necessary to take pictures which are synchronized with the laser pulse. This is done to make sure that if a plasma is generated by the laser pulse, this event is monitored and, else, a picture without an event is recorded. For reliable statements, several hundred of such pictures were taken in order to calculate the breakdown probability. The program estimated the area of events in pixel as shown in the following figures. An example picture is used in the subsequent steps of the program to illustrate how the algorithm works.



**Figure 4.37:** Picture as taken by the camera. Plasma event can be observed as yellow emission of radiation and in the following series of illustrations this event is used to show the function of the *MatLab* algorithm.

*Figure 4.37* is taken as an example for a recorded event which can be seen as yellow and red emission on a black background. In several steps the program will find the edge of the event and will estimate its area in pixel.

In the *Figure 4.38* the same picture is shown with the event outlined as the *MatLab* program found the edge. The first step in processing the picture is a conversion to gray scale, therefore, the gray scale picture is also shown in *Figure 4.38* in the subfigures (c) and (d) ((d) is the magnified event corresponding to (b)).





(a) The original color picture is shown. As overlay the detected edge is added outlining the plasma event.

(b) The original color picture as in (a) with the detected edge. The section containing the event is magnified for better illustration.

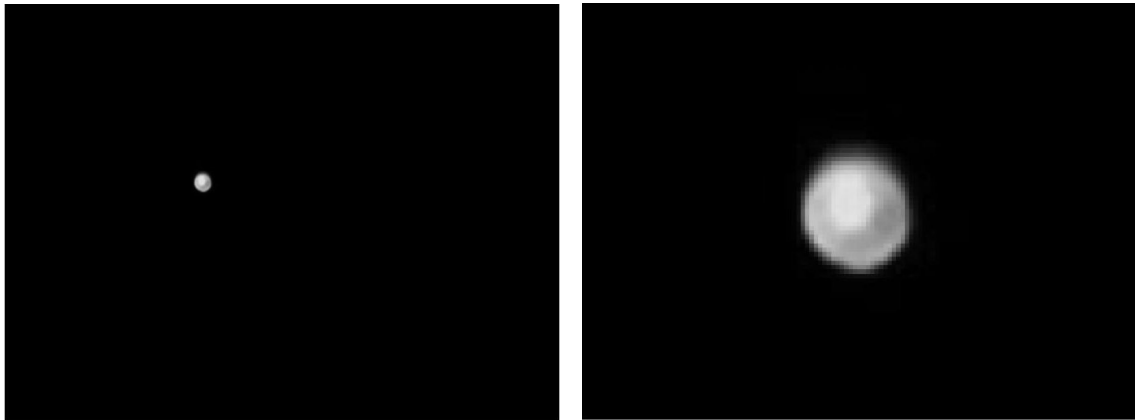


(c) Same picture as in (a) after conversion to gray scale. Conversion to grayscale is the first step in the program. Here, the edge is also overlaid as white line.

(d) The gray scale picture with the detected edge and the section containing the event magnified.

**Figure 4.38:** After processing the pictures with the program, events are recognized. The detected edge is shown as overlay to the sample picture (*Figure 4.37*) in subfigure (a) and the section containing the plasma events is also magnified as shown in subfigure (b). Subfigures (c) and (d) show the same measurement as subfigures (a) and (b) respectively but after conversion to gray scale as done by the program in a first step.

In order to obtain the area of events in pixel the program detects an edge as shown in *Figure 4.38*. The program converts the recorded picture to gray scale and then, in a second step a filter is applied to even out the background. In *Figure 4.39* the first two steps for the example picture (*Figure 4.37*) are shown. In the following the examples of the processing steps will be illustrated in the same way; the original sized picture on the left hand side and a magnified section containing the event on the right hand side.



(a) Picture as shown in *Figure 4.37* converted into gray scale.

(b) Magnified section of subfigure (a) containing the plasma event.



(c) A filter is applied to even the background. In this case no difference to the gray scale picture can be detected, but in measurements without event this filtering is necessary (refer to *Figure 4.40*).

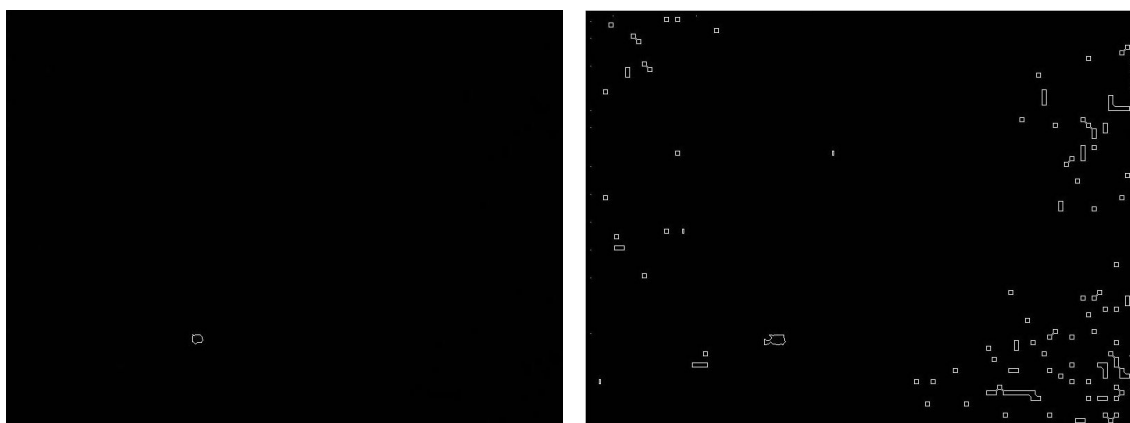
(d) A filter is applied to even the background and the section containing the event is magnified.

**Figure 4.39:** In a first processing step the recorded picture is converted to gray scale and then a filter is applied to even out the background. The function of the filter is more evident at pictures without event (refer to *Figure 4.40*).

After conversion to gray scale a filter is applied as shown in *Figure 4.39* (c) and (d). Here, no difference to the gray scale pictures in *Figure 4.39* (a) and (b) can be observed.

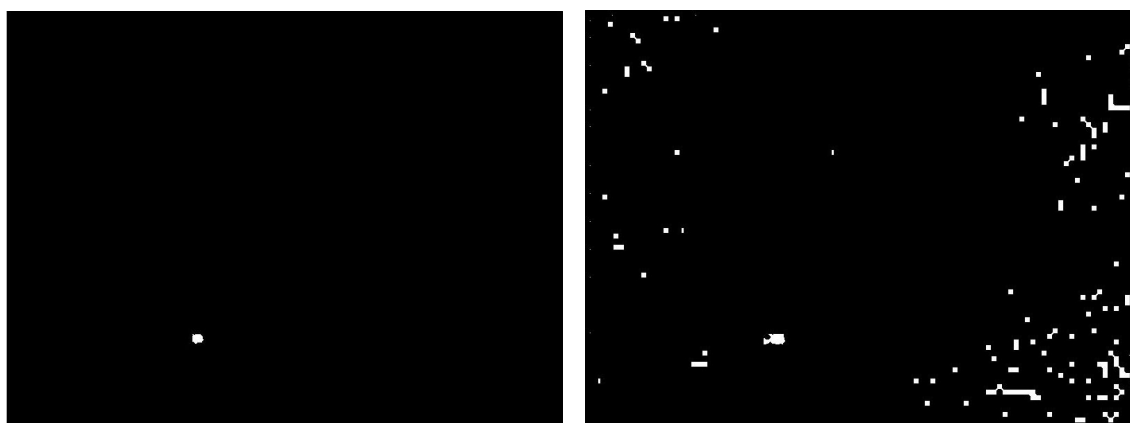
The necessity of the filter becomes more evident by processing a picture without event. In such a case the algorithm will detect very small gradients resulting in a huge overall area, which adulterates the measurements when leaving the filter away.

An example of such a case is shown in *Figure 4.40*. Here, a picture without event is processed using the filter in subfigure (a) and the processing without filter in subfigure (b). The pictures shown in *Figure 4.40* illustrate the last processing step and the steps in between are omitted in order to show the function of the filter.



(a) Measurement of a weak event, outlined as recognized by the program.

(b) Same processing as in (a). The event is outlined as recognized by the program but without applying the software filter.



(c) Same event as in (a). Here, interior gaps are filled as described in *Figure 4.41*.

(d) Same processing as in (c) but without applying the software filter.

**Figure 4.40:** Processing of a weak event, with and without using a filter. In (c) and (d) interior gaps are filled as described in *Figure 4.41*.

After conversion to gray scale and application of the filter an edge detection algorithm is used. It detects gradients in the color (or gray) value and finds an edge in this way (refer to *Figure 4.41*). At first gradients in the gray value are detected and the edge is outlined in white as shown in *Figure 4.41* subfigure (a) (or magnified in subfigure (b)).

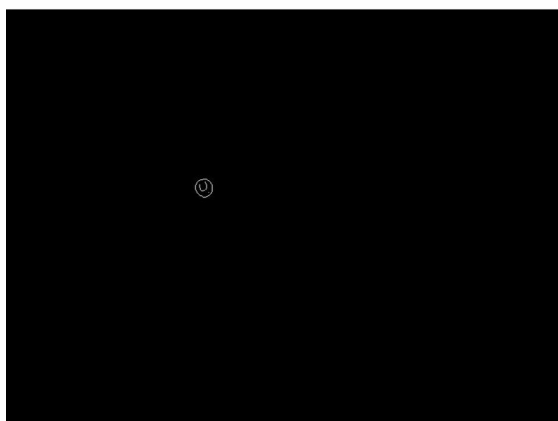
Then the detected edge is thickened in several steps (refer to subfigures (c) and (d)) and the resulting lines are tested for a connection. Connecting edges, meaning lines forming a closed object are recognized as belonging together.

In a subsequent step, interior gaps are filled with white color as shown *Figure 4.41* (e) and (f). The final result is such a black and white picture, where events are marked in white. The area of such events is the sum of all white pixel in a picture.

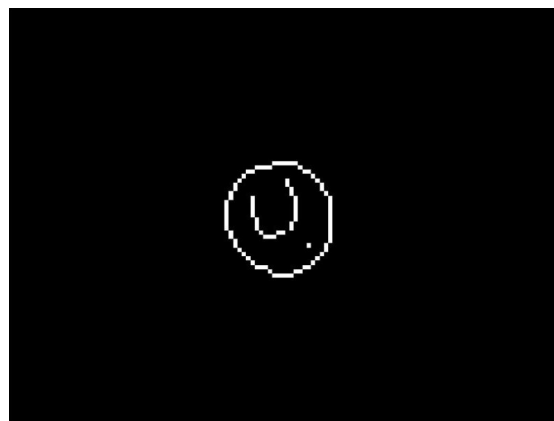
As a simple way to calculate breakdown probability the resulting black and white pictures are evaluated. If the area of white pixel is greater zero, meaning if white pixel exist, it counts as event, if the picture is black, it counts as no event. As already mentioned in the previous sections, breakdown probability is then the quotient of the number of pictures containing events per total number of evaluated pictures.

The program is calculating the total area in pixel and is not only testing if white pixel exist. This area size is recorded with the picture and can be used to evaluate samples at high concentrations. Especially when multiple plasma events are initiated by the laser pulse, the advantage of recording the total event area becomes evident (refer to *Section 4.2.3.1* for analysis of multiple events).

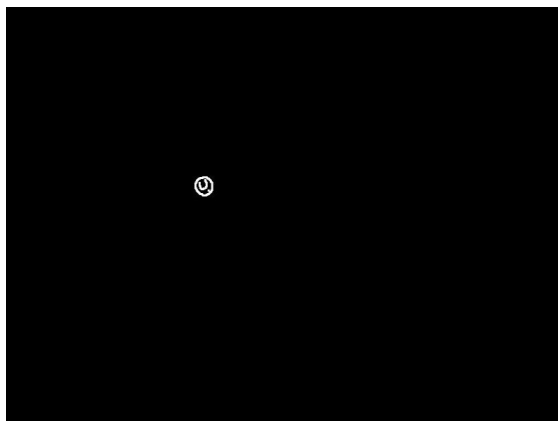
A problem with these simple calculation are pixel errors or some other effects causing some pixel to get exposed to radiation. This results in areas of a few pixel which shall not count as an event. Therefore, a threshold value has to be defined when an area is recognized as event and when not.



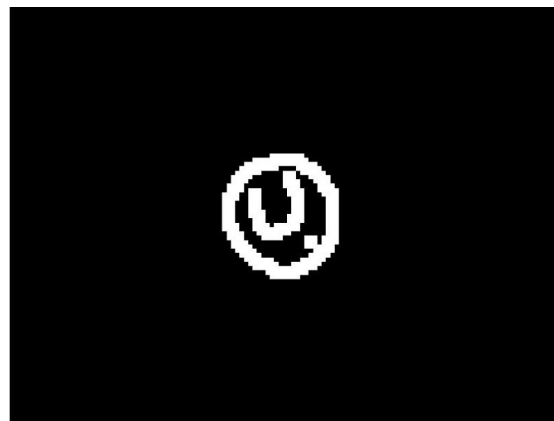
(a) Gradients are detected in the gray value and the detected edge is outlined.



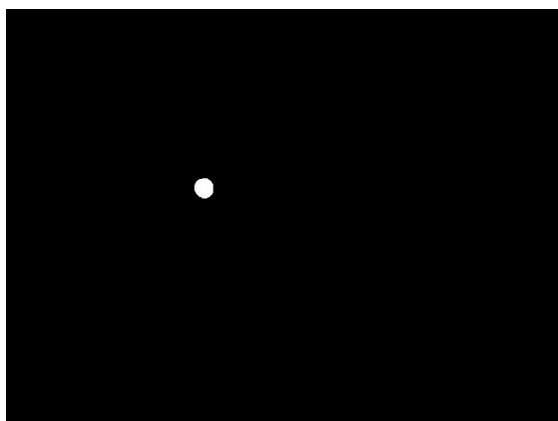
(b) Gradients are detected in the gray value as in subfigure (a) and a magnified section is shown.



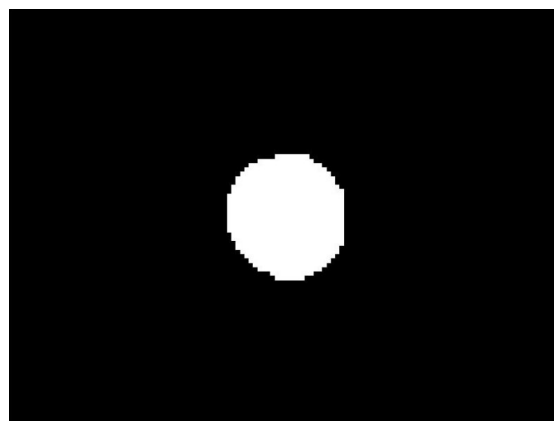
(c) Afterward, the detected edge is thickened in several steps.



(d) The edge is thickened in several steps and, again, a magnified version of the event in subfigure (c).



(e) Finally, not connected lines are discarded and objects with connected outlines interior gaps are filled.



(f) Filling of interior gaps and showing a magnified version of the event.

**Figure 4.41:** After conversion to gray scale and application of the filter, gradients in the gray value are detected and outlined as shown in subfigure (a) (again, in the right column are magnified versions of the section containing the plasma event). The detected edge will then be thickened several times in subsequent steps as shown e.g. in subfigure (c). Connected edges will be recognized as events, not connected lines are discarded. In a final step interior gaps are filled with white color.

In *Figure 4.42* results of two experiments for the calculation of breakdown probability are shown. The estimated event area of each picture in the series is plotted versus the picture number and sorted descending by size. For counting events, a threshold value has to be defined specifying the area in pixel which will count as an breakdown event. This threshold for counting as an event is set to fifty pixel in *Figure 4.42*. As can be seen in the figure, there are some non-zero areas which have a size of a few pixel only. These are no events, therefore, such a threshold value is necessary.

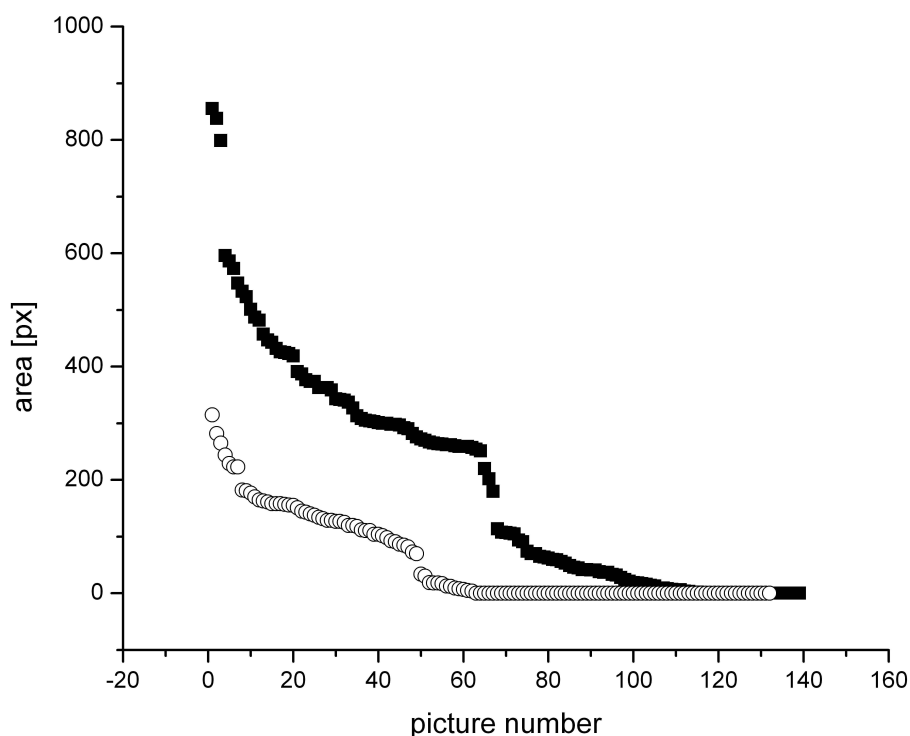


**Figure 4.42:** Area of breakdown events in the measurements estimated by the *MatLab* program. The area in pixel is calculated for each measurement and plotted for each picture. In this figure they are also sorted from highest estimated area to lowest.

As already mentioned above, for evaluation of breakdown probability, everything with an area greater than zero can count as a plasma event. That will theoretically suffice, but even after applying a filter to even the background signals there are small areas of a few pixel left. These small areas are no events, therefore, a minimal size for plasma events has to be defined. As shown in *Figure 4.42*, the event area can differ from series to series. This may be caused by changes in the distance of camera and cuvette or by slightly different angles in placing the cuvette in relation to the incident laser beam and the camera.

For the example in *Figure 4.42* a threshold value of about 50 pixel would be appropriate for the experiment with the open circles whereas a threshold value of about 150 pixel would be good for the experiment with the filled boxes.

Another interesting point is the shape of the curves, which seems always to have a step in it when ordered by size of the area in pixel. For the experiment with the filled boxes in *Figure 4.42* this is at about picture number 70. A step can also be observed in the other experiment in this figure (with the open circles), here at about picture number 50.

#### 4.2.2.2 Estimating Breakdown Area in Colloidal Suspension

Estimation of the area of breakdown events is done by the *MatLab* program as described above. After the edge detection algorithm is applied, events are localized in the picture as described before in this chapter. The area of a breakdown event is filled with white color, the rest of the picture is filled with black. After processing a recorded picture in this way, all white pixel in the recorded photo are counted and this results in the total area of events in pixel.

As a matter of fact, for calculation of breakdown probability, the area of events in a picture has to be calculated first. At least the program has to run till filling interior gaps, checking for white colored pixel and counting them until reaching a certain value. Only if the area exceeds a predefined threshold value it counts as an event. Therefore, an estimation of breakdown area has to be carried out for the program to identify events. After that, the breakdown probability can be calculated.

For determination of breakdown probability to states are discriminated, "event" or "no event". The advantage of using the total area of events would be a finer differentiation in form of the area size. This fact becomes notable at high breakdown probability, especially if multiple events are generated in a measurement (refer to *Section 4.2.3.1*).

In *Figure 4.43* experiments were carried out showing the estimated pixel area of events at varying laser pulse energy. The samples correspond to the measurements in *Figure 4.36*, here also *Sample09* at a concentration of  $2.0 \cdot 10^5 \text{ cm}^{-3}$ , *Sample10* at a concentration of  $8.6 \cdot 10^4 \text{ cm}^{-3}$  and distilled water were analyzed. For each sample a series of measurements was carried out at varying laser pulse energy. The plasma event area was estimated by the program as described above.

The difference between the two samples (*Sample09* and *Sample10*) is the mean particle diameter. *Sample09* contains particulates of a larger size with an average diameter of  $2.0 \mu\text{m}$  than *Sample10*, which contains particulates of an average diameter of  $0.35 \mu\text{m}$ .

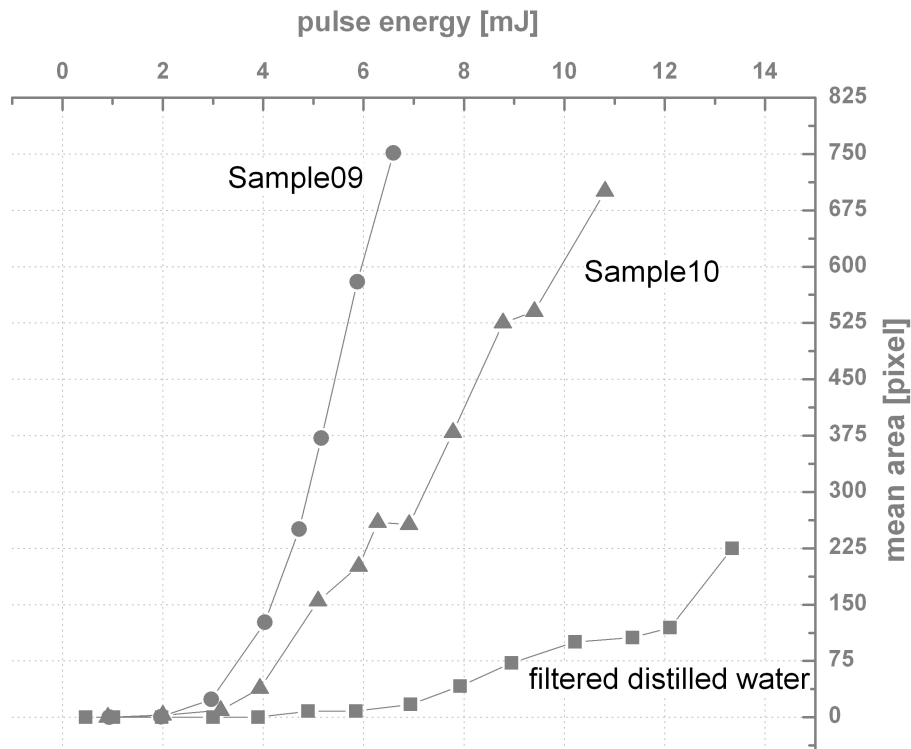


**Figure 4.43:** Estimated area of breakdown events at different pulse energies. Here, *Sample09* was used at a concentration of  $2.0 \cdot 10^5 \text{ cm}^{-3}$  in comparison to *Sample10* at a concentration of  $8.6 \cdot 10^4 \text{ cm}^{-3}$  and distilled water. Breakdown probability for this experiments is shown in *Figure 4.36*, here the corresponding mean areas in pixel are plotted (refer also to *Figure 4.44* for comparison of breakdown probability and estimated area).

With increasing laser pulse energy, plasma breakdown probability increases resulting in a larger plasma event area. These experiments show the same tendency as the measurements concerning breakdown probability. The larger particles (*Sample09*) have a lower breakdown threshold and, therefore, plasma generation can occur at lower pulse energy. In contrast to the experiments shown in *Figure 4.36*, the graphs did not form an *S*-shape, but the area continues to increase. This is due to taking multiple events into account, were two or more events in one recorded picture have a greater area than one event, whereas in breakdown probability one or more plasma events, would count simply as event (refer to *Section 4.2.3.1*).

### 4.2.3 Correlating the Breakdown Probability and its Estimated Area

In the experiments evaluation of data files (recorded pictures) was carried out with the help of the *MatLab* program. The program analyzes the files and gives the breakdown



probability for the experiment. An experiment, in this case, is meant to be understood as a series of measurements varying a parameter like concentration or laser pulse energy. Each measurement in the series consists, in turn, of many recorded pictures, typically several hundred. In addition to the breakdown probability the total area of events in pixel is recorded.

As mentioned above, breakdown probability measurements discriminates two states only, "event" or "no event". The number of events per number of measurements gives the breakdown probability, thus, this value can range between zero and one or one hundred percent. At high breakdown probabilities, multiple events are likely to occur (refer to *Section 4.2.3.1*). In this case it will still count as "event" for the calculation of breakdown probability and no differentiation is made.

By recording the total pixel area of events, differentiation of multiple events becomes feasible in the sense that the area increases even when the breakdown probability has reached one (or one hundred percent). At lower breakdown probability the curves are qualitatively similar, therefore total area can be used instead of breakdown probability. At high breakdown probabilities, the area estimation has the additional advantage of taking multiple events into account.

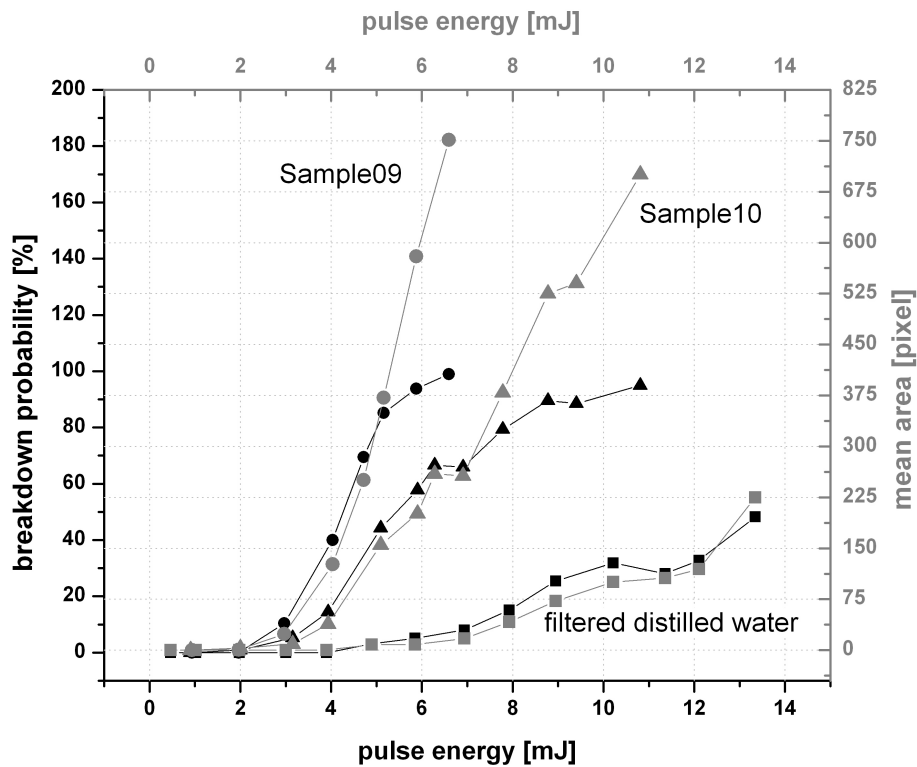


**Figure 4.44:** Estimated area of breakdown events at different laser pulse energies. Here, *Sample09* was investigated at a concentration of  $2.0 \cdot 10^5 \text{ cm}^{-3}$  in comparison to *Sample10* at a concentration of  $8.6 \cdot 10^4 \text{ cm}^{-3}$  and filtered distilled water.

In further experiments the program was used for data evaluation. In addition to the breakdown probability (also calculated by program) the area of all events was recorded. This new aspect of the evaluation of the breakdown events has the main advantage of perceiving multiple events in one recorded picture.

The graph in *Figure 4.45* shows a comparison of breakdown probability as counted by eye and the breakdown probability calculated by the program. Additionally, the area is plotted with all data normalized.

Concentrations are in relation to a sample suspension which was set to a concentration of one. Here, estimation of breakdown probability was investigated when counting by hand or by program.

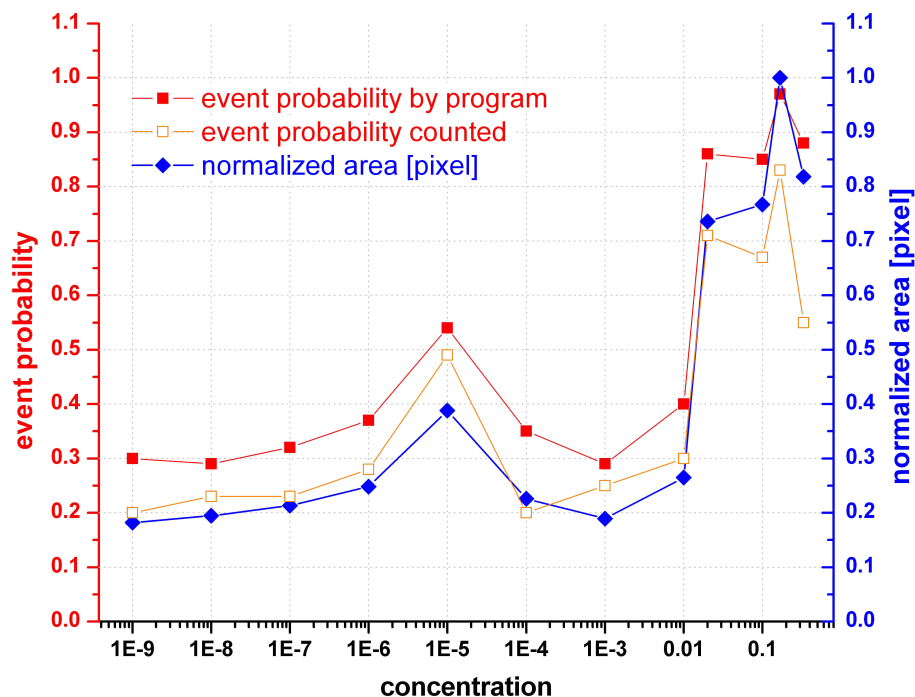


**Figure 4.45:** Total event area as evaluated by the *MatLab* program in comparison to its breakdown probability estimated by eye and by software.

#### 4.2.3.1 Analysis of Multiple Events Based on Area Estimation

After adjusting the laser system and optimizing the *MatLab* program, prepared silica dioxide particulates were investigated. In an initial measurement, three samples were analyzed. Breakdown probability and total pixel area was recorded and plotted against the pulse energy. The samples included distilled water for comparison. Additionally, the distilled water sample was filtered using a 0.45  $\mu\text{m}$  filter in order to ensure purity without using a clean room. The other two samples contained silica dioxide colloids of different size. *Sample09* consists of 0.35  $\mu\text{m}$  particulates in distilled water and *Sample10* contained colloids with a diameter of 2  $\mu\text{m}$ . Nearly matching concentrations were chosen for both sample colloid suspensions ( $2.0 \cdot 10^5 \text{ cm}^{-3}$  for *Sample09* and  $8.6 \cdot 10^4 \text{ cm}^{-3}$  for *Sample10* respectively). Laser pulse energy was adjusted using an iris lens, which simultaneously changed the beam diameter. In the range of pulse energies used for these investigations, this change of beam diameter did not have an observable impact. It may be noted, however, that a much bigger diameter leads to more scattering before the focal zone and thus causes disturbances in the measurement. Also, by changing the beam diameter, or by cutting off a part, the beam profile can not be considered a gaussian profile. This fact is

neglected in these experiments, but may become important if calculations of particle size distributions were carried out.

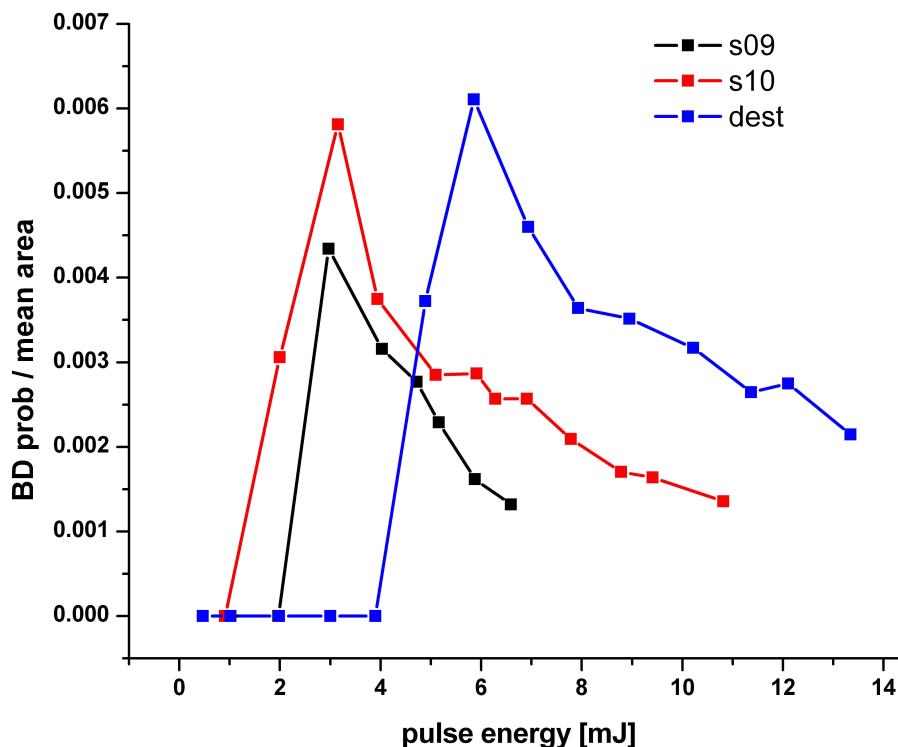


**Figure 4.46:** Quotient of breakdown probability and total pixel area (refer to *Figure 4.44*).

In *Figure 4.46* the quotient of BD probability and total pixel area as calculated in order to show their comparability clearer. These investigations have been done with *Sample09*, *Sample10* and distilled water (refer to *Figure 4.44*). More data has to be acquired for these kind of calculations, which should be done future investigations.

In the measurements described in this part,  $\text{SiO}_2$  was used as sample colloidal substance. Silica dioxide is a white powder which was solved in distilled water (refer to *Chapter 3*). In order to test the setup and have a wider range of applicability, two kinds of black particles were tested. These are graphite and activated carbon.

The scattering was much higher with these colloids and all parameters had to be readjusted. With these particulates first test measurements were carried out. These investigations have to be continued in order to measure breakdown probability and calculate concentrations of these particles.

## Chapter 5

### Summary and Conclusion

This work aimed at the detection of pesticides in environmental compartments. One focus was the mapping of pesticide distributions on natural surfaces like leaves in regard to a fast optical assessment of pesticide coverage. Laser induced fluorescence (LIF) spectroscopy was the chosen method to achieve this goal by investigating interactions of sample pesticides with a fluorescent tracer material. Different setups were tested ranging from fluorescence measurements of single spots to scanning and simple imaging techniques. The ambition of the second part was the detection of pesticide active components in water. These normally show a low solubility benefiting the formation of colloids, tiny particulates in the nanometer range. Colloidal particulates are neglected in chemical water standard analysis, where filters with a pore size of 450 nm are used. For the detection of nanosized particulates at low concentrations laser induced breakdown detection (LIBD) was the chosen method.

Optical methods have the advantage of counting as non-invasive, and a fast online analysis of samples is possible due to the very short interaction times of radiation with matter. For both methods used in this work, laser induced fluorescence and laser induced breakdown detection, a preparation of the samples is not required. These are essential prerequisites for *in vivo* and *in situ* investigations of biological material or measurements regarding environmental questions.

For a fast optical assessments of pesticide coverage on surfaces like leaves, laser induced fluorescence spectroscopy was used. Fluorescence spectroscopy has wide applications for biological and environmental questions. Natural surfaces like leaves have the additional difficulty of a matrix fluorescence stemming from substances in the leaf. Notably in green leaves is the chlorophyll molecule but also other substances like ferulic acid which can be found in cell walls. In order to achieve a measure of independence from the signals of these bio-emitters, a fluorescing tracer material has been used. The experiments did not focus on the detection of the tracer material but in changes of the fluorescence

properties such as shifts in wavelength, intensity, or life times in presence or absence of a sample pesticide. Shifts in fluorescence parameters may stem from complexation or other interactions with the sample pesticide and the fluorescence tracer material. It has been shown, that these changes could be used to differentiate pesticide containing droplets from droplets of pure water. Additionally, the quantity of these shifts depends on the concentration of the sample pesticide allowing a limited concentration measurement.

For analysis of pesticide coverage, a focused laser beam was used for fluorescence excitation and the sample leaf was put on a movable stage. This setup allowed a scanning over the leaf which results in a mapping of pesticide distributions. In this work, experiments of scanning along a line over a droplet have been shown. Moving the xy-stage was carried out by micrometer screws manually, and measuring time was about 10 s per point which results in a long experiment time. Therefore, only a measurement over a line was evaluated, but the process could be automated by a motor driven stage and measuring time is reducible by shorter integration times or an improved camera.

Additionally, simple and low cost imaging systems have been investigated. As straight forward setup, a sample leaf was placed under an UV-C light source (lamp of a clean bench) and a photo was taken by a commercially available CCD camera (a 2 megapixel digital camera). It could be shown that it is feasible to use such a system for the detection of coverage, but these experiments did not provide any spectral information. Component discrimination or identification is therefore not possible. As a second imaging system, a fluorescence microscope was used to investigate the sample leaves. One advantage of this setup was the investigation of dissolution of the fluorescence tracer material in a droplet of distilled water. The microscope was equipped with a video CCD camera and single pictures could be stored. The dry dye micro-crystals did not show a fluorescence signal but when dissolved in water a strong fluorescence emission was observable.

The simple imaging setup can be used for detection of coverage, while the scanning experiments utilizing laser induced fluorescence spectroscopy additionally delivers spectral information. Scanning over a leaf provides good results for the detection of pesticides as well as estimating coverage and being able to discriminate pesticide containing droplets from pure water droplets. As a future step an automation of the scanning unit would be desirable for a better scanning over the leaf surface.

For field application, some test plants have to be pretreated with the fluorescent marker prior to pesticide application. Then the changes in fluorescence properties of the labeling substance can be used for detection of the pesticide on the plant. Still, the experimental setup has also to be tested in the field before any practical application can be suggested. The auto-fluorescence of the pesticides did not provide reliable results due to the rather weak signals and matrix effects originating from the plants organic composition. The one exception investigated in this work was the pesticide *Gesatop 50*, which shown a strong

auto-fluorescence. This pesticide may be investigated directly by its auto-fluorescence and for a practical application no treatments of test plants would be required.

Aiming at the detection of pesticide colloidal suspensions, experiments utilizing laser induced breakdown detection are conducted. Pesticides are typically composed of an active ingredient which comes with surfactants or other substances in an emulsion. The emulsion aids the active component to reach their place of action e.g. by penetrating the cuticula of a leaf. Since the active components usually show low solubility, the emulsion also helps getting solved in water. Due to the low solubility, the active ingredients are likely to form colloids once getting into the soil or water systems.

Colloids are tiny particulates of solid matter, their size ranges from 1 nm to 1  $\mu\text{m}$  in diameter. In this work also particulates of 2  $\mu\text{m}$  in diameter were used, but for a simpler mode of speech all particulates are referred to as colloids. In standard chemical water analysis filters with a pore size of 450 nm are used, which results in neglecting particulates of a smaller diameter. For the detection of colloids in water a method is required which is able to detect such tiny particulates and is also sensitive to these particles at low concentrations. For this purpose laser induced breakdown detection (LIBD) was used in this work.

This optical method uses a pulsed laser beam focused into a cuvette containing water and the sample colloidal suspension. Plasma breakdown detection is based on different breakdown threshold values of solid matter, liquids, and gases where gases have the highest threshold value and solids the lowest. Utilizing this fact, laser pulse energy is adjusted in a way, that no plasma events occur when focused into the sample liquid, distilled water in this work. A sample containing the solid particulates is then investigated. If a colloid enters the focal region of the laser beam a plasma is generated at the particulate due to the lower breakdown value of solid matter. The measurements are not disturbed by gas bubbles because the gas requires even higher pulse energies for plasma breakdown than the liquid.

If a particulate enters the focal region and a plasma is generated depends on the concentration and size of the colloids. Concentration measurements are carried out by analyzing the breakdown probability. Breakdown probability requires many pulses to be investigated and is calculated as the number of plasma events per number of total laser pulses. If a plasma is generated in the sample this results in an acoustical and in an optical signal stemming from the fast volume expansion and from the recombination of electrons respectively.

Either signal can be used for the detection of plasma breakdown events, for a subsequent calculation of the particulate mean diameter, however, the optical detection is required (extend of the focal zone can be measured and together with the breakdown probability, the mean diameter can be calculated). In order to have the possibility to implement size

determination in the future, the optical detection was employed in this work. Pictures of the focal region are taken by a CCD camera synchronized with the laser pulse. For the calculation of breakdown probability these photos are analyzed. Due to the large amount of data a self written *MatLab* program was used in this work for an automation of this process. The program identifies plasma events in a picture and estimates an event area in pixel. The event area is used for calculation of breakdown probability where only *event* or *no event* in a given picture is needed.

It could be shown that total event area and breakdown probability correlate well at lower values. At higher values, meaning higher breakdown probability, the total event area has the advantage of taking multiple plasma events (due to their larger area) into account whereas with the breakdown probability such differentiation is not possible and a maximum is reached at one hundred percent.

The first steps in the construction of a setup for quantification of pesticide colloidal suspensions are shown in this work. Here, silica dioxide ( $SiO_2$ ) sample colloidal suspensions are used for testing feasibility of the method and for evaluation of experiment parameters. Silica dioxide is a white substance and first experiments with black particulates were also conducted. As black colloids active carbon and graphite suspension were prepared.

To continue these experiments measurements with the black particles will have to be carried out as well as investigations of sample organic material such as yeast cells. The setup also has to be tested with colloidal pesticide active components. Additionally, field experiments should be conducted for investigating feasibility of the method in the natural environment. Another addition to the laser induced breakdown detection would be a combination with breakdown spectroscopy. Therefore, a timed recording of the spectral dispersed radiation stemming from the plasma event is required in order to detect atomic lines. This more complex setup would have the advantage of element identification which would result in a better pesticide determination.



# Appendix A

## Pesticide Properties and Data Sheets

In this appendix information about the used pesticides is compiled. This information is taken from the safety data sheets or instruction manuals.

### Patoran FL

Material Safety Data Sheet

Date: 17/02/2004

Supersedes: 10/02/2004

---

#### 01 IDENTIFICATION OF THE SUBSTANCE/PREPARATION AND OF THE COMPANY

Product name: PATORAN FL  
Name: Belchim Crop Protection Deutschland

#### 02 COMPOSITION / INFORMATION ON INGREDIENTS

Chemical nature: Herbicide  
Hazardous constituents: Metobromuron (CAS: 003060-89-7, EINECS: 221-301-5)  
500 g/L

#### 09 PHYSICAL AND CHEMICAL PROPERTIES

Physical state: Suspension concentrate  
Color: White (milky)  
pH: 6.0 – 8.0 (susp. 1 %)  
Flammability characteristics:  
- Flash point: > 100 °C  
Specific gravity: 1.22 g/cm<sup>3</sup> – 1.25 g/cm<sup>3</sup> at 20 °C  
Dynamic viscosity: 750 mPas – 1000 mPas at 20 °C

---

**Table A.1:** Material Safety Data Sheet: Patoran FL (Extract)

## Roundup UltraMax

Material Safety Data Sheet

Date: 19/10/2005

---

### 01 IDENTIFICATION OF THE SUBSTANCE/PREPARATION AND OF THE COMPANY

Product name: Roundup UltraMax  
Name: Spiess-Urania Chemicals GmbH

### 02 COMPOSITION / INFORMATION ON INGREDIENTS

Chemical nature: Herbicide  
Hazardous constituents: Glyphosate monoisopropylamine salt (CAS: 38641-94-0, Eines: 254-056-8, EC classification: N; R51/53): 51.0 %  
Surfactant (CAS: 68478-96-6, EC classification: Xn, N; R22-41-51/53): 7.5 %

### 09 PHYSICAL AND CHEMICAL PROPERTIES

Physical state: liquid  
Color: yellow  
Odor: aromatic  
pH: 5.1 (10 g/L at 20 °C)  
Flammability characteristics:  
- Flash point: not flammable  
- Auto-ignition temperature: no auto-ignition  
Specific gravity: 1.193 g/cm<sup>3</sup> at 20 °C  
Solubility:  
- in water: Dispersible.  
Kinematic viscosity: 86.32 mm<sup>2</sup>/s at 25 °C

---

**Table A.2:** Material Safety Data Sheet: Roundup UltraMax (Extract)

## Duplosan DP

Material Safety Data Sheet

Date: 04/05/2005

Supersedes: 30/11/2004

---

### 01 IDENTIFICATION OF THE SUBSTANCE/PREPARATION AND OF THE COMPANY

Product name: DUPLOSAN DP

Name: Nufarm Deutschland GmbH

### 02 COMPOSITION / INFORMATION ON INGREDIENTS

Chemical nature: Herbicide

Hazardous constituents: Dichloprop-P potassium salt (CAS: 113963-87-4, Eines: 430-580-9, EC classification: Xn; R22-38-41-43): 55.0 %  
2,4-Dichlorophenol (CAS: 120-83-2, Eines: 204-429-6, EC classification: T, N; R22-24-34-51/53): 0.1 %

### 09 PHYSICAL AND CHEMICAL PROPERTIES

Physical state: liquid at 20 °C

Color: brown

Odor: aromatic

pH: 10 – 12 at 20 °C

Flammability characteristics:

- Flash point: no data

- Auto-ignition temperature: no data

Specific gravity: 1.26 g/cm<sup>3</sup> – 1.32 g/cm<sup>3</sup> at 20 °C

Solubility:

- in water: Soluble.

Dynamic viscosity: 27.22 mPas at 20 °C

---

**Table A.3:** Material Safety Data Sheet: Duplosan DP (Extract)

## Goltix 700 SC

Material Safety Data Sheet

Date: 12/11/2004

Supersedes: 06/08/2004

---

### 01 IDENTIFICATION OF THE SUBSTANCE/PREPARATION AND OF THE COMPANY

Product name: Goltix 700 SC  
Name: Feinchemie Schwebda GmbH

### 02 COMPOSITION / INFORMATION ON INGREDIENTS

Chemical nature: Herbicide  
Hazardous constituents: Metamitron (CAS: 41394-05-2, Einecs: 255-349-3, EC classification: Xn, N; R20 - 50): 50 – 60 %  
Propane-1,2-diol (Einecs: 200-338-0): 0.5 – 2 %  
Glycerin (Einecs: 200-289-5): 1 – 10 %  
3(2H)-Isothiazolone,5-chloro-2-methyl-, mixt. with 2-methyl-3(2H)-isothiazolone (CAS: 55965-84-9, EC classification: T, C, N; R23/24/25-34-43-50-53): 0.0015 – <0.06 %

### 09 PHYSICAL AND CHEMICAL PROPERTIES

Physical state: liquid  
Color: beige  
Odor: weak, characteristic  
pH: 6.3 (1 %)  
Flammability characteristics:  
- Flash point: 73 °C  
- Auto-ignition temperature: 475 °C  
Specific gravity: 1.20 g/mL at 20 °C  
Solubility:  
- in water: dispersible  
Dynamic viscosity: 157.3 {mPas at 20 °C  
Surface tension: 21.5 mN/m

---

**Table A.4:** Material Safety Data Sheet: Goltix 700 SC (Extract)

## Arelon Fluessig

Material Safety Data Sheet

Date: 19/09/2005

---

### 01 IDENTIFICATION OF THE SUBSTANCE/PREPARATION AND OF THE COMPANY

Product name: Arelon flüssig  
Name: Nufarm Deutschland GmbH

### 02 COMPOSITION / INFORMATION ON INGREDIENTS

Chemical nature: Herbicide  
Hazardous constituents: Isoproturon (CAS: 34123-59-6, EINECS: 251-835-4, EC classification: N, Xn; R40, R50/53): 45.0 %  
Ethylene glycol (CAS: 107-21-1, EINECS: 203-473-3, EC classification: Xn; R22): 5 – 10 %  
Alkyletherphosphate Na-salt (EC classification: Xi; R36, R38): 3.0 %

### 09 PHYSICAL AND CHEMICAL PROPERTIES

Physical state: liquid  
Color: gray-beige  
Odor: characteristic  
pH: 7.8  
Flammability characteristics:  
- Flash point: > 100 °C  
- Auto-ignition temperature:  
not flammable  
Dynamic viscosity: no data

---

**Table A.5:** Material Safety Data Sheet: Arelon Fluessig (Extract)

## Centium 36 CS

Material Safety Data Sheet

Date: 09/11/2004

Supersedes: 17/12/2003

---

### 01 IDENTIFICATION OF THE SUBSTANCE/PREPARATION AND OF THE COMPANY

Product name: CENTIUM 36 CS

Name: FMC Chemical

### 02 COMPOSITION / INFORMATION ON INGREDIENTS

Chemical nature: Herbicide based on Clomazone

Hazardous constituents: Clomazone (CAS: 81777-89-1, EC auto-class.: Xn; R20/22 - R52): 34.83 %

Sodium nitrate (CAS: 7631-99-4, EINECS: 231-554-3, EC classification: R8 -Xn; R22 - Xi; R36/37/38): 4.5 %

Calcium chloride (CAS: 10043-52-4, EINECS: 233-140-8, EC classification: Xi; R36): 4.5 %

### 09 PHYSICAL AND CHEMICAL PROPERTIES

Physical state: Liquid

Color: brown

Odor: slight aromatic

pH: 8.87 (Aqueous dispersion - 1 %)

Flammability characteristics:

- Flash point: > 98 °C

- Auto-ignition temperature: 392 °C

Specific gravity: 1.16 g/cm<sup>3</sup> at 20 °C

Solubility:

- in water: Dispersible.

Dynamic viscosity: 143 mPas – 412 mPas at 20 °C

Surface tension: 68.9 mN/m at 20.5 °C

---

**Table A.6:** Material Safety Data Sheet: Centium 36 CS (Extract)

## Lexus

Material Safety Data Sheet

Date: 22/07/2004

---

### 01 IDENTIFICATION OF THE SUBSTANCE/PREPARATION AND OF THE COMPANY

Product name: Lexus PX

Synonyma: Lexus,  
B11176335

Name: Du Pont de Numours (Deutschland) GmbH

### 02 COMPOSITION / INFORMATION ON INGREDIENTS

Chemical nature: Herbicide

Hazardous constituents: Flupyr-sulfuron-methyl (CAS: 144740-54-5, EC classification: N; R50 - R53): 50 %

### 09 PHYSICAL AND CHEMICAL PROPERTIES

Physical state: solid

Color: white, yellow-brown

Odor: none

pH: 7 – 9 at 10 g/L and 20 °C

Flammability characteristics:

- Flash point: not applicable

Bulk density: 720 kg/m<sup>3</sup> – 820 kg/m<sup>3</sup>

Solubility:

- in water: dispersible.

---

**Table A.7:** Material Safety Data Sheet: Lexus (Extract)

## Reglone

Material Safety Data Sheet

Date: 05/01/2006

---

### 01 IDENTIFICATION OF THE SUBSTANCE/PREPARATION AND OF THE COMPANY

Product name: Reglone  
Name: Syngenta Agro GmbH

### 02 COMPOSITION / INFORMATION ON INGREDIENTS

Chemical nature: Herbicide  
Hazardous constituents: Diquat dibromide (CAS: 85-00-7, Einecs: 201-579-4,  
EC classification: T+, N; R22-26-36/37/38-43-48/25-  
50/53): 32.2 % (equals 17.1 % Diquat ion)  
Pyridine bases H (EC classification: Xn; R10-21/22): 0 –  
5 % (w/w)

### 09 PHYSICAL AND CHEMICAL PROPERTIES

Physical state: liquid  
Color: light brown  
Odor: characteristic for pyridine bases  
pH: 6.11  
Flammability characteristics:  
- Flash point: > 100 °C  
- Auto-ignition temperature: > 625 °C  
Specific gravity: 1.173 g/mL at 20 °C  
Solubility:  
- in water: dispersible

---

**Table A.8:** Material Safety Data Sheet: Reglone (Extract)



## Gesatop 50

Material Safety Data Sheet

Date: 09/11/2004

Supersedes: 17/12/2003

---

### 01 IDENTIFICATION OF THE SUBSTANCE/PREPARATION AND OF THE COMPANY

Product name: Gesatop  
Name: Orion Crop Protection Limited

### 02 COMPOSITION / INFORMATION ON INGREDIENTS

Chemical nature: Triazine herbicide  
Hazardous constituents: Simazine (CAS: 122-34-9): 500 g/l

### 09 PHYSICAL AND CHEMICAL PROPERTIES

Physical state: flowable suspension  
Color: light green  
Odor: non specific  
pH: 6.5 – 8.5 (aqueous - 1 %)  
Flammability characteristics:  
- Flash point: > 61 °C (closed cup)  
- Auto-ignition temperature: not available  
Specific gravity: 1.09 g/cm<sup>3</sup> at 20 °C  
Solubility:  
- in water: 6.2 g/L (pH 7, 20 °C) (simazine)

---

**Table A.9:** Material Safety Data Sheet: Gesatop 50 (Extract)

## Tamaron

Material Safety Data Sheet

Date: 25/02/2005

---

### 01 IDENTIFICATION OF THE SUBSTANCE/PREPARATION AND OF THE COMPANY

Product name: Tamaron  
Name: Bayer CropScience AG

### 02 COMPOSITION / INFORMATION ON INGREDIENTS

Chemical nature: Insecticide  
Hazardous constituents: Methamidophos (CAS: 10265-92-6, EINECS: 233-606-0, EC classification: T+, N; R24, R26/28, R50): 48.40 %  
Diethylene glycol (CAS: 111-46-6, EINECS: 203-872-2, EC classification: Xn; R22): 30.00 %  
Poly (oxy-1,2-ethanediyl), alpha-(isononylphenyl)-omega-hydroxy- (CAS: 37205-87-1, EC classification: Xn; R22, R41, R51/53): 5.00 %

### 09 PHYSICAL AND CHEMICAL PROPERTIES

Physical state: clear liquid  
Color: blue  
Odor: slight  
pH: 2.0 – 3.5 at 10 g/L (aqueous solution)  
Flammability characteristics:  
- Flash point: 56 °C  
- Auto-ignition temperature: 392 °C  
Specific gravity: 1.25 g/cm<sup>3</sup> at 20 °C  
Solubility:  
- in water: clear soluble

---

**Table A.10:** Material Safety Data Sheet: Tamaron (Extract)

# List of Figures

2.1	General experimental setup for spectroscopy measurements . . . . .	5
2.2	Jablonski diagram illustrating decay processes . . . . .	7
2.3	Schematic overview of plasma generation and breakdown. . . . .	12
2.4	Schematic of LIBD mechanisms. . . . .	13
3.1	Schematic setup of the nitrogen laser system. . . . .	22
3.2	Setup of the Nd:YAG-laser system used for time resolved measurements.	27
3.3	Setup of the Nd:YAG laser system used for laser induced breakdown de- tection of colloids or fine particulate material in liquids. . . . .	29
4.1	Absorption measurements of the sample pesticides recorded by a pho- tometer. . . . .	38
4.2	Picture of <i>Rhodamine 101</i> and <i>Rhodamine 6G</i> on the surface of a cover slip. . . . .	40
4.3	Comparison of different particulate dyes on the surface of a glass carrier material. . . . .	41
4.4	Comparison of <i>Rhodamine 6G</i> on the surface of a cover slip and solved in a cuvette. . . . .	42
4.5	Investigation of <i>CdSe</i> nanoparticles on a glass carrier material. . . . .	43
4.6	Waterfall diagram of <i>CdSe</i> nanoparticles on glass carrier material. . . . .	44
4.7	Cuts along the time axis of <i>Figure 4.6</i> . . . . .	45

4.8	Investigation of <i>CdSe</i> nanoparticles on thick and thin layer areas. . . . .	46
4.9	Fluorescence spectra of <i>Arelon flüssig</i> and <i>Gesatop 50</i> applied to a leaf coated with a <i>Rhodamine 6G</i> layer. . . . .	47
4.10	Auto-fluorescence of the sample pesticides. . . . .	49
4.11	Pesticide active ingredients applied to a cover slip coated with a <i>Rhodamine 101</i> layer. . . . .	50
4.12	Fluorescence of pesticides on the surface of the glass carrier material. . . . .	51
4.13	Fluorescence of pesticides on the surface of the glass carrier material coated with a layer of <i>Rhodamine 6G</i> . . . . .	52
4.14	Fluorescence of an untreated leaf compared to an added droplet of water. . . . .	53
4.15	Fluorescence of a leaf with a dry <i>Rhodamine 6G</i> layer compared to added droplets of two sample pesticides. . . . .	54
4.16	Images of a fluorescence microscope monitoring the dissolution of a <i>Rhodamine 6G</i> crystallite. . . . .	55
4.17	Images of a fluorescence microscope monitoring the dissolution of a <i>Rhodamine 6G</i> crystallite and subsequent drying of the suspension. . . . .	56
4.18	Fluorescence intensity of a <i>Rhodamine 6G</i> layer on the surface of an ivy leaf. . . . .	58
4.19	Fluorescence intensity of a <i>Rhodamine 6G</i> layer on the surface of a cover slip. . . . .	59
4.20	Shift in <i>Rhodamine 6G</i> fluorescence wavelength due to the interaction of the dye with a pesticide containing droplet. . . . .	60
4.21	Spectral shift of the <i>Rhodamine 6G</i> fluorescence due to interaction with a droplet containing the pesticide <i>Arelon flüssig</i> at different concentrations. . . . .	61
4.22	Shift in <i>Rhodamine 6G</i> fluorescence wavelength due to the interaction of the dye with a droplet containing the pesticide <i>Roundup UltraMax</i> . . . . .	62
4.23	Time resolved fluorescence spectrum of <i>Rhodamine 6G</i> in (a) cuvette and (b) on leaf . . . . .	63
4.24	Time resolved fluorescence spectra of the sample pesticides (Part I). . . . .	64

4.24	Time resolved fluorescence spectra of the sample pesticides (Part II). . . . .	65
4.25	Time resolved fluorescence spectra of a <i>Rhodamine 6G</i> solution in <i>Arelon flüssig</i> and in distilled water applied to a leaf surface. . . . .	66
4.26	Emission spectra of <i>Rhodamine 6G</i> in <i>Arelon flüssig</i> and distilled water on a leaf surface. . . . .	67
4.27	Scanning over a droplet of pesticide applied to the surface of a <i>Rhodamine 6G</i> coated ivy leaf. . . . .	69
4.28	Scanning over a droplet on a <i>Rhodamine 6G</i> coated ivy leaf and displaying full fluorescence spectra. . . . .	70
4.29	Fluorescence image of an ivy leaf recorded by a digital camera. . . . .	71
4.30	Example of an optical measurement utilizing LIBD. . . . .	73
4.31	Cutouts of pictures taken by the camera. . . . .	75
4.32	Cutouts of pictures taken by the camera in gray scale. . . . .	76
4.33	Pictures of a weak event the event enhanced by software. . . . .	77
4.34	Example events of different intensity. . . . .	78
4.35	Breakdown probability in dependence of the concentration of a sample solution. . . . .	80
4.36	Breakdown probability of two sample suspensions containing $SiO_2$ and filtered distilled water over pulse energy is shown. . . . .	81
4.37	Example of a picture as taken by the camera. . . . .	84
4.38	Pictures of events after processing by the program. . . . .	85
4.39	Processing steps of the program (Part I). . . . .	86
4.40	Processing of a weak event, with and without using a filter. . . . .	87
4.41	Processing steps of the program (Part II). . . . .	89
4.42	Estimation of the area of breakdown events by a <i>MatLab</i> program. . . . .	90
4.43	Estimated area of breakdown events at different pulse energies. . . . .	92

---

4.44	Estimated area and breakdown probability of events at different laser pulse energies. . . . .	94
4.45	Breakdown probability by program and by eye in comparison with total area. . . . .	95
4.46	Quotient of breakdown probability and total pixel area (refer to <i>Figure 4.44</i> ). . . . .	96

# List of Tables

2.1	Example of biomagnification . . . . .	17
3.1	Technical Data: Nitrogen Laser System . . . . .	23
3.2	Technical Data: Detection Unit . . . . .	24
3.3	Technical Data: Non-linear Crystals . . . . .	24
3.4	Technical data: Nd:YAG Laser System for TR-LIF . . . . .	25
3.5	Technical Data: Detection Unit . . . . .	26
3.6	Technical data: UV-lamb and CCD-camera . . . . .	30
3.7	Technical data: Fluorescence Microscope . . . . .	31
3.8	Technical Data: Dyes . . . . .	33
3.9	Data: Used Pesticides with Mode of Action . . . . .	34
A.1	Material Safety Data Sheet: Patoran FL (Extract) . . . . .	101
A.2	Material Safety Data Sheet: Roundup UltraMax (Extract) . . . . .	102
A.3	Material Safety Data Sheet: Duplosan DP (Extract) . . . . .	103
A.4	Material Safety Data Sheet: Goltix 700 SC (Extract) . . . . .	104
A.5	Material Safety Data Sheet: Arelon Fluessig (Extract) . . . . .	105
A.6	Material Safety Data Sheet: Centium 36 CS (Extract) . . . . .	106
A.7	Material Safety Data Sheet: Lexus (Extract) . . . . .	107

---

A.8	Material Safety Data Sheet: Reglone (Extract) . . . . .	108
A.9	Material Safety Data Sheet: Gesatop 50 (Extract) . . . . .	109
A.10	Material Safety Data Sheet: Tamaron (Extract) . . . . .	110



# Bibliography

- [1] Miller, G. *Living in the Environment Principles, Connections, and Solutions*. Books/Cole Publishing Company, 11 edition, (2000).
- [2] Kiely, T., Donaldson, D., and Grube, A. *Pesticides Industry Sales and Usage - 2000 and 2001 Market Estimates*. Biological and Economic Analysis Division, Office of Pesticide Programs, Office of Prevention, Pesticides, and Toxic Substances, U.S. Environmental Protection Agency, , May (2004).
- [3] Swarup, D. and Patra, R. Environmental pollution and its impact on domestic animals and wildlife. *Indian Journal of Animal Science* **75**(2), 231–240 (2005).
- [4] Lunney, A., Zeeb, B., and Reimer, K. Uptake of weathered DDT in vascular plants: Potential for phytoremediation. *Environmental Science & Technology* **38**(22), 6147–6154 (2004).
- [5] Close, M. and Flintoft, M. National survey of pesticides in groundwater in New Zealand 2002. *New Zealand Journal of Marine and Freshwater Research* **38**(2), 289–299 (2004).
- [6] Rao, S. and Mamatha, P. Water quality in sustainable water management. *Current Science* **87**(7), 942–947 (2004).
- [7] Hahn, D. W. Laser-induced breakdown spectroscopy for sizing and elemental analysis of discrete aerosol particles. *Applied Physics Letters* **72**(23), 2960–2962, June (1998).
- [8] Poulain, D. and Alexander, D. Influences on concentration measurements of liquid aerosols by laser-induced breakdown spectroscopy. *Applied Spectroscopy* **49**(5), 569–579, May (1995).
- [9] Wagner, T., Bundschuh, T., Schick, R., and Koster, R. Detection of aquatic colloids in drinking water during its distribution via a water pipeline network. *Water Science And Technology* **50**(12), 27–37 (2004).

- [10] Bundschuh, T., Knopp, R., Winzenbacher, R., Kim, J. I., and Koster, R. Quantification of aquatic nano particles after, different steps of bodensee water purification with laser-induced breakdown detection (LIBD). *Acta Hydrochimica et Hydrobiologica* **29**(1), 7–15, July (2001).
- [11] Saito, M., Izumida, S., Onishi, K., and Akazawa, J. Detection efficiency of microparticles in laser breakdown water analysis. *Journal Of Applied Physics* **85**(9), 6353–6357, May (1999).
- [12] Filella, M., Deville, C., Chanudet, V., and Vignati, D. Variability of the colloidal molybdate reactive phosphorous concentrations in freshwaters. *Water Research* **40**(17), 3185–3192, October (2006).
- [13] Chanudet, V. and Filella, M. A non-perturbing scheme for the mineralogical characterization and quantification of inorganic colloids in natural waters. *Environmental Science & Technology* **40**(16), 5045–5051, August (2006).
- [14] Chanudet, V. and Filella, M. Particle size and mineralogical composition of inorganic colloids in glacier-melting water and overlying ice in an alpine glacier, oberaargletscher, switzerland. *Journal Of Glaciology* **52**(178), 473–475 (2006).
- [15] Hauser, W., Geckeis, H., Kim, J. I., and Fierz, T. A mobile laser-induced breakdown detection system and its application for the in situ-monitoring of colloid migration. *Colloids And Surfaces A-Physicochemical And Engineering Aspects* **203**(1-3), 37–45, April (2002).
- [16] Walther, C., Bitea, C., Hauser, W., Kim, J. I., and Scherbaum, F. J. Laser induced breakdown detection for the assessment of colloid mediated radionuclide migration. *Nuclear Instruments & Methods In Physics Research Section B-Beam Interactions With Materials And Atoms* **195**(3-4), 374–388, October (2002).
- [17] Degueudre, C., Pfeiffer, H.-R., Alexander, W., Wernli, B., and Bruetsch, R. Colloid properties in granitic groundwater systems. I: Sampling and characterisation. *Applied Geochemistry* **11**, 677 (1996).
- [18] Walther, C., Cho, H. R., and Fanghanel, T. Measuring multimodal size distributions of aquatic colloids at trace concentrations. *Applied Physics Letters* **85**(26), 6329–6331, December (2004).
- [19] Walther, C., Buchner, S., Filella, M., and Chanudet, V. Probing particle size distributions in natural surface waters from 15 nm to 2  $\mu\text{m}$  by a combination of LIBD and single-particle counting. *Journal of Colloid and Interface Science* **301**(2), 532–537, September (2006).
- [20] Atteia, O., Perret, D., Adatte, T., Kozel, R., and Rossi, P. Characterization of natural colloids from a river and spring in a karstic basin. *Environmental Geology* **34**(4), 257–269, June (1998).

- [21] Rosse, P. and Loizeau, J. L. Use of single particle counters for the determination of the number and size distribution of colloids in natural surface waters. *Colloids And Surfaces A-Physicochemical And Engineering Aspects* **217**(1-3), 109–120, April (2003).
- [22] McCarthy, J. and Zachara, J. Subsurface transport of contaminants - mobile colloids in the subsurface environment may alter the transport of contaminants. *Environmental Science & Technology* **23**(5), 496–502, May (1989).
- [23] Kersting, A. B., Efurud, D. W., Finnegan, D. L., Rokop, D. J., Smith, D. K., and Thompson, J. L. Migration of plutonium in ground water at the nevada test site. *Nature* **397**(6714), 56–59, January (1999).
- [24] Degueldre, C., Bilewicz, A., Hummel, W., and Loizeau, J. L. Sorption behaviour of am on marl groundwater colloids. *Journal Of Environmental Radioactivity* **55**(3), 241–253 (2001).
- [25] Lakowicz, J. R. *Principles of Fluorescence Spectroscopy*. Springer Science+Business Media, LCC, third edition, (2006).
- [26] Kitamori, T., Yokose, K., Suzuki, K., Sawada, T., and Gohshi, Y. Laser breakdown acoustic effect of ultrafine particle in liquids and its application to particle counting. *Japanese Journal Of Applied Physics Part 2 - Letters* **27**(6), L983–L985, June (1988).
- [27] Kitamori, T., Yokose, K., Sakagami, M., and Sawada, T. Detection and counting of ultrafine particles in ultrapure water using laser breakdown acoustic method. *Japanese Journal Of Applied Physics Part 1 - Regular Papers Short Notes & Review Papers* **28**(7), 1195–1198, July (1989).
- [28] Fujimori, H., Matsui, T., Ajiro, T., Yokose, K., Hsueh, Y. M., and Izumi, S. Detection of fine particles in liquids by laser breakdown method. *Japanese Journal Of Applied Physics Part 1 - Regular Papers Short Notes & Review Papers* **31**(5A), 1514–1518, May (1992).
- [29] Cervenak, M. and Isenor, N. Multiphoton ionization yield curves for gaussian laser-beams. *Optics Communications* **13**(2), 175–178 (1975).
- [30] Walther, C., Herlert, A., Kim, J. I., Scherbaum, F. J., Schweikhard, L., and Vogel, M. Absolute cross-sections for the nonresonant multi-photon ionization of toluene and xylene in the gas phase. *Chemical Physics* **265**(2), 243–250, April (2001).
- [31] Radziemski, L. From LASER to LIBS, the path of technology development. *Spectrochimica Acta Part B* **57**, 1109–1113 (2002).

- [32] Maker, P., Terhune, R., and Savage, C. Optical third harmonic generation. In *Proceedings of Third International Conference on Quantum Electronics*, volume 2, 1559. Columbia University Press, New York, (1964).
- [33] Buravlev, Y., Nadezha, B., and Babanskaya, L. Use of a laser in spectral analysis of metals and alloys. *Zavodskaya Laboratoriya* **410**, 165–171 (1974).
- [34] Cremers, D. and Radziemski, L., editors. *Handbook of Laser-Induced Breakdown Spectroscopy*. John Wiley & Sons, Ltd, (2006).
- [35] Tognoni, E., Palleschi, V., Corsi, M., and Cristoforetti, G. Quantitative micro-analysis by laser-induced breakdown spectroscopy: a review of the experimental approaches. *Spectrochimica Acta Part B* **57**, 1115–1130 (2002).
- [36] Izumida, S., Onishi, K., and Saito, M. Estimation of laser-induced breakdown threshold of microparticles in water. *Japanese Journal Of Applied Physics Part 1-Regular Papers Short Notes & Review Papers* **37**(4A), 2039–2042, April (1998).
- [37] Niemz, M. Threshold dependence of laser-induced optical-breakdown on pulse duration. *Applied Physics Letters* **66**(10), 1181–1183, March (1995).
- [38] Sacchi, C. Laser-induced electric breakdown in water. *Journal Of The Optical Society Of America B-Optical Physics* **8**(2), 337–345, February (1991).
- [39] Radziemski, L. and Cremers, D., editors. *Laser-Induces Plasmas and Application*. Marcel Dekker, Inc., (1989).
- [40] Bundschuh, T., Wagner, T. U., and Koster, R. Laser-induced breakdown detection (LIBD) for the highly sensitive quantification of aquatic colloids. Part I: Principle of LIBD and mathematical model. *Particle & Particle Systems Characterization* **22**(3), 172–180, November (2005).
- [41] Bundschuh, T., Yun, J. I., and Knopp, R. Determination of size, concentration and elemental composition of colloids with laser-induced breakdown detection/spectroscopy (LIBD/S). *Fresenius J Anal Chem* **371**(8), 1063–1069, Dec (2001).
- [42] Knollenberg, R. and Veal, D. Optical-particle monitors, counters, and spectrometers - performance characterization, comparison, and use. *Journal Of The IES* **35**(2), 64–81, March (1992).
- [43] Kim, J., Zeh, P., and Delakwitz, B. Chemical interactions of actinide ions with groundwater colloids in gorleben aquifer system. *Radiochimica Acta* **58**, 147 (1992).
- [44] Bundschuh, T. *Entwicklung und Anwendung der Laser-induzierten Breakdown Detektion zur Quantifizierung aquatischer Kolloide und Actinidenkolloide*. PhD thesis, Technische Universitaet Muenchen, (1999).

- [45] Knopp, R. *Laserinduzierte Breakdowndetektion zur Charakterisierung und Quantifizierung aquatischer Kolloide*. PhD thesis, Technische Universitaet Muenchen, (1996).
- [46] EPA. What is a Pesticide?, U.S. Environmental Protection Agency. <http://www.epa.gov/pesticides/about/>, , January (2007).
- [47] EPA. Pesticides, U.S. Environmental Protection Agency. <http://www.epa.gov/ebtpages/pesticides.html>, , December (2006).
- [48] Reeve, R. *Environmental Analysis*. John Wiley & Sons, (1994).
- [49] Sharma, V. DDT: The fallen angel. *Current Science* **85**(11), 1532–1537 (2003).
- [50] Brackmann, U. *Lambdachrome Laser Dyes*. Goettingen: Lambda Physik AG, 3rd edition, (2000).
- [51] Peterson, R. B., Oja, V., and Laisk, A. Chlorophyll fluorescence at 680 and 730 nm and leaf photosynthesis. *Photosynthesis Research* **70**(2), 185–196 (2001).
- [52] Vacha, F., Adamec, F., Valenta, J., and Vacha, M. Spatial location of photosystem pigment-protein complexes in thylakoid membranes of chloroplasts of *pisum sativum* studied by chlorophyll fluorescence. *Journal Of Luminescence* **122**, 301–303, January (2007).
- [53] Lichtenthaler, H. and Schweiger, J. Cell wall bound ferulic acid, the major substance of the blue-green fluorescence emission of plants. *Journal of Plant Physiology* **152**(2-3), 272–282, March (1998).



# Curriculum Vitae

name	Harald Hake
place of birth	Langenhagen, Germany
date of birth	07.11.1974
school carrier	<i>08/1981 - 07/1985: Grundschule Bissendorf 08/1985 - 07/1987: Orientierungsstufe Bissendorf 08/1987 - 07/1995: Gymnasium Mellendorf</i>
school qualification	<i>Abitur</i>
military service	<i>08/1995 - 07/1996: Grundwehrdienst in Munster</i>
university carrier	<i>10/1996 - 06/2002: study of physics at the University of Hannover 11/2000 - 07/2002: studentische Hilfskraft, supervising students in practical exercises (biology and physics) 08/2002 - 06/2007: Supervising students in practical exercises (biology and physics) 01/2003 - 09/2003: preparation of dissertation project, application for funding 10/2003 - 06/2007: doctorate studies 01/2006 - 02/2006: Minerva Short-Term Research Grant of the Max Planck Gesellschaft for working at the Technion - Israel Institute of Technology, Haifa, Israel</i>
university qualification	<i>diploma in physics</i>





# Publications

## Publications

H. Hake, R. Ben-Zur, I. Schechter and A. Anders

*Fast optical assessment of pesticide coverage on plants*

Analytica Chimica Acta 596, 1-8 (2007)

## Poster

T. Reeck, R. Raetzold, H. Hake and A. Anders

*A detection of the wood preservative Hylotox 59 and its active component DDT by using laser induced fluorescence (LIF) spectroscopy*

Norddeutscher Lasertag, Hannover, Germany (December 2002)

T. Reeck, R. Raetzold, H. Hake and A. Anders

*A detection of the wood preservative Hylotox 59 and its active component DDT by using laser induced fluorescence (LIF) spectroscopy*

Analytica Conference 2002, Munich, Germany (April 2002)



# Danksagung

An dieser Stelle möchte ich ganz herzlich Frau Prof. Dr. Angelika Anders für die Betreuung des Promotionsprojekts danken sowie für ihre freundliche Unterstützung während der Arbeit.

Außerdem geht mein Dank an Herrn Prof. Dr. Israel Schechter für seine freundliche Übernahme des Korreferats, sowie sein Interesse während der Arbeit und für die vielen Anregungen und auch die Gespräche drumherum. In diesem Zusammenhang möchte ich auch der Max Planck Gesellschaft für die Bewilligung eines Minerva Short-Term Research Grants danken, wodurch ein Besuch und die Mitarbeit in der Arbeitsgruppe von Herrn Prof. Dr. Schechter (Januar/Februar 2006) möglich war.

Für aufmunternde Worte und Diskussionen möchte ich mich vor allem bei PD Dr. Carsten Zeilinger und PD Dr. Anaclet Ngezahayo bedanken. Auch für ihre Unterstützung bei Fragen und im Labor. Gleiches gilt für Dr. Valery Bulatov, für dessen Hilfe während meines Aufenthalts in Israel ich mich ganz herzlich bedanken möchte.

Für seine Bemühungen und seine Unterstützung gerade zu Beginn meiner Arbeit und auch für nette Abende außerhalb des Instituts möchte ich Dr. Ralf Pätzold meinen Dank aussprechen. Zusätzlich möchte ich an dieser Stelle auch Oliver Enders, Melanie Steffens, Dr. Meike Keuntje, Dr. Merve Meinhardt und Thilo Reeck nennen.

Für ihre Unterstützung im Labor und dem Ansetzen diverser Proben geht mein Dank an Ingrid und Heidi, ohne deren Hilfe so mancher am Institut Schwierigkeiten hätte.

Für Gespräche auch außerhalb des Arbeitsgebiets und Einblicke in andere Bereiche geht mein Dank an Sabrina und Willem. Auch Jörgen, Ilona und Tobias möchte ich danken für die interessanten Gespräche auch abseits des Fachlichen.

Ich möchte allen Mitarbeitern des Instituts für Biophysik danken für die nette Arbeitsumgebung. Ich habe mich immer sehr wohl gefühlt und das ist natürlich allen Mitarbeitern zu verdanken.

Für die Überlassung der Pestizide möchte ich mich beim Pflanzenschutzamt Hannover und ebenso beim Institut für Pflanzenkrankheiten und Pflanzenschutz der Universität Hannover bedanken.

Für ihre Freundschaft in all den Jahren geht mein Dank an Markus, Lena, Mirco, Markus, Thorsten und Frank. Ebenso mein Dank an Natasha und Pavel für die Mitnahme bei vielen tollen Unternehmungen in Israel.

I would like to thank Israel Schechter for his kind support of my work and the nice chats and interesting discussions. And Valery Bulatov has my thanks for his help while I stayed at the Technion. It was a great time in Israel and only fond memories remain.

Meine tief empfundene Dankbarkeit geht an meine Eltern, die mir erst das Studium ermöglicht haben. Neben der finanziellen Unterstützung in all der Zeit, möchte ich mich für ihren Rückhalt auch in schwierigen Phasen bedanken. Zusprache und Motivation waren ebenfalls immer zu bekommen, obwohl es für euch selbst sicher nicht immer leicht war.

Meiner lieben Oma möchte ich meine tiefe Zuneigung aussprechen, auch wenn sie diesen Augenblick leider nicht mehr mit mir teilen kann. Doch ich freue mich auch, einige Zeit mit Bennet (dem neuesten Mitglied der Familie) verbringen zu können.

Memento mori: Frieda Hake, Karl-Heinz Köppe, Andreas Hake, Matthias Wiechmann